

ISTANBUL TECHNICAL UNIVERSITY ★ GRADUATE SCHOOL OF SCIENCE
ENGINEERING AND TECHNOLOGY

**NUMERICAL SIMULATION OF TWO-PHASE
OIL AND WATER FLOW**

M.Sc. THESIS

Atakan SEVER

Department of Petroleum and Natural Gas Engineering

Petroleum and Natural Gas Engineering

JANUARY 2012

ISTANBUL TECHNICAL UNIVERSITY ★ GRADUATE SCHOOL OF SCIENCE
ENGINEERING AND TECHNOLOGY

**NUMERICAL SIMULATION OF TWO-PHASE
OIL AND WATER FLOW**

M.Sc. THESIS

**Atakan SEVER
(505091516)**

Department of Petroleum and Natural Gas Engineering

Petroleum and Natural Gas Engineering

Thesis Advisor: Prof. Dr. Mustafa ONUR

JANUARY 2012

İSTANBUL TEKNİK ÜNİVERSİTESİ ★ FEN BİLİMLERİ ENSTİTÜSÜ

**İKİ FAZLI PETROL VE SU AKIŞININ
SAYISAL SİMÜLASYONU**

YÜKSEK LİSANS TEZİ

**Atakan SEVER
(505091516)**

Perol ve Doğal Gaz Mühendisliği Anabilim Dalı

Petrol ve Doğal Gaz Mühendisliği Programı

Tez Danışmanı: Prof. Dr. Mustafa ONUR

OCAK 2012

Atakan Sever, a **M.Sc.** student of ITU **Graduate School of Science Engineering and Technology** student ID **505091516**, successfully defended the **thesis** entitled “**NUMERICAL SIMULATION OF TWO-PHASE OIL AND WATER FLOW**”, which he prepared after fulfilling the requirements specified in the associated legislations, before the jury whose signatures are below.

Thesis Advisor : **Prof. Dr. Mustafa ONUR**

İstanbul Technical University

Jury Members : **Prof. Dr. Mustafa ONUR**

İstanbul Technical University

Assist. Prof. Ö. İnanç TÜREYEN

İstanbul Technical University

Assoc. Prof. Dr. Ayşe KAŞLILAR

İstanbul Technical University

Date of Submission : 19 December 2011

Date of Defense : 25 January 2012

To my family and wife,

FOREWORD

First of all I would like to thank my parents and my wife who were giving me support all the time I need.

I would like to thank my thesis advisor Prof. Dr. Mustafa ONUR for giving me his valuable times and guiding me throughout this study. His working discipline will be a norm and his lessons will form a fundamental basis of me.

I would like to thank Assistant Prof. Dr. Ö. İnanc TÜREYEN for his help at the all stages of this work.

I would like to thank Research Assistant Dr. Murat ÇINAR for his help on CMG software. I would also like to thank Research Assistant Cihan ALAN for his help of developing the matrix solver.

I extend my special thanks to the member of the Examining Committee ; Assist. Prof. Dr. İnanc TÜREYEN and Assoc. Prof. Dr. Ayşe KAŞLILAR for their attention.

December 2011

Atakan SEVER
Petroleum and Natural
Gas Engineer

1. TABLE OF CONTENTS

	<u>Page</u>
FOREWORD	ix
TABLE OF CONTENTS	xi
ABBREVIATIONS	xiii
LIST OF SYMBOLS	xvi
LIST OF TABLES	xvii
LIST OF FIGURES	xix
SUMMARY	xxi
ÖZET	xxiii
1. INTRODUCTION	1
1.1 Purpose and Scope of Thesis.....	2
2. MATHEMATICAL MODEL	5
2.1 Assumptions	5
2.2 Derivation of Continuity Equation	5
2.3 Integration of Darcy's Law	7
2.4 Initial and Outer Reservoir Boundary Conditions.....	8
2.5 Well (or Inner) Boundary Conditions	10
3. FINITE DIFFERENCE FORMULATION	13
3.1 Difference Equations.....	13
3.1.1 Reservoir difference equations.....	14
3.1.2 Well constraint equations.....	21
3.2 Method of Solutions	22
3.2.1 Newton's method.....	23
3.2.2 Implicit pressure - explicit saturation (IMPES) method	32
3.2.3 Example matrix structures	40
3.3 Matrix Problem Solver	43
4. VERIFICATION OF THE RESULTS	45
4.1 Case 1 - Injection.....	45
4.2 Case 2 - Injection - Falloff - Production	51
4.3 Case 3 - Injection.....	54
5. APPLICATIONS	59
5.1 Effect of Initial Time Step of Simulation.....	59
5.2 Analysis of Derivatives for Injection - Falloff - Production Periods	59
5.3 Effect of End Point Mobility Ratio	64
5.4 Effect of Skin in Injection - Falloff Tests	66
6. CONCLUSIONS AND RECOMMENDATIONS	75
REFERENCES	77
APPENDICES	79
APPENDIX A.1	81
CURRICULUM VITAE	91

ABBREVIATIONS

CMG	: Computer Modelling Group
FIMPS	: Fully Implicit Solution of Both Pressure and Saturation
IMEX	: Implicit-Explicit Black Oil Simulator
IMPES	: Implicit Pressure-Explicit Saturation

LIST OF SYMBOLS (NOMENCLATURE)

A	: Surface area, ft^2
B	: Formation volume factor, RB / STB
b	: Inverse of formation volume factor, STB / RB
c	: Compressibility, psi^{-1}
f	: Given function
f'	: Derivative of given function
J	: Jacobian matrix
k	: Permeability, md
M^*	: End point mobility ratio, unitless
Max	: Maksimum
\mathbf{n}	: Orthogonal vector
noi	: Number of open interval
P	: Pressure, psi
q	: Flow rate, STB / D
r	: Radial direction
S	: Saturation
s	: Skin factor
T	: Transmissibility, $md \times ft / cp$
t	: Time, day
V	: Constant related to fluid volume of a grid block, defined by Eqs. 3.65-3.68.
V_b	: Bulk volume, ft^3
z	: Vertical direction
z'	: Reference point

Greek Symbols

Δ	: Difference operator
δ	: Difference operator
ε	: Tolerance limit
ϕ	: Porosity
γ	: Fluid gradient, psi / ft
λ	: Mobility, md / cp
μ	: Viscosity, cp
v	: Velocity, ft / s
θ	: Thera direction

ρ	: Density, lbm / ft^3
ω	: Perturbation
∂	: Derivative operator

Subscripts

r	: Rock
i	: Index for radial direction
j	: Index for theta direction
k	: Index for vertical direction
m	: Fluid phase (oil or water)
o	: Oil
w	: Water

Superscripts

n	: Present time level
n+1	: Next time level
T	: Transpose

LIST OF TABLES

	<u>Page</u>
Table 4.1 : Data for Case 1 and Case 2	47
Table 4.2 : Data from Levitan's paper	55
Table 5.1 : Injection-falloff data	64

LIST OF FIGURES

	<u>Page</u>
Figure 3.1 : Control volume in $r - \theta - z$ coordinate system	16
Figure 3.2 : Grid structure for r direction using MacDonaldis - Coats method (taken from Gok, 2004).	39
Figure 3.3 : Schematic presentation of grids in $r - z$ direction.....	39
Figure 3.4 : Schematic presentation of grids in $r - \theta$ direction (taken from Gok, 2004).	40
Figure 3.5 : Simple reservoir structure in $r - \theta - z$ direction.....	41
Figure 3.6 : Jacobian matrix structure for the FIMPS (or Newton) method	42
Figure 3.7 : Matrix structure for IMPES method.....	43
Figure 4.1 : Pressure vs. time for Case 1 ($N_r = 200$)	48
Figure 4.2 : Saturation profile in r direction for Case 1 (end of injection) ($N_r = 200$)	48
Figure 4.3 : Bottom-hole pressures from IMPES method for different values of N_r for Case 1.	49
Figure 4.4 : Water saturation versus radial distance from IMPES method for different values of N_r for Case 1.	49
Figure 4.5 : Bottom-hole pressures from Newton method for different values of N_r for Case 1	50
Figure 4.6 : Water saturation versus radial distance from Newton method for different values of N_r for Case 1.	50
Figure 4.7 : Pressure vs. time plot for Case 2	52
Figure 4.8 : Saturation profile in r direction (end of fall off) for Case 2	52
Figure 4.9 : Saturation profile in r direction for Case 2 (end of production)	53
Figure 4.10 : Pressure vs. time plot for Case 2	54
Figure 4.11 : Rate normalized ΔP and $\Delta P'$ vs time (finite wellbore) for Levitan's (2003) case (Case 3).	56
Figure 4.12 : Rate normalized ΔP and $\Delta P'$ vs time (infinite wellbore) for Levitan's (2003) case (Case 3)	57
Figure 5.1 : Rate normalized ΔP and $\Delta P'$ vs time (infinite wellbore).....	60
Figure 5.2 : ΔP and $\Delta P'$ vs time for injection period	61
Figure 5.3 : ΔP and $\Delta P'$ vs time for falloff period.	62
Figure 5.4 : ΔP and $\Delta P'$ vs time for production period.....	63
Figure 5.5 : Total mobility change ($\mu_o = 3$ cp, $\mu_w = 0.5$)	63
Figure 5.6 : Comparison of favorable and unfavorable case for injection period. ...	65
Figure 5.7 : Comparison of favorable and unfavorable case for falloff period	66
Figure 5.8 : Effect of skin on injection period (favorable).	70
Figure 5.9 : Effect of skin on injection period (unfavorable).	70
Figure 5.10 : Effect of skin on falloff period (favorable).	72
Figure 5.11 : Effect of skin on falloff period (unfavorable).	73
Figure 5.12 : Effect of skin radius (unfavorable, $s = 4.75$).....	74

Figure A.1 : Effect of skin radius (unfavorable, $s = 4.75$)..... 85

NUMERICAL SIMULATION OF TWO-PHASE OIL AND WATER FLOW

SUMMARY

Two-phase oil and water flow is a subject of variety of applications in reservoir engineering processes. For instance, waterflooding is a widely used secondary recovery technique, based on the simultaneous flow of oil and water, to increase the oil production. In this technique, water is injected into an oil reservoir through injection wells to displace oil towards production wells. Another application of two-phase oil and water flow is encountered in injection/falloff pressure transient tests. Injection and fall-off tests are run for well and reservoir characterization purposes. Especially in offshore fields, due to environmental concerns, water injection into an oil reservoir is a common practice to test the wells for appraisal and development of the oil reservoirs. Flow rate and pressure data under two-phase flow of oil and water are stored and analyzed to obtain reservoir properties affecting the future development of the field.

Diffusivity equations describing the two-phase flow of oil and water in a porous and permeable medium are non-linear partial differential equations. Such equations are not easily solvable by analytical methods. However, there exist numerous articles that attempt to develop and present analytical solutions in the literature for the two-phase flow of oil and water under some restricted assumptions (e.g., homogenous reservoir). Analytical solutions may be easy and fast to apply, but may not well represent the oil and water flow because of their restrictive assumptions. On the other hand, numerical methods are more appealing to solve the oil and water phase flow for more general cases. Due to its generality, in this study, we consider numerical based methods (i.e., finite difference methods) to solve the diffusivity equation for oil-water flow and investigate the pressure and water saturation behaviors of a vertical well and reservoir for the cases where analytical solutions are not available.

A general discretized equation is derived for simulating two-phase water and oil flow in three-dimensional (3-D) r - θ - z cylindrical coordinate system using the finite difference method. Then, this general difference equation is solved by considering two different methods. The first method is based on a fully implicit solution of both pressure and saturation (FIMPS) using the Newton method, and the other method is based on a fully implicit solution of pressure and explicit solution of saturation, which is known as the IMPES method. Derivations for both methods are given in this study. The solutions generated from the simulators developed during the course of this work were compared and validated with the solutions generated from a commercial software CMG - IMEX. Moreover, we also validate the simulator for some benchmark cases taken from the papers presented in the literature.

Finally, some well-test applications are run with the simulator and pressure differences and their derivatives (diagnostic plots) are analyzed. This process is

achieved with the commercial well-test software ECRIN. Behaviour and effects of mechanical skin on diagnostic plots for injection and fall-off tests are discussed.

İKİ FAZLI PETROL VE SU AKIŞININ SAYISAL SİMÜLASYONU

ÖZET

İki fazlı petrol ve su akışı, pek çok rezervuar mühendisliği uygulamasının konusunu oluşturmaktadır. Örneğin, su ile petrolü öteleme, rezervuarlardan ek petrol üretimini arttırmak için en yaygın olarak kullanılan ikincil yöntemlerden biridir. En basit haliyle, su ile ötelemenin amacı enjeksiyon kuyuları aracılığıyla suyun rezervuara enjekte edilerek petrol üretim kuyularına ötelenmeye çalışılmasıdır. Bu nedenle su ile petrol öteleme sürecinin planlanabilmesi için iki fazlı petrol ve su akışının temellerinin bilinmesi gerekmektedir.

İki fazlı petrol ve su akışının uygulama bulduğu bir diğer alan ise enjeksiyon ve basınç-düşüm kuyu testleridir. Son yıllarda çevresel endişeler ve duyarlılık nedeniyle, özellikle açıkdenizde delinen kuyularda yapılan testler, rezervuara su basılarak yapılmaktadır. Bu tür testler, yüzeyde üretim ve toplama tankları gerektirmediğinden tercih edilmektedir. Bu testler, rezervuar öndeğerlendirmesi ve gelişimi hakkında önemli bilgiler sunar. Su ile öteleme projelerinde, enjeksiyon ve basınç düşüm testleri rezervuar karakterizasyonu için önemlidir. Debi ve basınç dataları kaydedilip analiz edilmekte ve sahanın gelişimini etkileyebilecek rezervuar parametreleri bulunmaya çalışılmaktadır.

Yaygın kullanımı ve önemi nedeniyle bu çalışmanın amacı, iki fazlı petrol ve su akışının temellerinin anlaşılması ve basınç-saturasyon davranışlarının gözlemlenebilmesi için tek kuyulu bir sistem için silindirik koordinat sisteminde simülatör geliştirmektir.

Gözenekli ve geçirgen bir ortamda iki fazlı petrol ve su akışını tanımlayan veya modelleyen difusivite denklemleri doğrusal olmayan kısmi diferansiyel denklemlerdir. Bu tür denklemler, bazı basitleştirici varsayımlar yapılmadıkça, analitik yöntemlerle çözümlenmesi zor olmaktadır. Literatürde su ve petrolün iki fazlı akışı için bazı sınırlayıcı varsayımlar altında (örneğin homojen rezervuar varsayımı gibi) geliştirilmiş bir çok analitik çözüm bulunmaktadır. Analitik çözümler uygulanması kolay ve hızlı olmakla beraber içerdiği kısıtlayıcı varsayımlar nedeniyle, çok amaçlı genel bir kullanıma uygun değildirler. Buna karşın, daha genel olduğu ve sınırlayıcı varsayımların kullanımını gerektirmediğinden, sayısal yöntemler su ve petrol akış problemlerini çözmek için daha çok tercih edilmektedir. Bu nedenle, bu çalışmada sayısal tabanlı sonlu fark yöntemleri kullanarak iki fazlı petrol ve su akışını tanımlayan difusivite denklemleri çözülmüş ve analitik çözümlerin yetersiz kaldığı bazı durumlar için basınç ve su duymuşluk dağılımlarının davranışı incelenmiştir.

Çalışmada ilk önce matematiksel model belirlenmiş ve çalışma süresince uygulanacak varsayımlar verilmiştir. Gözenekli ortamda iki fazlı petrol ve su akışını tanımlayan difusivite denklemi kütle korunum yasası ve gözenekli ortamda hızı tanımlayan Darcy denklemi kullanılarak türetilmiştir. Türetilen difusivite denklemi üç boyutlu r-Q-z silindirik koordinat sisteminde iki fazlı su-petrol akışı simülasyonu için sonlu farklar yöntemi kullanılarak çözülmüştür ve genel fark denklemleri türetilmiştir. Daha sonra fark denklemleri iki farklı yöntemle çözülmüştür ve bu yöntemlere göre türetimler bu çalışmada verilmiştir.

Çalışmada uygulanan yöntemlerden birincisi hem basıncın hem de doymuşluğun Newton yöntemiyle kapalı olarak çözüldüğü, Tümüyle Kapalı Basınç ve Doymuşluk (TKBD) olarak da isimlendirilen yöntemdir. Yöntemde genel fark denklemleri tekrar düzenlenerek petrol, su ve kuyu kalıcı (residual) denklemleri bulunmuştur. Bulunan denklemler kullanılarak Jacobian matrisi oluşturulmuş ve matris içindeki türevler nümerik yöntemle hesaplanmıştır. Newton prosedürüne göre matris vektör problemi çözümlenerek kuyu dibi basıncı, gridlerdeki basınç ve su saturasyonu değerleri hesaplanmıştır.

İkinci olarak, basıncın kapalı, doymuşluğun açık olarak çözüldüğü, Kapalı Basınç-Açık Doymuşluk (KBAD) olarak da isimlendirilen sayısal çözümleme yöntemi uygulanmıştır. Bu yöntemde ise petrol ve su genel fark denklemleri birleştirilerek basınç denklemi oluşturulmuştur. Kuyu denklemi ve basınç denklemi kullanılarak kuyu dibi basıncı ve gridlerdeki basınç değerleri kapalı olarak hesaplanmıştır. Bulunan basınç değerleri su denkleminde yerine konularak gridlerdeki su saturasyonu açık olarak hesaplanmıştır.

Çalışmada silindirik koordinat sisteminde gridler r yönünde MacDonaldis and Coat yöntemi uygulanarak oluşturulmuştur. Yöntem sayesinde değişimin en fazla olduğu kuyu dibinde daha küçük gridler kullanılırken kuyudan uzaklaştıkça grid büyüklükleri artmaktadır. Q ve z yönünde ise eşit aralıklı gridler kullanılmıştır.

Grid sınırlarındaki geçirgenlikler harmonik ortalama kullanılarak hesaplanmıştır. Görelî geçirgenlik grid merkezlerinde Power-Law model kullanılarak hesaplanmıştır. Grid sınırlarında ise akış yönüne (upstreaming) göre belirlenmiştir. Akış yüksek basınçlı ortamdaki düşük basınçlı ortama doğru olacağından, iki grid sınırındaki görelî geçirgenlik değeri, bu iki gridin merkezlerindeki basınç değerlerinin karşılaştırılmasıyla bulunmuştur. Petrol ve su formasyon hacim faktörü ve gözenekliliğin basıncın bir fonksiyonu olduğu varsayılmış ve grid sınırlarındaki değerleri aritmetik ortalama kullanılarak hesaplanmıştır. Yukarıda bahsedilen parametrelerin grid ve rezervuar sınırlarında hesaplanması Appendix – A’ da detaylı olarak verilmiştir.

Geliştirilen simülatörde logaritmik olarak artan zaman aralıkları kullanılmıştır. Bu şekilde değişimin fazla olduğu erken zamanlarda küçük zaman aralıkları kullanılmıştır. Artan zaman ile değişimin azalması daha büyük zaman aralıklarını kullanımına izin vermektedir. Bu nedenle logaritmik olarak artan zaman aralıkları kullanmak toplam çözüm süresini kısaltmasından dolayı avantaj sağlamaktadır.

Çözüm için uygulanan iki farklı yöntem için ortaya çıkacak matris yapıları basit bir rezervuar sisteminin gridlere ayrılmasıyla gösterilmiştir. Oluşan matris yapılarının seyrek matris (sparse matrix) olması nedeniyle depolama (storage) ve uzun çözüm süreleri problemlerinden kurtulmak amacıyla Yale Üniversite'sinde geliştirilen çözüm paketi kullanılmıştır. Bu çözüm paketi sadece matris içindeki sıfır olmayan elementleri depolamakta ve kendi içindeki özel algoritmayı kullanarak matrisin bütün elemanlarını depolayan çözüm yöntemlerine göre çok daha kısa sürede çözüm yapabilmektedir.

Tümüyle Kapalı Basınç ve Doymuşluk ve Kapalı Basınç-Açık Doymuşluk yöntemlerini kullanan simülatörün doğruluğu ticari bir yazılım olan CMG - IMEX ile kontrol edilmiştir. Ayrıca, geliştirilen simülatörün çözümleri, literatürde sunulan makalelerden alınan baz durumlara ait çözümler ile de test edilmiştir. Üç farklı durum için yapılan bu testlerle, geliştirilen simülatörün doğruluğu hem basınç hemde saturasyon için çizilen grafiklerle gösterilmiştir.

Kontrol aşamasında Kapalı Basınç-Açık Doymuşluk yöntemi kullanılırken uygun grid yapısı kullanılmadığında saturasyonun açık olarak çözülmesinden dolayı karşılaşılabilecek stabilite problemi bir örnekle gösterilmiştir.

Simülatörün doğruluğu test edildikten sonra son olarak literatürde bulunan bazı örnek kuyu-testi verileri kullanılarak simülatör çalıştırılmış ve basınç farkı-basınç farkı türevi grafikleri simülatörden alınan basınç sonuçlarına göre çizilmiştir. Bu işlem ticari bir yazılım olan ECRİN programıyla yapılmıştır. Farklı parametrelerin etkileri simülatör kullanılarak incelenmiştir.

Çalışmada ilk olarak simülasyonun başlangıç zamanının basınç farkı türevi üzerine etkisi gösterilmiştir. Daha sonra enjeksiyon ve basınç düşüm periyodlarının basınç farkı-basınç farkı türevi davranışları incelenmiş ve literatürden yapılan araştırmaya göre radyal akış periyodlarının türev değerlerinin sayısal olarak nasıl bulunacağı gösterilmiştir. Sonrasında sınır noktalar göz önüne alınarak bulunan mobilite oranının basınç farkı-basınç farkı türevi davranışları üzerine etkileri hem enjeksiyon hemde basınç düşüm periyodları için ayrı ayrı incelenmiştir.

Son olarak zar etkisi Hawkins formülasyonu kullanılarak simülatöre uygulanmış ve zar etkisinin basınç farkı-basınç farkı türevi grafigine etkileri enjeksiyon ve basınç düşüm periyodları için incelenmiş ve elde edilen sonuçlar tartışılmıştır. Ayrıca, Hawkins formülasyonundaki parametrelerden biri olan zar etkisi yarıçapının basınç farkı-basınç farkı türevi davranışını nasıl değiştirdiği farklı zar etkisi yapıçapı değerleri seçilerek enjeksiyon periyodu için gösterilmiştir.

Çalışma sonuçların ve önerilerin verilmesiyle sonlandırılmıştır.

1. INTRODUCTION

Two-phase oil and water flow finds variety of applications in reservoir engineering. For instance, waterflooding is a widely used secondary recovery technique, based on the simultaneous flow of oil and water, to increase the oil production. Once water is injected to reservoir, oil is swept and displaced towards the production wells. The design of this process in the field and the performance predictions of additional oil production via this process require the fundamental understanding and the solution of two-phase oil and water flow in a porous and a permeable medium (Craig 1971, Willhite 1986).

Another application of two-phase oil and water flow is for transient formation and well tests involving injection and falloff periods. Injection and fall-off tests are run for well and reservoir characterization purposes. Due to recent environmental concerns regarding the handling of fluids to be produced at the surface in production tests, water injection into an oil reservoir, especially in offshore where there is abundance of water, is a common practice to test the wells for appraisal and development of the oil reservoirs. The pressure and rate data collected under two-phase flow of oil and water are stored and analyzed to obtain reservoir properties affecting the future performance and development of the reservoir. Over the last 30 years, there is an increased interest in developing analytical and numerical solutions for the two-phase oil and water flow problems in porous and permeable media. For example, Abbaszadeh and Kamal (1989) investigated the pressure transient testing of water injection wells by considering analytical approach solving the diffusivity equations for oil and water. Bratvold and Horne (1990) presented procedures to interpret injection and falloff test data following cold water injection into a hot-oil reservoir. Levitan and Michael (2003) developed a semi-analytical solution for the variable rate injection and falloff tests in homogeneous single-layer reservoirs. Peres et al. (2006) provided analytical solutions for analyzing the falloff tests following injection tests. Amina (2007) provided a comprehensive investigation of injection and falloff testing of vertical, limited-entry, and horizontal wells and developed

analytical solutions for the analysis of such well tests. Chen (2007) investigated the in-situ determination of oil-water relative permeability curves from injection and falloff tests.

Unlike the diffusivity equation for describing the single-phase liquid oil or water flow, the diffusivity equations describing the two-phase flow of oil and water in a porous and permeable medium are non-linear partial differential equations. Such equations are not easily solvable by analytical methods. As stated and cited above, there exist several articles that attempt to develop and present analytical solutions in the literature for the two-phase flow of oil and water under some restricted assumptions (e.g., homogenous reservoir). Analytical solutions may be easy and fast to apply, but may not well represent the oil and water flow because of their restrictive assumptions. On the other hand, numerical methods are more appealing to solve the oil and water phase flow under more general cases. Hence, in this study, we consider numerical based methods (i.e., finite difference methods) to solve the diffusivity equation for oil-water flow and investigate the pressure and water saturation behaviors of a vertical well and reservoir for the cases where analytical solutions are not available.

1.1 Purpose and the Scope of Thesis

The main purpose of this study is to develop a general single-well simulator to simulate pressure and saturation behavior of water and oil two-phase three-dimensional flow in a 3-D cylindrical reservoir. The simulator can treat the reservoir with homogeneous or heterogeneous porosity and isotropic or anisotropic permeability fields. Another objective is to study the behavior of injection and falloff tests by constructing diagnostic plots for the interpretation of injection and falloff periods using the pressure and pressure-derivative results of the developed simulator.

In the second chapter, considering both oil and water, with the integration of Darcy's law, the diffusivity equations, which are non-linear partial differential equations, for describing two phase flow of oil and water, will be derived. In Chapter III, we consider the solutions of these non-linear partial differential equations with the appropriate initial and boundary conditions by using two different numerical methods based on the finite difference technique; fully implicit pressure and saturation (FIMPS) and implicit pressure and explicit saturation methods (IMPES).

In Chapter IV, the solutions generated from the simulators developed during the course of this study were compared and validated with the solutions generated from a commercial software IMEX-CMG. Moreover, the solutions from our simulators are also validated with the solutions for some benchmark cases taken from the papers presented in the literature. In Chapter V, we present some applications with the simulator. Here, we use the simulator as a forward (direct) solution tool to simulate various production, injection and falloff test cases to understand the pressure and saturation behavior of the reservoir. Although not considered in the thesis, the simulator developed can also be used as a tool for history matching or inverse problem applications to infer the reservoir properties from observed pressure and/or saturation data.

2. MATHEMATICAL MODEL

To solve the two-phase flow of oil and water in porous media we must first consider the mathematical model. In this chapter, diffusivity equation is derived and initial and boundary conditions are presented.

2.1 Assumptions

In this study, we assume immiscible flow of oil and water in a horizontal, isothermal reservoir. We will neglect the gravity and capillary effects. Reservoir is assumed to be in cylindrical shape with a vertical well located at the center. Oil and water viscosities are assumed to be constant with pressure. We also assume that the absolute permeability of the reservoir does not change with pressure. Of course, oil and water relative permeability change with water saturation. We assume that the power-law model for relative permeability of oil and water is applicable. Formation volume factors of oil and water as well as porosity are treated as a function of pressure. We treat oil and water as slightly compressible fluids.

2.2 Derivation of Continuity Equation

The continuity equation is a partial differential equation, which describes the flow in porous media. When considering a multiphase flow in a three-dimensional space, the continuity equation is derived by using the law of mass conservation. To derive the continuity equation, we must start from general mass (or material) balance equation given in the field units as follows:

$$-\iint_A (\rho_m \mathbf{v}_m \cdot \mathbf{n}) dA = \frac{1}{c_1} \iiint_V \frac{\partial(\phi \rho_m S_m)}{\partial t} dV \quad (2.1)$$

c_1 : constant and equals to 5.615

m : phase of fluid (oil or water)

ρ : density of the fluid

\mathbf{v} : velocity of the fluid

$(\rho\mathbf{v})$: mass-flux vector

ϕ : porosity

S : saturation

t : time

The integral in the left-hand side of Eq. 2.1 is performed over a surface area A perpendicular to flow direction, whereas the integral in the right-hand side of Eq. 2.1 is performed over the volume. The symbol “ \bullet ” in the left-hand side of Eq. 2.1 is used to represent the vector scalar product operation between the mass-flux vector $(\rho\mathbf{v}_m)$ and the unit normal outward vector \mathbf{n} to surface dA . We can relate the surface integral in Eq. 2.1 to a volume integral by using the divergence theorem (Kreyszig 1979). Then, we can rewrite the general material balance equation as follows.

$$-\iiint_V (\nabla \bullet \rho_m \mathbf{v}_m) dV = \frac{1}{c_1} \iiint_V \frac{\partial(\phi \rho_m S_m)}{\partial t} dV \quad (2.2)$$

or

$$-(\nabla \bullet \rho_m \mathbf{v}_m) = \frac{1}{c_1} \frac{\partial(\phi \rho_m S_m)}{\partial t} \quad (2.3)$$

where ∇ is the gradient operator or vector, and the solid dot represents the scalar product or divergence of the mass-flux. The divergence of of the mass-flux in cylindrical coordinate system is given by (Kreyszig 1979):

$$(\nabla \bullet \rho_m \mathbf{v}_m) = \frac{1}{r} \frac{\partial}{\partial r} (r \rho_m v_{m,r}) + \frac{1}{r} \frac{\partial}{\partial \theta} (\rho_m v_{m,\theta}) + \frac{\partial}{\partial z} (\rho_m v_{m,z}) \quad (2.4)$$

Where the subscripts r , θ , and z will be used for the directions in this study.

If we substitute Eq. 2.4 in Eq. 2.3,

$$-\left(\frac{1}{r} \frac{\partial}{\partial r}(r \rho_m v_{m,r}) + \frac{1}{r} \frac{\partial}{\partial \theta}(\rho_m v_{m,\theta}) + \frac{\partial}{\partial z}(\rho_m v_{m,z})\right) = \frac{1}{c_1} \frac{\partial(\phi \rho_m S_m)}{\partial t} \quad (2.5)$$

Eq. 2.5 is called the continuity equation for phase m in cylindrical coordinate system considering fluid flow in a three-dimensional space in the directions of r , θ and z .

2.3 Integration of Darcy's Law

Velocity term in Eq. 2.5 is defined by the well-known Darcy's Law. Velocities (assuming a horizontal reservoir) in $r-\theta-z$ coordinate system in field units are defined by.

$$v_{m,r} = -c_2 \frac{k_r k_{rm}}{B_m \mu_m} \frac{\partial P_m}{\partial r} \quad (2.6)$$

$$v_{m,\theta} = -c_2 \frac{k_\theta k_{rm}}{r B_m \mu_m} \frac{\partial P_m}{\partial \theta} \quad (2.7)$$

$$v_{m,z} = -c_2 \frac{k_z k_{rm}}{B_m \mu_m} \left(\frac{\partial P_m}{\partial z} - \gamma_m \frac{\partial z}{\partial z} \right) \quad (2.8)$$

c_2 : constant equal to 1.127×10^{-3}

P : pressure

B : formation volume factor

μ : viscosity

k_r : absolute permeability in the r direction

k_θ : absolute permeability in the θ direction

k_z : absolute permeability in the z direction

k_{rm} : relative permeability of phase m

γ_m : gradient of phase m

It is important to note that as we neglect the effect of capillary pressure, i.e., we take $P_c = P_{non-wetting} - P_{wetting} = 0$, water and oil phase pressures are the same and equal to P ($P_w = P_o = P$) and hence Eqs. 2.6 and 2.8 can be expressed in term of the pressure P .

Recall that, we assume gravity effect is negligible. Therefore, we rewrite velocity in the z direction as

$$v_{m,z} = -c_2 \frac{k_z k_{rm}}{B_m \mu_m} \frac{\partial P}{\partial z} \quad (2.9)$$

If we substitute Eq. 2.6, Eq. 2.7, and Eq. 2.9 into Eq. 2.5, we obtain

$$c_2 \left(\frac{1}{r} \frac{\partial}{\partial r} \left(r \rho_m \frac{k_r k_{rm}}{B_m \mu_m} \frac{\partial P}{\partial r} \right) + \frac{1}{r^2} \frac{\partial}{\partial \theta} \left(\rho_m \frac{k_\theta k_{rm}}{B_m \mu_m} \frac{\partial P}{\partial \theta} \right) + \frac{\partial}{\partial z} \left(\rho_m \frac{k_z k_{rm}}{B_m \mu_m} \frac{\partial P}{\partial z} \right) \right) = \frac{1}{c_1} \frac{\partial (\phi \rho_m S_m)}{\partial t} \quad (2.10)$$

Eq. 2.10 represents the diffusivity equation for phase m (oil or water) in cylindrical coordinate system considering flow in three-directions; r , θ , and z . In this study, we will approximate Eq. 2.10 by using two different finite difference formulation as to be discussed later.

A constraint that we need consider in solving Eq. 2.10 is that the sum of the oil and water phase saturations at any given time in the reservoir should add up to unity, i.e.,

$$S_o + S_w = 1 \quad (2.11)$$

where S_o is the oil saturation, and S_w is the water saturation at a given time and point in the reservoir.

2.4 Initial and Outer Reservoir Boundary Conditions

Eq. 2.10 is a three-dimensional second order partial differential equation involving two dependent variables P and saturation S_m . We will solve Eq. 2.10 subject to appropriately defined initial and boundary conditions to find a unique solution. Since we would like to solve both pressure (P) and one of the phase saturations (S_m , $m = w$ or o), we need two initial conditions:

$$P(r, \theta, z, t = 0) = P_i \quad (2.12)$$

$$S_m(r, \theta, z, t = 0) = S_{m,i} \quad (2.13)$$

P_i is the initial pressure assumed to be uniform, and $S_{m,i}$ is the initial saturation of phase m .

Regarding outer reservoir boundary conditions, we consider all no-flow (a Neumann type) boundary conditions at all reservoir outer boundaries. Hence, a no-flow outer boundary condition in the r direction at $r = r_e$ is considered and can be expressed as:

$$\left(r \frac{\partial P}{\partial r} \right)_{r=r_e, \theta, z} = 0 \quad 0 \leq \theta \leq 2\pi, 0 \leq z \leq h \quad (2.14)$$

Moreover, it is also assumed that no-flow top and bottom boundaries are present at $z = 0$ (bottom of the reservoir) and $z = h$ (top of the reservoir). Therefore, we can write no-flow top and bottom outer boundary conditions at z as follows.

$$\left(\frac{\partial P}{\partial z} \right)_{r, \theta, z=0} = 0 \quad r_w \leq r \leq r_e, 0 \leq \theta \leq 2\pi \quad (2.15)$$

$$\left(\frac{\partial P}{\partial z} \right)_{r, \theta, z=h} = 0 \quad r_w \leq r \leq r_e, 0 \leq \theta \leq 2\pi \quad (2.16)$$

In this study, we consider two different boundary conditions for the θ direction. The first consideration is for the case where the reservoir extends from 0 degrees (=0 radians) to 360 degrees (= 2π radians) in the θ direction; i.e., a full reservoir sector with $\theta = 360^\circ$. In this case we must consider the continuity of flux for phase m , pressure, and saturation at $\theta = 0^\circ$ and $\theta = 360^\circ$. Therefore, the appropriate boundary conditions for this case are expressed as follows:

$$\left(\frac{k_{rm} k_\theta}{\mu_m} \frac{\partial p}{\partial \theta} \right)_{r, \theta=0, z} = \left(\frac{k_{rm} k_\theta}{\mu_m} \frac{\partial p}{\partial \theta} \right)_{r, \theta=2\pi, z} \quad r_w \leq r \leq r_e, 0 \leq z \leq h \quad (2.17)$$

$$p(r, \theta = 0, z) = p(r, \theta = 2\pi, z) \quad r_w \leq r \leq r_e, 0 \leq z \leq h \quad (2.18)$$

$$S_m(r, \theta = 0, z) = S_m(r, \theta = 2\pi, z) \quad r_w \leq r \leq r_e, 0 \leq z \leq h \quad (2.19)$$

The second consideration is for the case where the reservoir extends from $\theta = \theta_b$ to $\theta = \theta_e$, where θ_e , is less than 360 degrees and greater than θ_b . This consideration is useful for simulating pressure and saturation behavior of wedge-shaped reservoirs with no-flow boundary conditions in the θ direction. So, the appropriate no-flow boundary conditions for this case in the θ direction are expressed as:

$$\left(\frac{\partial P}{\partial \theta} \right)_{r, \theta = \theta_b, z} = 0 \quad r_w \leq r \leq r_e, 0 \leq z \leq h \quad (2.20)$$

$$\left(\frac{\partial P}{\partial \theta} \right)_{r, \theta = \theta_e, z} = 0 \quad r_w \leq r \leq r_e, 0 \leq z \leq h \quad (2.21)$$

2.5 Well (or Inner) Boundary Conditions

In this study, we will solve Eq. 2.10 subject to a specified water injection rate or total (oil and water) production rate history at the well. We ignore the wellbore storage effects for simplicity. This assumption would be realistic if the gauge is placed to middle of the open interval and/or if the downhole shut-in is operational during buildups and falloffs.

In the case where we specify the total production rate as the inner boundary condition, we use the following well constraint equation:

$$q_{surface} = c_2 \int_{\theta = \theta_b}^{\theta = \theta_e} \int_{z = h_1}^{z = h_2} \left(\left(\frac{k_r k_{rw}}{B_w \mu_w} + \frac{k_r k_{ro}}{B_o \mu_o} \right) r \frac{\partial P}{\partial r} \right)_{r=r_w, z, \theta} dz d\theta \quad (2.22)$$

The inner boundary condition given in Eq. 2.22 is general. It can be used for either a fully penetrating vertical well or a limited entry vertical well. In Eq. 2.22, h_1 and h_2 represent the beginning and ending points of the open interval measured positive from the bottom of the formation in the z direction. In the case where we consider a

fully penetrating well, we set $h_1 = 0$ and $h_2 = h$, where h is the total reservoir thickness. For the case where we model a limited-entry vertical well, it is convenient to rewrite Eq. 2.22 as

$$q_{surface} = c_2 \sum_{l=1}^{N_{top}} \int_{\theta=\theta_b}^{\theta=\theta_e} \int_{z=h_{1,l}}^{z=h_{2,l}} \left[k_r \left(\frac{k_{rw}}{\mu_w B_w} + \frac{k_{ro}}{\mu_o B_o} \right) r \frac{\partial P}{\partial r} \right]_{r=r_w, z, \theta} dz d\theta \quad (2.23)$$

where N_{top} represents the total number of open intervals, and $h_{1,l}$ and $h_{2,l}$ represents the beginning and ending points of the l th open interval in the z -direction. Note that Eq. 2.22 is quite general in the sense that it allows us to consider multiple open segments along the wellbore.

It is important to note that Eqs. 2.22 and 23 considers that the open interval extends from $\theta = \theta_b$ to $\theta = \theta_e$ in the θ direction. For a full sector reservoir, we set $\theta_b = 0$ and $\theta_e = 2\pi$. It is also worth noting that $q_{surface}$ in Eqs. 2.22 and 2.23 represents the specified total surface production rate (in STB/D) and is specified as positive, i.e., $q_{surface} > 0$.

For the case where we consider water injection at a specified surface rate, then we use the following equation as the well constraint equation:

$$q_w = c_2 \int_{\theta=\theta_b}^{\theta=\theta_e} \int_{z=h_1}^{z=h_2} \left(\frac{k_r k_{rw}}{\mu_w B_w} r \frac{\partial P}{\partial r} \right)_{r=r_w, z, \theta} dz d\theta \quad (2.24)$$

For a fully penetrating well and a full sector reservoir, we set $\theta_b = 0$ and $\theta_e = 2\pi$, $h_1 = 0$ and $h_2 = h$ in Eq. 2.24. Similarly, for a limited-entry vertical well with a specified water injection rate, the appropriate well constraint equation is given by:

$$q_w = c_2 \sum_{l=1}^{N_{top}} \int_{\theta=\theta_b}^{\theta=\theta_e} \int_{z=h_{1,l}}^{z=h_{2,l}} \left(\frac{k_r k_{rw}}{\mu_w B_w} r \frac{\partial P}{\partial r} \right)_{r=r_w, z, \theta} dz d\theta \quad (2.25)$$

It is worth noting that q_w in Eqs. 2.24 and 2.25 represents the specified surface water injection rate (in STB/D) and is specified as negative, i.e., $q_w < 0$.

For simulating a buildup period following a production period or a falloff period following an injection period, we simply set $q_{surface} = 0$ in Eqs. 2.22 and 2.23 and $q_w = 0$ in Eqs. 2.24 and 2.25.

3. FINITE DIFFERENCE FORMULATION

In numerical solution approach, partial differential equations are converted to algebraic set of nonlinear equations by using finite difference methods and then this set of equations are solved by direct or iterative techniques. Therefore, finite difference methods plays a central role for the solution of differential equations, especially boundary value problems.

3.1 Difference Equations

Three basic finite difference methods are given as follows.

- Forward Difference
- Backward Difference
- Central Difference

And their formulation for the first derivative of any function $f(x_0)$ are given as follows, respectively.

$$f'(x_0) = \frac{f(x_0 + \Delta x) - f(x_0)}{\Delta x} \quad (3.1)$$

$$f'(x_0) = \frac{f(x_0) - f(x_0 - \Delta x)}{\Delta x} \quad (3.2)$$

$$f'(x_0) = \frac{f(x_0 + \Delta x) - f(x_0 - \Delta x)}{2\Delta x} \quad (3.3)$$

For simplicity, the following notations will be used for the differences.

$$f'(x_0) = \frac{f_{i+1} - f_i}{\Delta x} \quad \text{Forward} \quad (3.4)$$

$$f'(x_0) = \frac{f_i - f_{i-1}}{\Delta x} \quad \text{Backward} \quad (3.5)$$

$$f'(x_0) = \frac{f_{i+1} - f_{i-1}}{2\Delta x} \quad \text{Central} \quad (3.6)$$

3.1.1 Reservoir difference equation

In Chapter 2, the derivation of the general continuity equation for immiscible multiphase flow has been presented. Since it is a nonlinear partial differential equation, the continuity equation must be solved by using analytical or numerical solution methods. In this study, we will derive the numerical solution for two-phase flow of oil and water in $r - \theta - z$ directions.

Let's recall the general material balance equation given in Eq. 2.1.

$$-\iint_S (\rho_m v_m \cdot \mathbf{n}) dS = \frac{1}{c_1} \iiint_V \frac{\partial(\phi \rho_m S_m)}{\partial t} dV \quad (3.7)$$

As is well known, the formation volume factor for a phase m is defined by.

$$B_m = \frac{V_m}{V_{m,sc}} \quad (3.8)$$

B_m : formation volume factor for phase m

V_m : volume of phase m at reservoir conditions

$V_{m,sc}$: volume of phase m at standard conditions

We can also write formation volume factor in the form of density as.

$$B_m = \frac{\rho_m}{\rho_{m,sc}} \quad (3.9)$$

ρ_m : density of phase m at reservoir conditions

$\rho_{m,sc}$: density of phase m at standard conditions

If we substitute Eq. 3.9 in material balance equation given in Eq. 3.7 we obtain the following equation.

$$-\iint_A \left(\frac{\mathbf{v}_m \cdot \mathbf{n}}{B_m} \right) dA = \frac{1}{c_1} \iiint_V \frac{\partial}{\partial t} \left(\frac{\phi S_m}{B_m} \right) dV \quad (3.10)$$

Now, we express Eq. 3.10 on control volume as shown in **Fig. 3.1**. Note that when using a numerical method based on a finite difference, we divide the reservoir into gridblocks. So the control volume shown in Fig. 3.1 can be considered as the gridblock with the indices (i,j,k) , having a bulk volume of $V_{b,i,j,k}$, where i , j , and k represent the indices for the r , θ , and z directions, respectively.

Let us consider the accumulation term or time derivative term in right hand side of Eq. 3.10. Multiplying and dividing by the bulk volume $V_{b,i,j,k}$, we can rewrite Eq. 3.10 as follows.

$$\frac{1}{c_1} \iiint_V \frac{\partial}{\partial t} \left(\frac{\phi S_m}{B_m} \right) dV = \frac{V_{b,i,j,k}}{c_1} \frac{\partial}{\partial t} \left(\frac{1}{V_{b,i,j,k}} \iiint_{V_{i,j,k}} \left(\frac{\phi S_m}{B_m} \right)_{i,j,k} dV \right) \quad (3.11)$$

$$V_{b,i,j,k} = \frac{1}{2} \left(r_{i+\frac{1}{2}}^2 - r_{i-\frac{1}{2}}^2 \right) \Delta \theta_j \Delta z_k \quad (3.12)$$

Using the definition of volumetric average, we can write,

$$\frac{V_{b,i,j,k}}{c_1} \frac{\partial}{\partial t} \left(\frac{1}{V_{b,i,j,k}} \iiint_{V_{i,j,k}} \left(\frac{\phi S_m}{B_m} \right)_{i,j,k} dV \right) = \frac{V_{b,i,j,k}}{c_1} \frac{\partial}{\partial t} \left(\frac{\phi S_m}{B_m} \right)_{i,j,k} \quad (3.13)$$

In Chapter 2, the continuity equation was derived using divergence theorem and a diffusivity equation was obtained in the form of partial differential equation. Of course, we could directly start by differencing the diffusivity equation given by Eq. 2.10 in the form of a partial differential equation. However, for convenience, we will start directly from Eq. 3.10 to derive our finite difference equations. Both approaches yield the same difference equations.

As it is clear from Fig. 3.1, there are six faces on the control volume. Therefore, we need to find six surface areas and break the integral in Eq. 3.10 into six and apply surface integral on each face. The surface areas for selected control volume are as follow.

Face at $r_{i-\frac{1}{2}}$ with area $A_1 \rightarrow \mathbf{n}(-1,0,0) \rightarrow A_1 = r_{i-\frac{1}{2}} \Delta\theta_j \Delta z_k$

Face at $r_{i+\frac{1}{2}}$ with area $A_2 \rightarrow \mathbf{n}(1,0,0) \rightarrow A_2 = r_{i+\frac{1}{2}} \Delta\theta_j \Delta z_k$

Face at $\theta_{i-\frac{1}{2}}$ with area $A_3 \rightarrow \mathbf{n}(0,-1,0) \rightarrow A_3 = \Delta r_i \Delta z_k$

Face at $\theta_{i+\frac{1}{2}}$ with area $A_4 \rightarrow \mathbf{n}(0,1,0) \rightarrow A_4 = \Delta r_i \Delta z_k$

Face at $z_{i-\frac{1}{2}}$ with area $A_5 \rightarrow \mathbf{n}(0,0,-1) \rightarrow A_5 = \frac{1}{2} \left(r_{i+\frac{1}{2}}^2 - r_{i-\frac{1}{2}}^2 \right) \Delta\theta_j$

Face at $z_{i+\frac{1}{2}}$ with area $A_6 \rightarrow \mathbf{n}(0,0,1) \rightarrow A_6 = \frac{1}{2} \left(r_{i+\frac{1}{2}}^2 - r_{i-\frac{1}{2}}^2 \right) \Delta\theta_j$

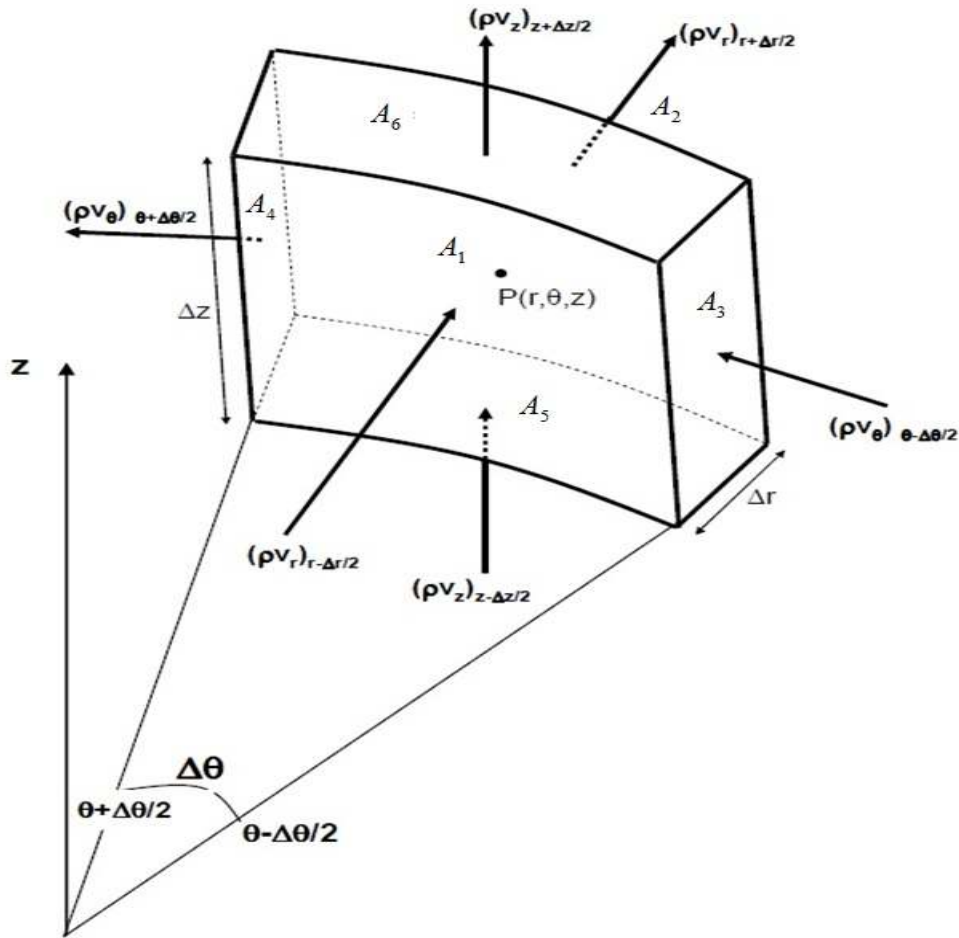


Figure 3.1 : Control volume in $r - \theta - z$ coordinate system

If we take the surface integral for six faces, we can write the surface term given in Eq. 3.10 as follows.

$$\begin{aligned}
& - \int_{z_{k-\frac{1}{2}}}^{z_{k+\frac{1}{2}}} \int_{\theta_{j-\frac{1}{2}}}^{\theta_{j+\frac{1}{2}}} \left(\frac{\mathbf{v}_{m,r}}{B_m} \right)_{i-\frac{1}{2},j,k} dA_1 + \int_{z_{k-\frac{1}{2}}}^{z_{k+\frac{1}{2}}} \int_{\theta_{j-\frac{1}{2}}}^{\theta_{j+\frac{1}{2}}} \left(\frac{\mathbf{v}_{m,r}}{B_m} \right)_{i+\frac{1}{2},j,k} dA_2 \\
& - \int_{z_{k-\frac{1}{2}}}^{z_{k+\frac{1}{2}}} \int_{r_{j-\frac{1}{2}}}^{r_{j+\frac{1}{2}}} \left(\frac{\mathbf{v}_{m,\theta}}{B_m} \right)_{i,j-\frac{1}{2},k} dA_3 + \int_{z_{k-\frac{1}{2}}}^{z_{k+\frac{1}{2}}} \int_{r_{j-\frac{1}{2}}}^{r_{j+\frac{1}{2}}} \left(\frac{\mathbf{v}_{m,\theta}}{B_m} \right)_{i,j+\frac{1}{2},k} dA_4 \\
& - \int_{\theta_{k-\frac{1}{2}}}^{\theta_{k+\frac{1}{2}}} \int_{r_{j-\frac{1}{2}}}^{r_{j+\frac{1}{2}}} \left(\frac{\mathbf{v}_{m,z}}{B_m} \right)_{i,j,k-\frac{1}{2}} dA_5 + \int_{\theta_{k-\frac{1}{2}}}^{\theta_{k+\frac{1}{2}}} \int_{r_{j-\frac{1}{2}}}^{r_{j+\frac{1}{2}}} \left(\frac{\mathbf{v}_{m,z}}{B_m} \right)_{i,j,k+\frac{1}{2}} dA_6 = - \sum_{l=1}^6 \iint_{S_l} \left(\frac{\mathbf{v}_m \cdot \mathbf{n}}{B_m} \right) dA
\end{aligned} \tag{3.14}$$

Substituting velocity definitions given in Chapter 2 (Eqs. 2.6, 2.7, and 2.8) into Eq. 3.14 and solving the integral, one can obtain the following equations:

$$\begin{aligned}
\int_{z_{k-\frac{1}{2}}}^{z_{k+\frac{1}{2}}} \int_{\theta_{j-\frac{1}{2}}}^{\theta_{j+\frac{1}{2}}} \left(\frac{\mathbf{v}_{m,r}}{B_m} \right)_{i-\frac{1}{2},j,k} dA_1 &= -c_2 \int_{z_{k-\frac{1}{2}}}^{z_{k+\frac{1}{2}}} \int_{\theta_{j-\frac{1}{2}}}^{\theta_{j+\frac{1}{2}}} \left(\frac{k_r k_{rm}}{B_m \mu_m} \frac{\partial P}{\partial r} \right)_{i-\frac{1}{2},j,k} r_{i-\frac{1}{2}} d\theta dz \\
&= -c_2 \left(\frac{k_r k_{rm}}{B_m \mu_m} \frac{\partial P}{\partial r} \right)_{i-\frac{1}{2},j,k} r_{i-\frac{1}{2}} \Delta\theta_j \Delta z_k
\end{aligned} \tag{3.15}$$

$$\begin{aligned}
\int_{z_{k-\frac{1}{2}}}^{z_{k+\frac{1}{2}}} \int_{\theta_{j-\frac{1}{2}}}^{\theta_{j+\frac{1}{2}}} \left(\frac{\mathbf{v}_{m,r}}{B_m} \right)_{i+\frac{1}{2},j,k} dA_2 &= c_2 \int_{z_{k-\frac{1}{2}}}^{z_{k+\frac{1}{2}}} \int_{\theta_{j-\frac{1}{2}}}^{\theta_{j+\frac{1}{2}}} \left(\frac{k_r k_{rm}}{B_m \mu_m} \frac{\partial P}{\partial r} \right)_{i+\frac{1}{2},j,k} r_{i+\frac{1}{2}} d\theta dz \\
&= c_2 \left(\frac{k_{m,r}}{B_m \mu_m} \frac{\partial P}{\partial r} \right)_{i+\frac{1}{2},j,k} r_{i+\frac{1}{2}} \Delta\theta_j \Delta z_k
\end{aligned} \tag{3.16}$$

$$\begin{aligned}
\int_{z_{k-\frac{1}{2}}}^{z_{k+\frac{1}{2}}} \int_{r_{j-\frac{1}{2}}}^{r_{j+\frac{1}{2}}} \left(\frac{v_{m,\theta}}{B_m} \right)_{i,j-\frac{1}{2},k} dA_3 &= \int_{z_{k-\frac{1}{2}}}^{z_{k+\frac{1}{2}}} \int_{r_{j-\frac{1}{2}}}^{r_{j+\frac{1}{2}}} \left(\frac{v_{m,\theta}}{B_m} \right)_{i,j-\frac{1}{2},k} drdz \\
&= -c_2 \int_{z_{k-\frac{1}{2}}}^{z_{k+\frac{1}{2}}} \int_{r_{j-\frac{1}{2}}}^{r_{j+\frac{1}{2}}} \frac{1}{r} \left(\frac{k_\theta k_{rm}}{B_m \mu_m} \frac{\partial P}{\partial \theta} \right)_{i,j-\frac{1}{2},k} drdz \\
&= -c_2 \left(\frac{k_\theta k_{rm}}{B_m \mu_m} \frac{\partial P}{\partial \theta} \right)_{i,j-\frac{1}{2},k} \ln \left(\frac{r_{i+\frac{1}{2}}}{r_{i-\frac{1}{2}}} \right) \Delta z_k
\end{aligned} \tag{3.17}$$

$$\begin{aligned}
\int_{z_{k-\frac{1}{2}}}^{z_{k+\frac{1}{2}}} \int_{r_{j-\frac{1}{2}}}^{r_{j+\frac{1}{2}}} \left(\frac{v_{m,\theta}}{B_m} \right)_{i,j+\frac{1}{2},k} dA_4 &= \int_{z_{k-\frac{1}{2}}}^{z_{k+\frac{1}{2}}} \int_{r_{j-\frac{1}{2}}}^{r_{j+\frac{1}{2}}} \left(\frac{v_{m,\theta}}{B_m} \right)_{i,j+\frac{1}{2},k} drdz \\
&= c_2 \int_{z_{k-\frac{1}{2}}}^{z_{k+\frac{1}{2}}} \int_{r_{j-\frac{1}{2}}}^{r_{j+\frac{1}{2}}} \frac{1}{r} \left(\frac{k_\theta k_{rm}}{B_m \mu_m} \frac{\partial P}{\partial \theta} \right)_{i,j+\frac{1}{2},k} drdz \\
&= c_2 \left(\frac{k_\theta k_{rm}}{B_m \mu_m} \frac{\partial P}{\partial \theta} \right)_{i,j+\frac{1}{2},k} \ln \left(\frac{r_{i+\frac{1}{2}}}{r_{i-\frac{1}{2}}} \right) \Delta z_k
\end{aligned} \tag{3.18}$$

$$\int_{\theta_{k-\frac{1}{2}}}^{\theta_{k+\frac{1}{2}}} \int_{r_{j-\frac{1}{2}}}^{r_{j+\frac{1}{2}}} \left(\frac{v_{m,z}}{B_m} \right)_{i,j,k-\frac{1}{2}} dA_5 = -\frac{c_2 \Delta \theta_j}{2} \left(r_{i+\frac{1}{2}}^2 - r_{i-\frac{1}{2}}^2 \right) \left(\frac{k_z k_{rm}}{B_m \mu_m} \frac{\partial P}{\partial z} \right)_{i,j,k-\frac{1}{2}} \tag{3.19}$$

$$\int_{\theta_{k-\frac{1}{2}}}^{\theta_{k+\frac{1}{2}}} \int_{r_{j-\frac{1}{2}}}^{r_{j+\frac{1}{2}}} \left(\frac{v_{m,z}}{B_m} \right)_{i,j,k+\frac{1}{2}} dA_6 = \frac{c_2 \Delta \theta_j}{2} \left(r_{i+\frac{1}{2}}^2 - r_{i-\frac{1}{2}}^2 \right) \left(\frac{k_z k_{rm}}{B_m \mu_m} \frac{\partial P}{\partial z} \right)_{i,j,k+\frac{1}{2}} \tag{3.20}$$

Using the approximated integral expressions given by Eqs. 3.15-3.20 and the accumulation term given by Eq. 3.13, we can rewrite Eq. 3.10 as:

$$\begin{aligned}
& c_2 \Delta \theta_j \Delta z_k \left[\left(\frac{k_r k_{rm}}{B_m \mu_m} r \frac{\partial P}{\partial r} \right)_{i+\frac{1}{2},j,k} - \left(\frac{k_r k_{rm}}{B_m \mu_m} r \frac{\partial P}{\partial r} \right)_{i-\frac{1}{2},j,k} \right] \\
& + c_2 \ln \left(\frac{r_{i+\frac{1}{2}}}{r_{i-\frac{1}{2}}} \right) \Delta z_k \left[\left(\frac{k_\theta k_{rm}}{B_m \mu_m} \frac{\partial P}{\partial \theta} \right)_{i,j+\frac{1}{2},k} - \left(\frac{k_\theta k_{rm}}{B_m \mu_m} \frac{\partial P}{\partial \theta} \right)_{i,j-\frac{1}{2},k} \right] \\
& + \frac{c_2 \Delta \theta_j}{2} \left(r_{i+\frac{1}{2}}^2 - r_{i-\frac{1}{2}}^2 \right) \left[\left(\frac{k_z k_{rm}}{B_m \mu_m} \frac{\partial P}{\partial z} \right)_{i,j,k+\frac{1}{2}} - \left(\frac{k_z k_{rm}}{B_m \mu_m} \frac{\partial P}{\partial z} \right)_{i,j,k-\frac{1}{2}} \right] = \frac{V_{b,i,j,k}}{c_1} \frac{\partial}{\partial t} \left(\frac{\phi S_m}{B_m} \right)_{i,j,k}
\end{aligned} \tag{3.21}$$

As mentioned earlier, finite difference approach is an important tool for the solution of partial derivatives. Hence, we can apply the convenient finite difference formula for the solution of position dependent partial derivatives.

$$\left(\frac{k_r k_{rm}}{B_m \mu_m} \frac{\partial P}{\partial r} \right)_{i+\frac{1}{2},j,k} = \left(\frac{b_m k_r k_{rm}}{\mu_m} \right)_{i+\frac{1}{2},j,k} \frac{P_{i+1,j,k} - P_{i,j,k}}{r_{i+1} - r_i} \tag{3.22}$$

$$\left(\frac{k_r k_{rm}}{B_m \mu_m} \frac{\partial P}{\partial r} \right)_{i-\frac{1}{2},j,k} = \left(\frac{b_m k_r k_{rm}}{\mu_m} \right)_{i-\frac{1}{2},j,k} \frac{P_{i,j,k} - P_{i-1,j,k}}{r_i - r_{i-1}} \tag{3.23}$$

$$\left(\frac{k_\theta k_{rm}}{B_m \mu_m} \frac{\partial P}{\partial \theta} \right)_{i,j+\frac{1}{2},k} = \left(\frac{b_m k_\theta k_{rm}}{\mu_m} \right)_{i,j+\frac{1}{2},k} \frac{P_{i,j+1,k} - P_{i,j,k}}{\theta_{j+1} - \theta_j} \tag{3.24}$$

$$\left(\frac{k_\theta k_{rm}}{B_m \mu_m} \frac{\partial P}{\partial \theta} \right)_{i,j-\frac{1}{2},k} = \left(\frac{b_m k_\theta k_{rm}}{\mu_m} \right)_{i,j-\frac{1}{2},k} \frac{P_{i,j,k} - P_{i,j-1,k}}{\theta_j - \theta_{j-1}} \tag{3.25}$$

$$\left(\frac{k_z k_{rm}}{B_m \mu_m} \frac{\partial P}{\partial z} \right)_{i,j,k+\frac{1}{2}} = \left(\frac{b_m k_z k_{rm}}{\mu_m} \right)_{i,j,k+\frac{1}{2}} \left(\frac{P_{i,j,k+1} - P_{i,j,k}}{z_{k+1} - z_k} \right) \tag{3.26}$$

$$\left(\frac{k_z k_{rm}}{B_m \mu_m} \frac{\partial P}{\partial z} \right)_{i,j,k-\frac{1}{2}} = \left(\frac{b_m k_z k_{rm}}{\mu_m} \right)_{i,j,k-\frac{1}{2}} \left(\frac{P_{i,j,k} - P_{i,j,k-1}}{z_k - z_{k-1}} \right) \tag{3.27}$$

$$b_m = \frac{1}{B_m} \quad (3.28)$$

As it is clear in Eq. 3.28, b_m is the inverse of formation volume factor. The reason to use inverse of formation volume factor is for the simplicity.

Furthermore, let us define the transmissibility terms as follows.

$$T_{m,r,i+\frac{1}{2},j,k} = c_2 r_{i+\frac{1}{2}} \frac{\Delta\theta_j \Delta z_k}{(r_{i+1} - r_i)} \left(\frac{b_m k_r k_{rm}}{\mu_m} \right)_{i+\frac{1}{2},j,k} \quad (3.29)$$

$$T_{m,r,i-\frac{1}{2},j,k} = c_2 r_{i-\frac{1}{2}} \frac{\Delta\theta_j \Delta z_k}{(r_i - r_{i-1})} \left(\frac{b_m k_r k_{rm}}{\mu_m} \right)_{i-\frac{1}{2},j,k} \quad (3.30)$$

$$T_{m,\theta,i,j+\frac{1}{2},k} = c_2 \ln \left(\frac{r_{i+\frac{1}{2}}}{r_{i-\frac{1}{2}}} \right) \frac{\Delta z_k}{(\theta_{j+1} - \theta_j)} \left(\frac{b_m k_\theta k_{rm}}{\mu_m} \right)_{i,j+\frac{1}{2},k} \quad (3.31)$$

$$T_{m,\theta,i,j-\frac{1}{2},k} = c_2 \ln \left(\frac{r_{i+\frac{1}{2}}}{r_{i-\frac{1}{2}}} \right) \frac{\Delta z_k}{(\theta_j - \theta_{j-1})} \left(\frac{b_m k_\theta k_{rm}}{\mu_m} \right)_{i,j-\frac{1}{2},k} \quad (3.32)$$

$$T_{m,z,i,j,k+\frac{1}{2}} = \frac{c_2}{2} \left(r_{i+\frac{1}{2}}^2 - r_{i-\frac{1}{2}}^2 \right) \frac{\Delta\theta_j}{(z_{k+1} - z_k)} \left(\frac{b_m k_z k_{rm}}{\mu_m} \right)_{i,j,k+\frac{1}{2}} \quad (3.33)$$

$$T_{m,z,i,j,k-\frac{1}{2}} = \frac{c_2}{2} \left(r_{i+\frac{1}{2}}^2 - r_{i-\frac{1}{2}}^2 \right) \frac{\Delta\theta_j}{(z_k - z_{k-1})} \left(\frac{b_m k_z k_{rm}}{\mu_m} \right)_{i,j,k-\frac{1}{2}} \quad (3.34)$$

Substituting the finite difference solutions from Eq. 3.22 to Eq. 3.27 and transmissibility definitions given from Eq. 3.29 to Eq. 3.34 in Eq. 3.20, we obtain the following equation.

$$\begin{aligned}
& T_{m,r,i+\frac{1}{2},j,k} (P_{i+1,j,k} - P_{i,j,k}) - T_{m,r,i-\frac{1}{2},j,k} (P_{i,j,k} - P_{i-1,j,k}) \\
& + T_{m,\theta,i,j+\frac{1}{2},k} (P_{i,j+1,k} - P_{i,j,k}) - T_{m,\theta,i,j-\frac{1}{2},k} (P_{i,j,k} - P_{i,j-1,k}) \\
& + T_{m,z,i,j,k+\frac{1}{2}} (P_{i,j,k+1} - P_{i,j,k}) - T_{m,z,i,j,k-\frac{1}{2}} (P_{i,j,k} - P_{i,j,k-1}) = \frac{V_{b,i,j,k}}{c_1} \frac{\partial}{\partial t} (b_m \phi S_m)_{i,j,k}
\end{aligned} \tag{3.35}$$

As it is clear, the finite difference approach must also be applied on the time dependent derivative in the accumulation term.

$$\frac{V_{b,i,j,k}}{c_1} \frac{\partial}{\partial t} (b_m \phi S_m)_{i,j,k} = \frac{V_{b,i,j,k}}{c_1 \Delta t^{n+1}} \left[(b_m \phi S_m)_{i,j,k}^{n+1} - (b_m \phi S_m)_{i,j,k}^n \right] \tag{3.36}$$

Here, the superscript n is used to represent the old time level, whereas the superscript $n+1$ represents the current time level at which the $(b_m \phi S_m)$ product in Eq. 3.36 is evaluated. In the right-hand side of Eq. 3.36, Δt^{n+1} denotes the time step taken from time t^n to t^{n+1} , i.e., $t^{n+1} = t^n + \Delta t^{n+1}$.

Finally, using Eq. 3.36 in Eq. 3.35, we can write general finite difference equation for each phase $m = o$ and w as:

$$\begin{aligned}
& T_{m,r,i+\frac{1}{2},j,k} (P_{i+1,j,k} - P_{i,j,k}) - T_{m,r,i-\frac{1}{2},j,k} (P_{i,j,k} - P_{i-1,j,k}) \\
& + T_{m,\theta,i,j+\frac{1}{2},k} (P_{i,j+1,k} - P_{i,j,k}) - T_{m,\theta,i,j-\frac{1}{2},k} (P_{i,j,k} - P_{i,j-1,k}) \\
& + T_{m,z,i,j,k+\frac{1}{2}} (P_{i,j,k+1} - P_{i,j,k}) - T_{m,z,i,j,k-\frac{1}{2}} (P_{i,j,k} - P_{i,j,k-1}) \\
& = \frac{V_{b,i,j,k}}{c_1 \Delta t^{n+1}} \left[(b_m \phi S_m)_{i,j,k}^{n+1} - (b_m \phi S_m)_{i,j,k}^n \right]
\end{aligned} \tag{3.37}$$

3.1.2 Well constraint equations

To be able to produce from or inject into the reservoir, we need well constraint equations where we specify the flow rate. As discussed in Chapter 2, in this study, we specify total flow rate at wellbore. Recall the inner boundary condition given in Eq. 2.23.

$$q_{surface} = c_2 \sum_{l=1}^{N_{top}} \int_{\theta=\theta_b}^{\theta=\theta_e} \int_{z=h_{1,j}}^{h_{2,l}} \left[k_r \left(\frac{k_{rw}}{\mu_w B_w} + \frac{k_{ro}}{\mu_o B_o} \right) r \frac{\partial P}{\partial r} \right]_{r=r_w, z, \theta} dz d\theta \quad (3.38)$$

Applying forward difference formulation at time t^{n+1} , we can approximate Eq. 3.38 with the following difference equation:

$$q_{surface}^{n+1} = \sum_{l=1}^{N_{top}} \sum_{k=n_{b,l}}^{n_{t,l}} \sum_{\theta=\theta_b}^{\theta=\theta_e} (T_{o,r,1/2,j,k} + T_{w,r,1/2,j,k}) (P_{1,j,k}^{n+1} - P_{0,j,k}^{n+1}) \quad (3.39)$$

$P_{1,j,k}$: pressure at $i = 1, \theta = j$, and $z = k$ grid

$P_{0,j,k}$: pressure at well or can also be represented as P_{wf}^{n+1} .

In Eq. 3.39, $n_{b,l}$ and $n_{t,l}$ represent the grid block numbers in the z-direction for bottom and top of the open interval l , respectively, for $l = 1, 2, \dots, N_{top}$. It is important to note that we consider an infinite conductivity wellbore so that wellbore pressure is uniform along the open interval in the z-direction.

In the case where we consider injection at a specified injection rate of q_w , we simply delete the oil transmissibility term in the left-hand side of Eq. 3.39 and replace q_{surf} by q_w so that we obtain the following equation:

$$q_w^{n+1} = \sum_{l=1}^{N_{top}} \sum_{k=n_{b,l}}^{n_{t,l}} \sum_{\theta=\theta_b}^{\theta=\theta_e} T_{w,r,1/2,j,k} (P_{1,j,k}^{n+1} - P_{0,j,k}^{n+1}) \quad (3.40)$$

The computation of the well oil and water transmissibility terms $T_{o,r,1/2,j,k}$ and $T_{w,r,1/2,j,k}$ in Eqs. 3.39 and 3.40 are discussed in Appendix A.

3.2 Method of Solutions

There exist different methods to solve reservoir finite difference equations (Eq. 3.37) together with the well constrain equations (Eq. 3.39 or 3.40). One of them is called Fully Implicit Pressure and Saturation Method (FIMPS) where pressure and saturation as well as their dependent variables are evaluated at time level t^{n+1} . Therefore, we need to rewrite general difference equation and well equation as follows.

$$\begin{aligned}
& T_{m,r,i+\frac{1}{2},j,k}^{n+1} \left(P_{i+1,j,k}^{n+1} - P_{i,j,k}^{n+1} \right) - T_{m,r,i-\frac{1}{2},j,k}^{n+1} \left(P_{i,j,k}^{n+1} - P_{i-1,j,k}^{n+1} \right) \\
& + T_{m,\theta,i,j+\frac{1}{2},k}^{n+1} \left(P_{i,j+1,k}^{n+1} - P_{i,j,k}^{n+1} \right) - T_{m,\theta,i,j-\frac{1}{2},k}^{n+1} \left(P_{i,j,k}^{n+1} - P_{i,j-1,k}^{n+1} \right) \\
& + T_{m,z,i,j,k+\frac{1}{2}}^{n+1} \left(P_{i,j,k+1}^{n+1} - P_{i,j,k}^{n+1} \right) - T_{m,z,i,j,k-\frac{1}{2}}^{n+1} \left(P_{i,j,k}^{n+1} - P_{i,j,k-1}^{n+1} \right) \\
& = \frac{V_{b,i,j,k}}{c_1 \Delta t^{n+1}} \left[(b_m \phi S_m)_{i,j,k}^{n+1} - (b_m \phi S_m)_{i,j,k}^n \right]
\end{aligned} \tag{3.41}$$

$$q_{surface}^{n+1} = \sum_{l=1}^{N_{top}} \sum_{k=n_{b,j}}^{n_{t,l}} \sum_{\theta=\theta_b}^{\theta=\theta_e} \left(T_{o,r,l/2,j,k} + T_{w,r,l/2,j,k} \right) \left(P_{1,j,k}^{n+1} - P_{0,j,k}^{n+1} \right) \tag{3.42}$$

3.2.1 Newton's method

Newton's Method, also known as Newton - Raphson Method, is a method for finding roots in numerical analysis and it describes an iterative procedure which is typically used in reservoir simulation. Suppose, we have n system of equations with N independent variables, i.e.,

$$\begin{aligned}
f_1 &= (x_1, x_2, \dots, x_N) = 0 \\
f_2 &= (x_1, x_2, \dots, x_N) = 0 \\
&\vdots \\
&\vdots \\
f_N &= (x_1, x_2, \dots, x_N) = 0
\end{aligned} \tag{3.43}$$

or, simply,

$$f_i = (x_1, x_2, \dots, x_N) = 0 \quad \text{for } i = 1, 2, \dots, N \tag{3.44}$$

We would like to solve x_l 's ($l = 1, 2, \dots, N$) so that $f_l = 0$ for each l .

Let

$$\mathbf{x} = (x_1, x_2, \dots, x_N) \tag{3.45}$$

Then, we can rewrite Eq. 3.42 as

$$f_i(\mathbf{x}) = 0 \quad 1 \leq i \leq N \quad (3.46)$$

We wish to find the solution

$$\hat{\mathbf{x}} = (\hat{\mathbf{x}}_1, \hat{\mathbf{x}}_2, \dots, \hat{\mathbf{x}}_N) \quad (3.47)$$

Such that

$$f_i(\hat{\mathbf{x}}) = 0 \quad 1 \leq i \leq N \quad (3.48)$$

If \mathbf{x} is close to $\hat{\mathbf{x}}$, the following Taylor series is approximately satisfied.

$$f_i(\hat{\mathbf{x}}) = f_i(\mathbf{x}) + \sum_{j=1}^N (\hat{\mathbf{x}}_j - \mathbf{x}_j) \frac{\partial f_i(\mathbf{x})}{\partial x_j} \quad i = 1, 2, \dots, N \quad (3.49)$$

Because $f_i(\hat{\mathbf{x}}) = 0$, we can rearrange Eq. 3.49 to obtain

$$\sum_{j=1}^N \frac{\partial f_i(\mathbf{x})}{\partial x_j} (\hat{\mathbf{x}}_j - \mathbf{x}_j) = -f_i(\mathbf{x}) \quad i = 1, 2, \dots, N \quad (3.50)$$

This suggests that the following iterative scheme with an iteration index n .

$$\sum_{j=1}^N \frac{\partial f_i(\mathbf{x}^n)}{\partial x_j} (\hat{\mathbf{x}}_j^{n+1} - \mathbf{x}_j^{n+1}) = -f_i(\mathbf{x}^n) \quad i = 1, 2, \dots, N \quad (3.51)$$

If we let δ_j^{n+1} denote

$$\delta_j^{n+1} = x_j^{n+1} - x_j^n \quad j = 1, 2, \dots, N \quad (3.52)$$

Then, we can rewrite Eq. 3.50 as

for $i = 1$

$$\frac{\partial f_1(\mathbf{x}^n)}{\partial x_1} \delta_1^{n+1} + \frac{\partial f_1(\mathbf{x}^n)}{\partial x_2} \delta_2^{n+1} + \dots + \frac{\partial f_1(\mathbf{x}^n)}{\partial x_N} \delta_N^{n+1} = -f_1(\mathbf{x}^n)$$

for $i = 2$

$$\frac{\partial f_2(\mathbf{x}^n)}{\partial x_1} \delta_1^{n+1} + \frac{\partial f_2(\mathbf{x}^n)}{\partial x_2} \delta_2^{n+1} + \dots + \frac{\partial f_2(\mathbf{x}^n)}{\partial x_N} \delta_N^{n+1} = -f_2(\mathbf{x}^n)$$

.

.

.

for $i = N$

$$\frac{\partial f_N(\mathbf{x}^n)}{\partial x_1} \delta_1^{n+1} + \frac{\partial f_N(\mathbf{x}^n)}{\partial x_2} \delta_2^{n+1} + \dots + \frac{\partial f_N(\mathbf{x}^n)}{\partial x_N} \delta_N^{n+1} = -f_N(\mathbf{x}^n)$$

(3.53)

Define the Jacobian matrix

$$\mathbf{J}(\mathbf{x}^n) = \begin{bmatrix} \frac{\partial f_1}{\partial x_1} & \frac{\partial f_1}{\partial x_2} & \dots & \dots & \frac{\partial f_1}{\partial x_N} \\ \frac{\partial f_2}{\partial x_1} & \frac{\partial f_2}{\partial x_2} & \dots & \dots & \frac{\partial f_2}{\partial x_N} \\ \dots & \dots & \dots & \dots & \dots \\ \frac{\partial f_N}{\partial x_1} & \frac{\partial f_N}{\partial x_2} & \dots & \dots & \frac{\partial f_N}{\partial x_N} \end{bmatrix} \quad (3.54)$$

Define

$$\boldsymbol{\delta}^{n+1} = \begin{bmatrix} \delta_1^{n+1} \\ \delta_2^{n+1} \\ \dots \\ \delta_N^{n+1} \end{bmatrix} \quad \mathbf{f}(\mathbf{x}^n) = \begin{bmatrix} f_1(\mathbf{x}^n) \\ f_2(\mathbf{x}^n) \\ \dots \\ f_N(\mathbf{x}^n) \end{bmatrix} \quad (3.55)$$

Then the system of equation given by Eq. 3.55 is

$$J(\mathbf{x}^n)\boldsymbol{\delta}^{n+1} = -\mathbf{f}(\mathbf{x}^n) \quad (3.56)$$

Newton's procedure can be described as :

Step (i) - Set $k = 0$, and guess $\mathbf{x}^0 = [x_1^0, x_2^0, \dots, x_N^0]^T$

Step (ii) - Form $J(\mathbf{x}^n)$ and $\mathbf{f}(\mathbf{x}^n)$

Step (iii) - Compute $\boldsymbol{\delta}^{n+1}$ from Eq. 3.56. Then propose a new iterate

$$\mathbf{x}^{n+1} = \mathbf{x}^n + \boldsymbol{\delta}^{n+1} \quad (3.57)$$

Check the following criterion for convergence:

$$\text{Max}_{1 \leq j \leq n} \left| \frac{x_j^{n+1} - x_j^n}{x_j^{n+1} + 10^{-13}} \right| \leq \varepsilon \quad (3.58)$$

If satisfied, accept \mathbf{x}^{n+1} as the solution and stop iterating.

Step (iv) - If Eq. 3.58 is not satisfied, set $n = n + 1$ and go to Step (ii).

This procedure will converge to $\hat{\mathbf{x}}$ provided

(i) - Inverse of Jacobian exists, i.e., \mathbf{J} is non - singular and \mathbf{J}^{-1} exists.

(ii) - $\frac{\partial^2 f_i}{\partial x_i \partial x_j}$ exist and are continuous in some neighborhood of $\hat{\mathbf{x}}$.

(iii) - \mathbf{x}^0 (initial guess) is sufficiently close to $\hat{\mathbf{x}}$.

Now, we apply the Newton's procedure to our difference equation given in Eq. 3.41.

As we deal with oil and water system, we write Eq. 3.41 for oil and water phases separately.

For oil (Eq. 3.41 with $m = o$) gives

$$\begin{aligned}
& T_{o,r,i+\frac{1}{2},j,k}^{n+1} \left(P_{i+1,j,k}^{n+1} - P_{i,j,k}^{n+1} \right) - T_{o,r,i-\frac{1}{2},j,k}^{n+1} \left(P_{i,j,k}^{n+1} - P_{i-1,j,k}^{n+1} \right) \\
& + T_{o,\theta,i,j+\frac{1}{2},k}^{n+1} \left(P_{i,j+1,k}^{n+1} - P_{i,j,k}^{n+1} \right) - T_{o,\theta,i,j-\frac{1}{2},k}^{n+1} \left(P_{i,j,k}^{n+1} - P_{i,j-1,k}^{n+1} \right) \\
& + T_{o,z,i,j,k+\frac{1}{2}}^{n+1} \left(P_{i,j,k+1}^{n+1} - P_{i,j,k}^{n+1} \right) - T_{o,z,i,j,k-\frac{1}{2}}^{n+1} \left(P_{i,j,k}^{n+1} - P_{i,j,k-1}^{n+1} \right) \\
& = \frac{V_{b,i,j,k}}{c_1 \Delta t^{n+1}} \left[(b_o \phi S_o)_{i,j,k}^{n+1} - (b_o \phi S_o)_{i,j,k}^n \right]
\end{aligned} \tag{3.59}$$

For water (Eq. 3.41 with $m = w$) gives

$$\begin{aligned}
& T_{w,r,i+\frac{1}{2},j,k}^{n+1} \left(P_{i+1,j,k}^{n+1} - P_{w,i,j,k}^{n+1} \right) - T_{w,r,i-\frac{1}{2},j,k}^{n+1} \left(P_{i,j,k}^{n+1} - P_{i-1,j,k}^{n+1} \right) \\
& + T_{w,\theta,i,j+\frac{1}{2},k}^{n+1} \left(P_{i,j+1,k}^{n+1} - P_{i,j,k}^{n+1} \right) - T_{w,\theta,i,j-\frac{1}{2},k}^{n+1} \left(P_{i,j,k}^{n+1} - P_{i,j-1,k}^{n+1} \right) \\
& + T_{w,z,i,j,k+\frac{1}{2}}^{n+1} \left(P_{i,j,k+1}^{n+1} - P_{i,j,k}^{n+1} \right) - T_{w,z,i,j,k-\frac{1}{2}}^{n+1} \left(P_{i,j,k}^{n+1} - P_{i,j,k-1}^{n+1} \right) \\
& = \frac{V_{b,i,j,k}}{c_1 \Delta t^{n+1}} \left[(b_w \phi S_w)_{i,j,k}^{n+1} - (b_w \phi S_w)_{i,j,k}^n \right]
\end{aligned} \tag{3.60}$$

Using requirement given in Eq. 2.11, that is, $S_o + S_w = 1$, we can rewrite oil equation as

$$\begin{aligned}
& T_{o,r,i+\frac{1}{2},j,k}^{n+1} \left(P_{i+1,j,k}^{n+1} - P_{i,j,k}^{n+1} \right) - T_{o,r,i-\frac{1}{2},j,k}^{n+1} \left(P_{i,j,k}^{n+1} - P_{i-1,j,k}^{n+1} \right) \\
& + T_{o,\theta,i,j+\frac{1}{2},k}^{n+1} \left(P_{i,j+1,k}^{n+1} - P_{i,j,k}^{n+1} \right) - T_{o,\theta,i,j-\frac{1}{2},k}^{n+1} \left(P_{i,j,k}^{n+1} - P_{i,j-1,k}^{n+1} \right) \\
& + T_{o,z,i,j,k+\frac{1}{2}}^{n+1} \left(P_{i,j,k+1}^{n+1} - P_{i,j,k}^{n+1} \right) - T_{o,z,i,j,k-\frac{1}{2}}^{n+1} \left(P_{i,j,k}^{n+1} - P_{i,j,k-1}^{n+1} \right) \\
& = \frac{V_{b,i,j,k}}{c_1 \Delta t^{n+1}} \left[(b_o \phi (1 - S_w))_{i,j,k}^{n+1} - (b_o \phi (1 - S_w))_{i,j,k}^n \right]
\end{aligned} \tag{3.61}$$

Rearranging oil equation given by Eq. 3.61 gives

$$\begin{aligned}
& T_{o,r,i-\frac{1}{2},j,k}^{n+1} P_{o,i-1,j,k}^{n+1} - T_{o,\theta,i,j-\frac{1}{2},k}^{n+1} P_{o,i,j-1,k}^{n+1} - T_{o,z,i,j,k-\frac{1}{2}}^{n+1} P_{o,i,j,k-1}^{n+1} \\
& - \left(\begin{array}{c} T_{o,r,i-\frac{1}{2},j,k}^{n+1} + T_{o,r,i+\frac{1}{2},j,k}^{n+1} + T_{o,\theta,i,j-\frac{1}{2},k}^{n+1} \\ + T_{o,\theta,i,j+\frac{1}{2},k}^{n+1} + T_{o,z,i,j,k-\frac{1}{2}}^{n+1} + T_{o,z,i,j,k+\frac{1}{2}}^{n+1} \end{array} \right) P_{o,i,j,k}^{n+1} + T_{o,r,i+\frac{1}{2},j,k}^{n+1} P_{o,i+1,j,k}^{n+1} \\
& + T_{o,\theta,i,j+\frac{1}{2},k}^{n+1} P_{o,i,j+1,k}^{n+1} + T_{o,z,i,j,k+\frac{1}{2}}^{n+1} P_{o,i,j,k+1}^{n+1} \\
& = \frac{V_{b,i,j,k}}{c_1 \Delta t^{n+1}} \left[(b_o \phi (1 - S_w))_{i,j,k}^{n+1} - (b_o \phi (1 - S_w))_{i,j,k}^n \right]
\end{aligned} \tag{3.62}$$

Rearranging water equation given by Eq. 3.60 gives

$$\begin{aligned}
& T_{w,r,i-\frac{1}{2},j,k}^{n+1} P_{i-1,j,k}^{n+1} - T_{w,\theta,i,j-\frac{1}{2},k}^{n+1} P_{i,j-1,k}^{n+1} - T_{w,z,i,j,k-\frac{1}{2}}^{n+1} P_{i,j,k-1}^{n+1} \\
& - \left(\begin{array}{c} T_{w,r,i-\frac{1}{2},j,k}^{n+1} + T_{w,r,i+\frac{1}{2},j,k}^{n+1} + T_{w,\theta,i,j-\frac{1}{2},k}^{n+1} \\ + T_{w,\theta,i,j+\frac{1}{2},k}^{n+1} + T_{w,z,i,j,k-\frac{1}{2}}^{n+1} + T_{w,z,i,j,k+\frac{1}{2}}^{n+1} \end{array} \right) P_{i,j,k}^{n+1} + T_{w,r,i+\frac{1}{2},j,k}^{n+1} P_{i+1,j,k}^{n+1} \\
& + T_{w,\theta,i,j+\frac{1}{2},k}^{n+1} P_{i,j+1,k}^{n+1} + T_{w,z,i,j,k+\frac{1}{2}}^{n+1} P_{i,j,k+1}^{n+1} \\
& = \frac{V_{b,i,j,k}}{c_1 \Delta t^{n+1}} \left[(b_w \phi S_w)_{i,j,k}^{n+1} - (b_w \phi S_w)_{i,j,k}^n \right]
\end{aligned} \tag{3.63}$$

For simplicity, let us define,

$$V_{o,i,j,k}^{n+1} = \frac{V_{b,i,j,k}}{c_1 \Delta t^{n+1}} (b_o \phi (1 - S_w))_{i,j,k}^{n+1} \tag{3.64}$$

$$V_{o,i,j,k}^n = \frac{V_{b,i,j,k}}{c_1 \Delta t^{n+1}} (b_o \phi (1 - S_w))_{i,j,k}^n \tag{3.65}$$

$$V_{w,i,j,k}^{n+1} = \frac{V_{b,i,j,k}}{c_1 \Delta t^{n+1}} (b_w \phi S_w)_{i,j,k}^{n+1} \tag{3.66}$$

$$V_{w,i,j,k}^n = \frac{V_{b,i,j,k}}{c_1 \Delta t^{n+1}} (b_w \phi S_w)_{i,j,k}^n \tag{3.67}$$

Then, we can form the oil and water residuals, respectively, to be used in Newton's method by the rearrangements of Eqs. 3.62 and 3.63 as follows:

$$\begin{aligned}
f_{o,i,j,k}^{n+1} &= T_{o,r,i-\frac{1}{2},j,k}^{n+1} P_{i-1,j,k}^{n+1} - T_{o,\theta,i,j-\frac{1}{2},k}^{n+1} P_{i,j-1,k}^{n+1} - T_{o,z,i,j,k-\frac{1}{2}}^{n+1} P_{i,j,k-1}^{n+1} \\
&\quad - \left(\begin{array}{ccc} T_{o,r,i-\frac{1}{2},j,k}^{n+1} & + T_{o,r,i+\frac{1}{2},j,k}^{n+1} & + T_{o,\theta,i,j-\frac{1}{2},k}^{n+1} \\ + T_{o,\theta,i,j+\frac{1}{2},k}^{n+1} & + T_{o,z,i,j,k-\frac{1}{2}}^{n+1} & + T_{o,z,i,j,k+\frac{1}{2}}^{n+1} \end{array} \right) P_{i,j,k}^{n+1} + T_{o,r,i+\frac{1}{2},j,k}^{n+1} P_{i+1,j,k}^{n+1} \\
&\quad + T_{o,\theta,i,j+\frac{1}{2},k}^{n+1} P_{i,j+1,k}^{n+1} + T_{o,z,i,j,k+\frac{1}{2}}^{n+1} P_{i,j,k+1}^{n+1} - V_{o,i,j,k}^{n+1} + V_{o,i,j,k}^n = 0
\end{aligned} \tag{3.68}$$

$$\begin{aligned}
f_{w,i,j,k}^{n+1} &= T_{w,r,i-\frac{1}{2},j,k}^{n+1} P_{i-1,j,k}^{n+1} - T_{w,\theta,i,j-\frac{1}{2},k}^{n+1} P_{i,j-1,k}^{n+1} - T_{w,z,i,j,k-\frac{1}{2}}^{n+1} P_{i,j,k-1}^{n+1} \\
&\quad - \left(\begin{array}{ccc} T_{w,r,i-\frac{1}{2},j,k}^{n+1} & + T_{w,r,i+\frac{1}{2},j,k}^{n+1} & + T_{w,\theta,i,j-\frac{1}{2},k}^{n+1} \\ + T_{w,\theta,i,j+\frac{1}{2},k}^{n+1} & + T_{w,z,i,j,k-\frac{1}{2}}^{n+1} & + T_{w,z,i,j,k+\frac{1}{2}}^{n+1} \end{array} \right) P_{i,j,k}^{n+1} + T_{w,r,i+\frac{1}{2},j,k}^{n+1} P_{i+1,j,k}^{n+1} \\
&\quad + T_{w,\theta,i,j+\frac{1}{2},k}^{n+1} P_{i,j+1,k}^{n+1} + T_{w,z,i,j,k+\frac{1}{2}}^{n+1} P_{i,j,k+1}^{n+1} - V_{w,i,j,k}^{n+1} + V_{w,i,j,k}^n = 0
\end{aligned} \tag{3.69}$$

for $i=1,2,\dots,N_r$, $j=1,2,\dots,N_\theta$, and $k=1,2,\dots,N_z$, where N_r , N_θ , and N_z denote the number of gridblocks in the r , θ , and z directions, respectively. Note that we can express the residual equations by using a block index (say l) instead of coordinate indices (i,j,k) . For example, if we order the difference equation first in the r -direction (i), then in the θ direction (j), and then in the z -direction (k), then we can define a block index l by the formula:

$$l = i + (j-1) \times N_r + (k-1) \times N_r \times N_\theta \tag{3.70}$$

For $i=1,2,\dots,N_r$, $j=1,2,\dots,N_\theta$, and $k=1,2,\dots,N_z$. Thus, we can express the residual (difference) equations given for oil and water ($f_{o,i,j,k}$ and $f_{w,i,j,k}$) and the unknowns $P_{i,j,k}$ and $S_{w,i,j,k}$ in terms of the grid block index l instead of the coordinate index (i,j,k) . Note that l goes from 1 to N_{gb} , where N_{gb} ($=N_r \times N_\theta \times N_z$) is the total number of grid blocks. In our ordering scheme, $l=1$ represents the grid block having coordinate indices ($i=1, j=1$, and $k=1$) (i.e., the bottommost grid block adjacent to the wellbore). Our ordering scheme is from the bottom to top in the z -direction, as will be illustrated later.

Pressure and water saturation are solved for each grid block from Eq. 3.68 and Eq. 3.69. Note that we solve water saturation and use Eq. 2.11 to find oil saturation. Of course, this is arbitrary and we could have expressed the right-hand side of Eqs. 3.62

and 3.63 in terms of oil saturation and solve the residual equations for oil saturation. Then use Eq. 2.11 to solve for the water saturation.

Using the residuals given by Eqs. 3.68 and 3.69, we can construct the Jacobian matrix to be used in Newton's method as by ordering as unknowns as pressure and water saturation using the grid block index. It should be noted that our first equation when forming the Jacobian matrix will be the well constraint equation and the reservoir residual equations for oil and water will respectively follow the well constraint residual equation. The unknowns are ordered as P_{wf}^{n+1} , P^{n+1} , and S_w^{n+1} .

$$\mathbf{J} = \begin{bmatrix}
 \frac{\partial f_{well}}{\partial P_{well}^{n+1}} & \frac{\partial f_{well}}{\partial P_1^{n+1}} & \frac{\partial f_{well}}{\partial S_{w,1}^{n+1}} & \frac{\partial f_{well}}{\partial P_2^{n+1}} & \frac{\partial f_{well}}{\partial S_{w,2}^{n+1}} & \cdot & \cdot & \cdot & \frac{\partial f_{well}}{\partial P_{N_{gb}}^{n+1}} & \frac{\partial f_{well}}{\partial S_{w,N_{gb}}^{n+1}} \\
 \frac{\partial f_{o,1}}{\partial P_{well}^{n+1}} & \frac{\partial f_{o,1}}{\partial P_1^{n+1}} & \frac{\partial f_{o,1}}{\partial S_{w,1}^{n+1}} & \frac{\partial f_{o,1}}{\partial P_2^{n+1}} & \frac{\partial f_{o,1}}{\partial S_{w,2}^{n+1}} & \cdot & \cdot & \cdot & \frac{\partial f_{o,1}}{\partial P_{N_{gb}}^{n+1}} & \frac{\partial f_{o,1}}{\partial S_{w,N_{gb}}^{n+1}} \\
 \frac{\partial f_{w,1}}{\partial P_{well}^{n+1}} & \frac{\partial f_{w,1}}{\partial P_1^{n+1}} & \frac{\partial f_{w,1}}{\partial S_{w,1}^{n+1}} & \frac{\partial f_{w,1}}{\partial P_2^{n+1}} & \frac{\partial f_{w,1}}{\partial S_{w,2}^{n+1}} & \cdot & \cdot & \cdot & \frac{\partial f_{w,1}}{\partial P_{N_{gb}}^{n+1}} & \frac{\partial f_{w,1}}{\partial S_{w,N_{gb}}^{n+1}} \\
 \frac{\partial f_{o,2}}{\partial P_{well}^{n+1}} & \frac{\partial f_{o,2}}{\partial P_1^{n+1}} & \frac{\partial f_{o,2}}{\partial S_{w,1}^{n+1}} & \frac{\partial f_{o,2}}{\partial P_2^{n+1}} & \frac{\partial f_{o,2}}{\partial S_{w,2}^{n+1}} & \cdot & \cdot & \cdot & \frac{\partial f_{o,2}}{\partial P_{N_{gb}}^{n+1}} & \frac{\partial f_{o,2}}{\partial S_{w,N_{gb}}^{n+1}} \\
 \frac{\partial f_{w,2}}{\partial P_{well}^{n+1}} & \frac{\partial f_{w,2}}{\partial P_1^{n+1}} & \frac{\partial f_{w,2}}{\partial P_1^{n+1}} & \frac{\partial f_{w,2}}{\partial P_2^{n+1}} & \frac{\partial f_{w,2}}{\partial S_{w,2}^{n+1}} & \cdot & \cdot & \cdot & \frac{\partial f_{w,2}}{\partial P_{N_{gb}}^{n+1}} & \frac{\partial f_{w,2}}{\partial S_{w,N_{gb}}^{n+1}} \\
 \cdot & \cdot & \cdot & \cdot & \cdot & \cdot & \cdot & \cdot & \cdot & \cdot \\
 \cdot & \cdot & \cdot & \cdot & \cdot & \cdot & \cdot & \cdot & \cdot & \cdot \\
 \cdot & \cdot & \cdot & \cdot & \cdot & \cdot & \cdot & \cdot & \cdot & \cdot \\
 \frac{\partial f_{o,N_{gb}}}{\partial P_{well}^{n+1}} & \frac{\partial f_{o,N_{gb}}}{\partial P_1^{n+1}} & \frac{\partial f_{o,N_{gb}}}{\partial S_{w,1}^{n+1}} & \frac{\partial f_{o,N_{gb}}}{\partial P_2^{n+1}} & \frac{\partial f_{o,N_{gb}}}{\partial S_{w,2}^{n+1}} & \cdot & \cdot & \cdot & \frac{\partial f_{o,N_{gb}}}{\partial P_{N_{gb}}^{n+1}} & \frac{\partial f_{o,N_{gb}}}{\partial S_{w,N_{gb}}^{n+1}} \\
 \frac{\partial f_{w,N_{gb}}}{\partial P_{well}^{n+1}} & \frac{\partial f_{w,N_{gb}}}{\partial P_1^{n+1}} & \frac{\partial f_{w,N_{gb}}}{\partial S_{w,1}^{n+1}} & \frac{\partial f_{w,N_{gb}}}{\partial P_2^{n+1}} & \frac{\partial f_{w,N_{gb}}}{\partial S_{w,2}^{n+1}} & \cdot & \cdot & \cdot & \frac{\partial f_{w,N_{gb}}}{\partial P_{N_{gb}}^{n+1}} & \frac{\partial f_{w,N_{gb}}}{\partial S_{w,N_{gb}}^{n+1}}
 \end{bmatrix} \quad (3.71)$$

and

$$\boldsymbol{\delta}^{n+1} = \begin{bmatrix} P_{well}^{n+1,k+1} - P_{well}^{n+1,k} \\ P_1^{n+1,k+1} - P_1^{n+1,k} \\ S_{w,1}^{n+1,k+1} - S_{w,1}^{n+1,k} \\ P_2^{n+1,k+1} - P_2^{n+1,k} \\ S_{w,2}^{n+1,k+1} - S_{w,2}^{n+1,k} \\ \vdots \\ \vdots \\ \vdots \\ P_{N_{gb}}^{n+1,k+1} - P_{N_{gb}}^{n+1,k} \\ S_{w,N_{gb}}^{n+1,k+1} - S_{w,N_{gb}}^{n+1,k} \end{bmatrix} \quad \mathbf{f}(\mathbf{P}^{n+1,k}) = \begin{bmatrix} f_{well}(\mathbf{P}^{n+1,k}) \\ f_{o,1}(\mathbf{P}^{n+1,k}) \\ f_{w,1}(\mathbf{P}^{n+1,k}) \\ f_{o,2}(\mathbf{P}^{n+1,k}) \\ f_{w,2}(\mathbf{P}^{n+1,k}) \\ \vdots \\ \vdots \\ \vdots \\ f_{o,N_{gb}}(\mathbf{P}^{n+1,k}) \\ f_{w,N_{gb}}(\mathbf{P}^{n+1,k}) \end{bmatrix} \quad (3.72)$$

where,

$$\mathbf{P}^{n+1,k} = \begin{bmatrix} P_{well}^{n+1,k} & P_1^{n+1,k} & P_2^{n+1,k} & \dots & P_{N_{gb}}^{n+1,k} \end{bmatrix}^T \quad (3.73)$$

Recall that we also need to integrate well equation given in Eq. 3.42 in the matrix as discussed later. So, the well residual equation to be used in the Newton method is obtained from the rearrangement of Eq. 39 or Eq. 40 depending on production or injection.

$$f_{well}^{n+1} = \sum_{l=1}^{N_{top}} \sum_{k=n_{b,l}}^{n_{t,l}} \sum_{\theta=\theta_b}^{\theta=\theta_e} (T_{o,r,l/2,j,k} + T_{w,r,l/2,j,k}) (P_{1,j,k}^{n+1} - P_{0,j,k}^{n+1}) - q_{surface}^{n+1} \quad (3.74)$$

$$f_{well}^{n+1} = \sum_{l=1}^{N_{top}} \sum_{k=n_{b,l}}^{n_{t,l}} \sum_{\theta=\theta_b}^{\theta=\theta_e} T_{w,r,l/2,j,k} (P_{1,j,k}^{n+1} - P_{0,j,k}^{n+1}) - q_w^{n+1} \quad (3.75)$$

Other details for the treatment of transmissibility and volume terms in the reservoir and well residual equations are given in Appendix A. We use a finite difference perturbation method to calculate the derivatives in Jacobian matrix (see Appendix A for details).

3.2.2 Implicit pressure – explicit saturation (IMPES) method

Another method to solve non-linear difference equations for the two-phase oil and water system is called the Implicit Pressure-Explicit Saturation (IMPES) method. The method is widely used since it decreases the size of matrix. However, it may also suffer from the stability problem because the saturation is solved explicitly in this method.

Recall the general finite difference equation for oil and water given Eq. 3.41.

$$\begin{aligned}
& T_{m,r,i+\frac{1}{2},j,k}^{n+1} (P_{i+1,j,k}^{n+1} - P_{i,j,k}^{n+1}) - T_{m,r,i-\frac{1}{2},j,k}^{n+1} (P_{i,j,k}^{n+1} - P_{i-1,j,k}^{n+1}) \\
& + T_{m,\theta,i,j+\frac{1}{2},k}^{n+1} (P_{i,j+1,k}^{n+1} - P_{i,j,k}^{n+1}) - T_{m,\theta,i,j-\frac{1}{2},k}^{n+1} (P_{i,j,k}^{n+1} - P_{i,j-1,k}^{n+1}) \\
& + T_{m,z,i,j,k+\frac{1}{2}}^{n+1} (P_{i,j,k+1}^{n+1} - P_{i,j,k}^{n+1}) - T_{m,z,i,j,k-\frac{1}{2}}^{n+1} (P_{i,j,k}^{n+1} - P_{i,j,k-1}^{n+1}) \\
& = \frac{V_{b,i,j,k}}{c_1 \Delta t^{n+1}} \left[(b_m \phi S_m)_{i,j,k}^{n+1} - (b_m \phi S_m)_{i,j,k}^n \right]
\end{aligned} \tag{3.76}$$

Let us define difference operator as follows.

$$\Delta_t u_{i,j,k}^{n+1} = u_{i,j,k}^{n+1} - u_{i,j,k}^n \tag{3.77}$$

where u is any function of r, θ, z , and t so that

$$\frac{(\Delta_t u_{i,j,k}^{n+1})}{\Delta t^{n+1}} \approx \frac{\partial u}{\partial t}(r_i, \theta_j, z_k, t^{n+1}) \tag{3.78}$$

Using the definition of difference operator, we can write derivative term in accumulation term as

$$\Delta_t (b_m \phi S_m) = (b_m \phi S_m)_{i,j,k}^{n+1} - (b_m \phi S_m)_{i,j,k}^n \tag{3.79}$$

We expand Eq. 3.79 as follows.

$$\Delta_t (b_m \phi S_m) = (b_m \phi)_{i,j,k}^{n+1} \Delta_t S_m + S_{m,i,j,k}^n \left[b_{m,i,j,k}^{n+1} \left(\frac{\phi_{i,j,k}^{n+1} - \phi_{i,j,k}^n}{P_{i,j,k}^{n+1} - P_{i,j,k}^n} \right) \Delta_t P + \phi_{i,j,k}^n \left(\frac{b_{m,i,j,k}^{n+1} - b_{m,i,j,k}^n}{P_{i,j,k}^{n+1} - P_{i,j,k}^n} \right) \Delta_t P \right] \tag{3.80}$$

Substituting Eq. 3.80 in Eq. 3.76 gives

$$\begin{aligned}
& T_{m,r,i+\frac{1}{2},j,k}^{n+1} \left(P_{i+1,j,k}^{n+1} - P_{i,j,k}^{n+1} \right) - T_{m,r,i-\frac{1}{2},j,k}^{n+1} \left(P_{i,j,k}^{n+1} - P_{i-1,j,k}^{n+1} \right) \\
& + T_{m,\theta,i,j+\frac{1}{2},k}^{n+1} \left(P_{i,j+1,k}^{n+1} - P_{i,j,k}^{n+1} \right) - T_{m,\theta,i,j-\frac{1}{2},k}^{n+1} \left(P_{i,j,k}^{n+1} - P_{i,j-1,k}^{n+1} \right) \\
& + T_{m,z,i,j,k+\frac{1}{2}}^{n+1} \left(P_{i,j,k+1}^{n+1} - P_{i,j,k}^{n+1} \right) - T_{m,z,i,j,k-\frac{1}{2}}^{n+1} \left(P_{i,j,k}^{n+1} - P_{i,j,k-1}^{n+1} \right) \\
& = \frac{V_{b,i,j,k}}{c_1 \Delta t^{n+1}} \left[(b_m \phi)_{i,j,k}^{n+1} \Delta_t S_m + S_{m,i,j,k}^n \left[b_{m,i,j,k}^{n+1} \left(\frac{\phi_{i,j,k}^{n+1} - \phi_{i,j,k}^n}{P_{i,j,k}^{n+1} - P_{i,j,k}^n} \right) \Delta_t P \right. \right. \\
& \left. \left. + \phi_{i,j,k}^n \left(\frac{b_{m,i,j,k}^{n+1} - b_{m,i,j,k}^n}{P_{i,j,k}^{n+1} - P_{i,j,k}^n} \right) \Delta_t P \right] \right] \tag{3.81}
\end{aligned}$$

Applying the same derivation given from Eq. 3.59 to Eq. 3.64 on the surface term given in the left hand side of Eq. 3.81, one can find following equations for oil and water, respectively,

$$\begin{aligned}
& \left[T_{o,r,i-\frac{1}{2},j,k}^{n+1} P_{i-1,j,k}^{n+1} - T_{o,\theta,i,j-\frac{1}{2},k}^{n+1} P_{i,j-1,k}^{n+1} - T_{o,z,i,j,k-\frac{1}{2}}^{n+1} P_{i,j,k-1}^{n+1} \right. \\
& - \left. \left(T_{o,r,i-\frac{1}{2},j,k}^{n+1} + T_{o,r,i+\frac{1}{2},j,k}^{n+1} + T_{o,\theta,i,j-\frac{1}{2},k}^{n+1} \right) P_{i,j,k}^{n+1} + T_{o,r,i+\frac{1}{2},j,k}^{n+1} P_{i+1,j,k}^{n+1} \right. \\
& \left. + T_{o,\theta,i,j+\frac{1}{2},k}^{n+1} + T_{o,z,i,j,k-\frac{1}{2}}^{n+1} + T_{o,z,i,j,k+\frac{1}{2}}^{n+1} \right) P_{i,j,k}^{n+1} \\
& + T_{o,\theta,i,j+\frac{1}{2},k}^{n+1} P_{i,j+1,k}^{n+1} + T_{o,z,i,j,k+\frac{1}{2}}^{n+1} P_{i,j,k+1}^{n+1} \left. \right] \\
& = \frac{V_{b,i,j,k}}{c_1 \Delta t^{n+1}} \left[(b_o \phi)_{i,j,k}^{n+1} \Delta_t S_o + S_{o,i,j,k}^n \left[b_{o,i,j,k}^{n+1} \left(\frac{\phi_{i,j,k}^{n+1} - \phi_{i,j,k}^n}{P_{i,j,k}^{n+1} - P_{i,j,k}^n} \right) \Delta_t P \right. \right. \\
& \left. \left. + \phi_{i,j,k}^n \left(\frac{b_{o,i,j,k}^{n+1} - b_{o,i,j,k}^n}{P_{i,j,k}^{n+1} - P_{i,j,k}^n} \right) \Delta_t P \right] \right] \tag{3.82}
\end{aligned}$$

$$\begin{aligned}
& \left[T_{w,r,i-\frac{1}{2},j,k}^{n+1} P_{i-1,j,k}^{n+1} - T_{w,\theta,i,j-\frac{1}{2},k}^{n+1} P_{i,j-1,k}^{n+1} - T_{w,z,i,j,k-\frac{1}{2}}^{n+1} P_{i,j,k-1}^{n+1} \right. \\
& - \left. \left(T_{w,r,i-\frac{1}{2},j,k}^{n+1} + T_{w,r,i+\frac{1}{2},j,k}^{n+1} + T_{w,\theta,i,j-\frac{1}{2},k}^{n+1} \right) P_{i,j,k}^{n+1} + T_{w,r,i+\frac{1}{2},j,k}^{n+1} P_{i+1,j,k}^{n+1} \right. \\
& \left. + T_{w,\theta,i,j+\frac{1}{2},k}^{n+1} + T_{w,z,i,j,k-\frac{1}{2}}^{n+1} + T_{w,z,i,j,k+\frac{1}{2}}^{n+1} \right) P_{i,j,k}^{n+1} \\
& + T_{w,\theta,i,j+\frac{1}{2},k}^{n+1} P_{i,j+1,k}^{n+1} + T_{w,z,i,j,k+\frac{1}{2}}^{n+1} P_{i,j,k+1}^{n+1} \left. \right] \\
& = \frac{V_{b,i,j,k}}{c_1 \Delta t^{n+1}} \left[(b_w \phi)_{i,j,k}^{n+1} \Delta_t S_w + S_{w,i,j,k}^n \left[b_{w,i,j,k}^{n+1} \left(\frac{\phi_{i,j,k}^{n+1} - \phi_{i,j,k}^n}{P_{i,j,k}^{n+1} - P_{i,j,k}^n} \right) \Delta_t P \right. \right. \\
& \left. \left. + \phi_{i,j,k}^n \left(\frac{b_{w,i,j,k}^{n+1} - b_{w,i,j,k}^n}{P_{i,j,k}^{n+1} - P_{i,j,k}^n} \right) \Delta_t P \right] \right] \tag{3.83}
\end{aligned}$$

Now, we can combine oil and water equation in single pressure equation which we will solve implicitly. To do so, we multiply oil equation (Eq. 3.82) by $1/b_{o,i,j,k}^{n+1}$ and water equation (Eq. 3.83) by $1/b_{w,i,j,k}^{n+1}$ and then add the resulting two equations to obtain:

$$\begin{aligned}
& \left(\frac{1}{b_{o,i,j,k}^{n+1}} T_{o,r,i-\frac{1}{2},j,k}^{n+1} + \frac{1}{b_{w,i,j,k}^{n+1}} T_{w,r,i-\frac{1}{2},j,k}^{n+1} \right) P_{i-1,j,k}^{n+1} - \left(\frac{1}{b_{o,i,j,k}^{n+1}} T_{o,\theta,i,j-\frac{1}{2},k}^{n+1} + \frac{1}{b_{w,i,j,k}^{n+1}} T_{w,\theta,i,j-\frac{1}{2},k}^{n+1} \right) P_{i,j-1,k}^{n+1} \\
& - \left(\frac{1}{b_{o,i,j,k}^{n+1}} T_{o,z,i,j,k-\frac{1}{2}}^{n+1} + \frac{1}{b_{w,i,j,k}^{n+1}} T_{w,z,i,j,k-\frac{1}{2}}^{n+1} \right) P_{i,j,k-1}^{n+1} \\
& - \left[\frac{1}{b_{o,i,j,k}^{n+1}} \left(\begin{array}{ccc} T_{o,r,i-\frac{1}{2},j,k}^{n+1} & + T_{o,r,i+\frac{1}{2},j,k}^{n+1} & + T_{o,\theta,i,j-\frac{1}{2},k}^{n+1} \\ + T_{o,\theta,i,j+\frac{1}{2},k}^{n+1} & + T_{o,z,i,j,k-\frac{1}{2}}^{n+1} & + T_{o,z,i,j,k+\frac{1}{2}}^{n+1} \end{array} \right) \right. \\
& \left. + \frac{1}{b_{w,i,j,k}^{n+1}} \left(\begin{array}{ccc} T_{w,r,i-\frac{1}{2},j,k}^{n+1} & + T_{w,r,i+\frac{1}{2},j,k}^{n+1} & + T_{w,\theta,i,j-\frac{1}{2},k}^{n+1} \\ + T_{w,\theta,i,j+\frac{1}{2},k}^{n+1} & + T_{w,z,i,j,k-\frac{1}{2}}^{n+1} & + T_{w,z,i,j,k+\frac{1}{2}}^{n+1} \end{array} \right) \right] P_{i,j,k}^{n+1} \\
& + \left(\frac{1}{b_{o,i,j,k}^{n+1}} T_{o,r,i+\frac{1}{2},j,k}^{n+1} + \frac{1}{b_{w,i,j,k}^{n+1}} T_{w,r,i+\frac{1}{2},j,k}^{n+1} \right) P_{i+1,j,k}^{n+1} + \left(\frac{1}{b_{o,i,j,k}^{n+1}} T_{o,\theta,i,j+\frac{1}{2},k}^{n+1} + \frac{1}{b_{w,i,j,k}^{n+1}} T_{w,\theta,i,j+\frac{1}{2},k}^{n+1} \right) P_{i,j+1,k}^{n+1} \\
& + \left(\frac{1}{b_{o,i,j,k}^{n+1}} T_{o,z,i,j,k+\frac{1}{2}}^{n+1} + \frac{1}{b_{w,i,j,k}^{n+1}} T_{w,z,i,j,k+\frac{1}{2}}^{n+1} \right) P_{i,j,k+1}^{n+1} \\
& = \frac{V_{b,i,j,k}}{c_1 \Delta t^{n+1}} \left[\begin{array}{l} (\phi)_{i,j,k}^{n+1} (\Delta_t S_o + \Delta_t S_w) + \left(\begin{array}{l} (S_{o,i,j,k}^n + S_{w,i,j,k}^n) \\ \left(\frac{\phi_{i,j,k}^{n+1} - \phi_{i,j,k}^n}{p_{i,j,k}^{n+1} - p_{i,j,k}^n} \right) \Delta_t P \end{array} \right) \\ + S_{o,i,j,k}^n \frac{\phi_{i,j,k}^n}{b_{o,i,j,k}^{n+1}} \left(\frac{b_{o,i,j,k}^{n+1} - b_{o,i,j,k}^n}{p_{i,j,k}^{n+1} - p_{i,j,k}^n} \right) \Delta_t P \\ + S_{w,i,j,k}^n \frac{\phi_{i,j,k}^n}{b_{w,i,j,k}^{n+1}} \left(\frac{b_{w,i,j,k}^{n+1} - b_{w,i,j,k}^n}{p_{i,j,k}^{n+1} - p_{i,j,k}^n} \right) \Delta_t P \end{array} \right]
\end{aligned} \tag{3.84}$$

Note that,

$$\begin{aligned}
& (\Delta_t S_o + \Delta_t S_w) = (S_{o,i,j,k}^{n+1} - S_{o,i,j,k}^n) + (S_{w,i,j,k}^{n+1} - S_{w,i,j,k}^n) \\
& = (S_{o,i,j,k}^{n+1} + S_{w,i,j,k}^{n+1}) - (S_{o,i,j,k}^n + S_{w,i,j,k}^n) = 1 - 1 = 0
\end{aligned} \tag{3.85}$$

For convenience, we define rock, oil and water isothermal compressibility as:

$$c_{r,i,j,k}^{n+1} = \frac{1}{\phi_{i,j,k}^n} \left(\frac{\phi_{i,j,k}^{n+1} - \phi_{i,j,k}^n}{p_{i,j,k}^{n+1} - p_{i,j,k}^n} \right) \quad (3.86)$$

$$c_{o,i,j,k}^{n+1} = \frac{1}{b_{o,i,j,k}^{n+1}} \left(\frac{b_{o,i,j,k}^{n+1} - b_{o,i,j,k}^n}{p_{i,j,k}^{n+1} - p_{i,j,k}^n} \right) \quad (3.87)$$

$$c_{w,i,j,k}^{n+1} = \frac{1}{b_{w,i,j,k}^{n+1}} \left(\frac{b_{w,i,j,k}^{n+1} - b_{w,i,j,k}^n}{p_{i,j,k}^{n+1} - p_{i,j,k}^n} \right) \quad (3.88)$$

Defining for simplicity,

$$\tilde{T}_{o,r,i\pm\frac{1}{2},j,k}^{n+1} = \frac{1}{b_{o,i,j,k}^{n+1}} T_{o,r,i\pm\frac{1}{2},j,k}^{n+1} \quad (3.89)$$

$$\tilde{T}_{w,r,i\pm\frac{1}{2},j,k}^{n+1} = \frac{1}{b_{w,i,j,k}^{n+1}} T_{w,r,i\pm\frac{1}{2},j,k}^{n+1} \quad (3.90)$$

$$\tilde{T}_{o,\theta,i,j\pm\frac{1}{2},k}^{n+1} = \frac{1}{b_{o,i,j,k}^{n+1}} T_{o,\theta,i,j\pm\frac{1}{2},k}^{n+1} \quad (3.91)$$

$$\tilde{T}_{w,\theta,i,j\pm\frac{1}{2},k}^{n+1} = \frac{1}{b_{w,i,j,k}^{n+1}} T_{w,\theta,i,j\pm\frac{1}{2},k}^{n+1} \quad (3.92)$$

$$\tilde{T}_{o,r,i,j,k\pm\frac{1}{2}}^{n+1} = \frac{1}{b_{o,i,j,k}^{n+1}} T_{o,r,i,j,k\pm\frac{1}{2}}^{n+1} \quad (3.93)$$

$$\tilde{T}_{w,z,i,j,k\pm\frac{1}{2}}^{n+1} = \frac{1}{b_{w,i,j,k}^{n+1}} T_{w,z,i,j,k\pm\frac{1}{2}}^{n+1} \quad (3.94)$$

Using the definitions given from Eq. 3.85 to Eq. 3.94, we can rewrite Eq. 3.84 as follows.

$$\begin{aligned}
& \left(\tilde{T}_{o,r,i-\frac{1}{2},j,k}^{n+1} + \tilde{T}_{w,r,i-\frac{1}{2},j,k}^{n+1} \right) P_{i-1,j,k}^{n+1} - \left(\tilde{T}_{o,\theta,i,j-\frac{1}{2},k}^{n+1} + \tilde{T}_{w,\theta,i,j-\frac{1}{2},k}^{n+1} \right) P_{i,j-1,k}^{n+1} \\
& - \left(\tilde{T}_{o,z,i,j,k-\frac{1}{2}}^{n+1} + \tilde{T}_{w,z,i,j,k-\frac{1}{2}}^{n+1} \right) P_{i,j,k-1}^{n+1} - \left(\begin{array}{c} \left(\tilde{T}_{o,r,i-\frac{1}{2},j,k}^{n+1} + \tilde{T}_{o,r,i+\frac{1}{2},j,k}^{n+1} + \tilde{T}_{o,\theta,i,j-\frac{1}{2},k}^{n+1} \right. \\ \left. + \tilde{T}_{o,\theta,i,j+\frac{1}{2},k}^{n+1} + \tilde{T}_{o,z,i,j,k-\frac{1}{2}}^{n+1} + \tilde{T}_{o,z,i,j,k+\frac{1}{2}}^{n+1} \right) \\ \left(\tilde{T}_{w,r,i-\frac{1}{2},j,k}^{n+1} + \tilde{T}_{w,r,i+\frac{1}{2},j,k}^{n+1} + \tilde{T}_{w,\theta,i,j-\frac{1}{2},k}^{n+1} \right. \\ \left. + \tilde{T}_{w,\theta,i,j+\frac{1}{2},k}^{n+1} + \tilde{T}_{w,z,i,j,k-\frac{1}{2}}^{n+1} + \tilde{T}_{w,z,i,j,k+\frac{1}{2}}^{n+1} \right) \end{array} \right) P_{i,j,k}^{n+1} \\
& + \left(\tilde{T}_{o,r,i+\frac{1}{2},j,k}^{n+1} + \tilde{T}_{w,r,i+\frac{1}{2},j,k}^{n+1} \right) P_{i+1,j,k}^{n+1} + \left(\tilde{T}_{o,\theta,i,j+\frac{1}{2},k}^{n+1} + \tilde{T}_{w,\theta,i,j+\frac{1}{2},k}^{n+1} \right) P_{i,j+1,k}^{n+1} \\
& + \left(\tilde{T}_{o,z,i,j,k+\frac{1}{2}}^{n+1} + \tilde{T}_{w,z,i,j,k+\frac{1}{2}}^{n+1} \right) P_{i,j,k+1}^{n+1} \\
& = \frac{V_{b,i,j,k} \phi_{i,j,k}^n}{c_1 \Delta t^{n+1}} \left[c_{r,i,j,k}^{n+1} \Delta_t P + c_{o,i,j,k}^{n+1} S_{o,i,j,k}^n \Delta_t P + c_{w,i,j,k}^{n+1} S_{w,i,j,k}^n \Delta_t P \right]
\end{aligned} \tag{3.95}$$

In IMPES method, we linearize the above pressure equation by backdating nonlinear coefficient to the old time step level. Also, assuming slightly compressible fluid, we can write Eq. 3.95 as follows.

$$\begin{aligned}
& \left(\tilde{T}_{o,r,i-\frac{1}{2},j,k}^n + \tilde{T}_{w,r,i-\frac{1}{2},j,k}^n \right) P_{i-1,j,k}^n - \left(\tilde{T}_{o,\theta,i,j-\frac{1}{2},k}^n + \tilde{T}_{w,\theta,i,j-\frac{1}{2},k}^n \right) P_{i,j-1,k}^{n+1} \\
& - \left(\tilde{T}_{o,z,i,j,k-\frac{1}{2}}^n + \tilde{T}_{w,z,i,j,k-\frac{1}{2}}^n \right) P_{i,j,k-1}^{n+1} - \left(\begin{array}{c} \left(\tilde{T}_{o,r,i-\frac{1}{2},j,k}^n + \tilde{T}_{o,r,i+\frac{1}{2},j,k}^n + \tilde{T}_{o,\theta,i,j-\frac{1}{2},k}^n \right. \\ \left. + \tilde{T}_{o,\theta,i,j+\frac{1}{2},k}^n + \tilde{T}_{o,z,i,j,k-\frac{1}{2}}^n + \tilde{T}_{o,z,i,j,k+\frac{1}{2}}^n \right) \\ \left(\tilde{T}_{w,r,i-\frac{1}{2},j,k}^n + \tilde{T}_{w,r,i+\frac{1}{2},j,k}^n + \tilde{T}_{w,\theta,i,j-\frac{1}{2},k}^n \right. \\ \left. + \tilde{T}_{w,\theta,i,j+\frac{1}{2},k}^n + \tilde{T}_{w,z,i,j,k-\frac{1}{2}}^n + \tilde{T}_{w,z,i,j,k+\frac{1}{2}}^n \right) \end{array} \right) P_{i,j,k}^{n+1} \\
& + \left(\tilde{T}_{o,r,i+\frac{1}{2},j,k}^n + \tilde{T}_{w,r,i+\frac{1}{2},j,k}^n \right) P_{i+1,j,k}^{n+1} + \left(\tilde{T}_{o,\theta,i,j+\frac{1}{2},k}^n + \tilde{T}_{w,\theta,i,j+\frac{1}{2},k}^n \right) P_{i,j+1,k}^{n+1} \\
& + \left(\tilde{T}_{o,z,i,j,k+\frac{1}{2}}^n + \tilde{T}_{w,z,i,j,k+\frac{1}{2}}^n \right) P_{i,j,k+1}^{n+1} \\
& = \frac{V_{b,i,j,k} \phi_{i,j,k}^n}{c_1 \Delta t^{n+1}} \left[c_{r,i,j,k}^n + c_{o,i,j,k}^n S_{o,i,j,k}^n + c_{w,i,j,k}^n S_{w,i,j,k}^n \right] \Delta_t P
\end{aligned} \tag{3.96}$$

Note that

$$\Delta_t P = P_{i,j,k}^{n+1} - P_{i,j,k}^n \quad (3.97)$$

For simplicity, we define

$$\tilde{V}_{i,j,k}^n = \frac{V_{b,i,j,k} \phi_{i,j,k}^n}{c_1 \Delta t^{n+1}} \left[c_{r,i,j,k}^n + c_{o,i,j,k}^n S_{o,i,j,k}^n + c_{w,i,j,k}^n S_{w,i,j,k}^n \right] \quad (3.98)$$

Finally, substituting Eq. 3.97 and Eq. 3.98 in Eq. 3.96,

$$\begin{aligned} & \left(\tilde{T}_{o,r,i-\frac{1}{2},j,k}^n + \tilde{T}_{w,r,i-\frac{1}{2},j,k}^n \right) P_{i-1,j,k}^n - \left(\tilde{T}_{o,\theta,i,j-\frac{1}{2},k}^n + \tilde{T}_{w,\theta,i,j-\frac{1}{2},k}^n \right) P_{i,j-1,k}^{n+1} \\ & - \left(\tilde{T}_{o,z,i,j,k-\frac{1}{2}}^n + \tilde{T}_{w,z,i,j,k-\frac{1}{2}}^n \right) P_{i,j,k-1}^{n+1} - \left(\begin{array}{l} \tilde{T}_{o,r,i-\frac{1}{2},j,k}^n + \tilde{T}_{o,r,i+\frac{1}{2},j,k}^n + \tilde{T}_{o,\theta,i,j-\frac{1}{2},k}^n \\ + \tilde{T}_{o,\theta,i,j+\frac{1}{2},k}^n + \tilde{T}_{o,z,i,j,k-\frac{1}{2}}^n + \tilde{T}_{o,z,i,j,k+\frac{1}{2}}^n \\ + \tilde{T}_{w,r,i-\frac{1}{2},j,k}^n + \tilde{T}_{w,r,i+\frac{1}{2},j,k}^n + \tilde{T}_{w,\theta,i,j-\frac{1}{2},k}^n \\ + \tilde{T}_{w,\theta,i,j+\frac{1}{2},k}^n + \tilde{T}_{w,z,i,j,k-\frac{1}{2}}^n + \tilde{T}_{w,z,i,j,k+\frac{1}{2}}^n + \tilde{V}_{i,j,k}^n \end{array} \right) P_{i,j,k}^{n+1} \\ & + \left(\tilde{T}_{o,r,i+\frac{1}{2},j,k}^n + \tilde{T}_{w,r,i+\frac{1}{2},j,k}^n \right) P_{i+1,j,k}^{n+1} + \left(\tilde{T}_{o,\theta,i,j+\frac{1}{2},k}^n + \tilde{T}_{w,\theta,i,j+\frac{1}{2},k}^n \right) P_{i,j+1,k}^{n+1} \\ & + \left(\tilde{T}_{o,z,i,j,k+\frac{1}{2}}^n + \tilde{T}_{w,z,i,j,k+\frac{1}{2}}^n \right) P_{i,j,k+1}^{n+1} = \tilde{V}_{i,j,k}^n P_{i,j,k}^n \end{aligned} \quad (3.99)$$

Eq. 3.99 is called as the pressure equation for IMPES method. Once we solve Eq. 3.99 for pressure, we can use either water or oil material balance equation to solve the water (or oil) saturation. We consider the material balance equation for water and solve for the water saturation. To solve water saturation, let us rewrite water equation given in Eq. 3.83 with the following modification to be consistent with the assumptions used, i.e., transmissibility will be evaluated at the old time step.

$$\begin{aligned}
& T^n_{w,r,i-\frac{1}{2},j,k} P^{n+1}_{i-1,j,k} - T^n_{w,\theta,i,j-\frac{1}{2},k} P^{n+1}_{i,j-1,k} - T^n_{w,z,i,j,k-\frac{1}{2}} P^n_{i,j,k-1} \\
& - \left(\begin{array}{c} T^n_{w,r,i-\frac{1}{2},j,k} + T^n_{w,r,i+\frac{1}{2},j,k} + T^n_{w,\theta,i,j-\frac{1}{2},k} \\ + T^n_{w,\theta,i,j+\frac{1}{2},k} + T^n_{w,z,i,j,k-\frac{1}{2}} + T^n_{w,z,i,j,k+\frac{1}{2}} \end{array} \right) P^{n+1}_{i,j,k} + T^n_{w,r,i+\frac{1}{2},j,k} P^{n+1}_{i+1,j,k} \\
& + T^n_{w,\theta,i,j+\frac{1}{2},k} P^{n+1}_{i,j+1,k} + T^n_{w,z,i,j,k+\frac{1}{2}} P^n_{i,j,k+1} \\
& = \frac{V_{b,i,j,k} \phi^n_{i,j,k} b_w^n}{c_1 \Delta t^{n+1}} \left[\Delta_t S_w + S^n_{w,i,j,k} (c_r^n + c_w^n) \Delta_t P \right]
\end{aligned} \tag{3.100}$$

Or solving for $\Delta_t S_w$ gives

$$\begin{aligned}
\Delta_t S_w &= \frac{1}{W^n_{i,j,k}} \left(\begin{array}{c} T^n_{w,r,i-\frac{1}{2},j,k} P^{n+1}_{i-1,j,k} - T^n_{w,\theta,i,j-\frac{1}{2},k} P^{n+1}_{i,j-1,k} - T^n_{w,z,i,j,k-\frac{1}{2}} P^n_{i,j,k-1} \\ \left(\begin{array}{c} T^n_{w,r,i-\frac{1}{2},j,k} + T^n_{w,r,i+\frac{1}{2},j,k} + T^n_{w,\theta,i,j-\frac{1}{2},k} \\ + T^n_{w,\theta,i,j+\frac{1}{2},k} + T^n_{w,z,i,j,k-\frac{1}{2}} + T^n_{w,z,i,j,k+\frac{1}{2}} \end{array} \right) P^{n+1}_{i,j,k} \\ + T^n_{w,r,i+\frac{1}{2},j,k} P^{n+1}_{i+1,j,k} + T^n_{w,\theta,i,j+\frac{1}{2},k} P^{n+1}_{i,j+1,k} + T^n_{w,z,i,j,k+\frac{1}{2}} P^n_{i,j,k+1} \end{array} \right) \\
& - S^n_{w,i,j,k} (c_r + c_w) (P^{n+1}_{i,j,k} - P^n_{i,j,k})
\end{aligned} \tag{3.101}$$

where we defined

$$W^n_{i,j,k} = \frac{V_{i,j,k} \phi^n_{i,j,k} b_w^n}{c_1 \Delta t^{n+1}} \tag{3.102}$$

Once we solve saturation equation given in Eq. 3.101, we can compute the water saturation as follows.

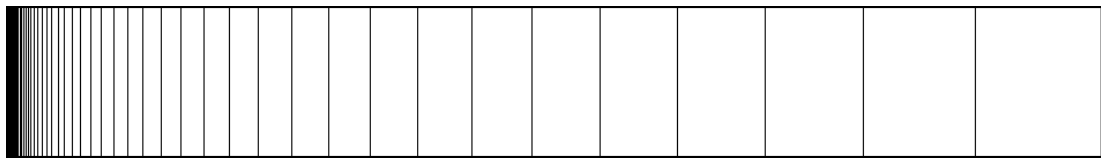
$$S^{n+1}_{w,i,j,k} = \Delta_t S_w + S^n_{w,i,j,k} \tag{3.103}$$

3.2.3 Example matrix structures

Here, we will present a matrix structure of one simple case for the Newton and IMPES methods. Firstly, gridding used in the r , θ , and z direction is described. Secondly, we consider a simple example application with with considered grid system to understand the structures of the matrices arising from the formulations of the Newton and IMPES methods.

As it is widely used in reservoir simulation, non-uniform block centered grids are used in r direction. MacDonald-Coats (1970) method used is to create grids in r direction. Simple example of gridding structure in r direction is given in **Figure 3.2**.

We also used block centered grids in θ and z directions. Schematical presentation of $r-z$ and $r-\theta$ directions are given in **Figure 3.3**. and **Figure 3.4**., respectively.



r_w r_e
Figure 3.2 : Grid structure for r direction using MacDonaldis - Coats method (taken from Gok, 2004).

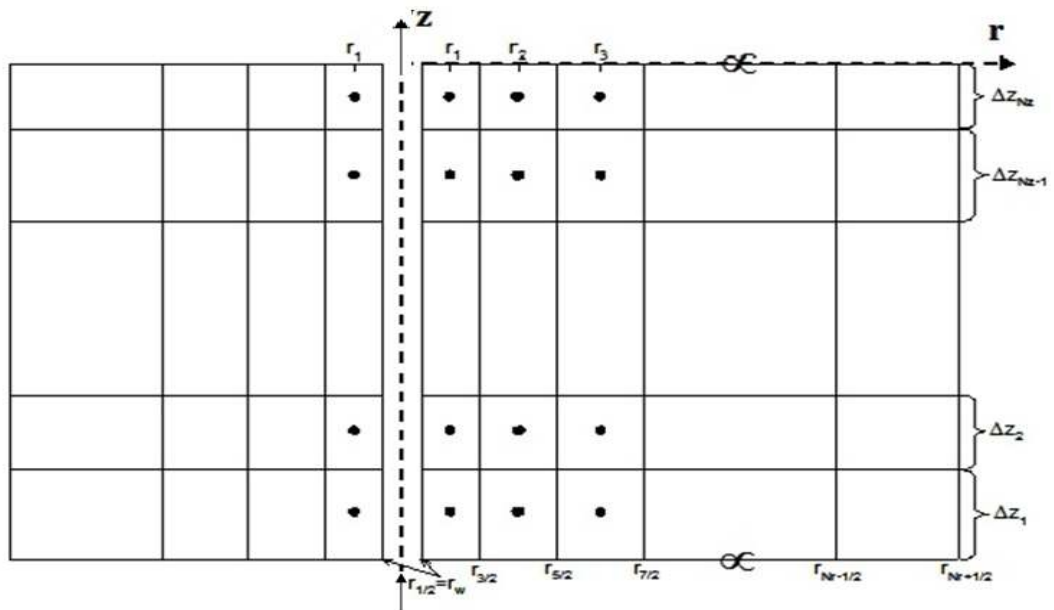


Figure 3.3 : Schematic presentation of grids in $r - z$ direction.

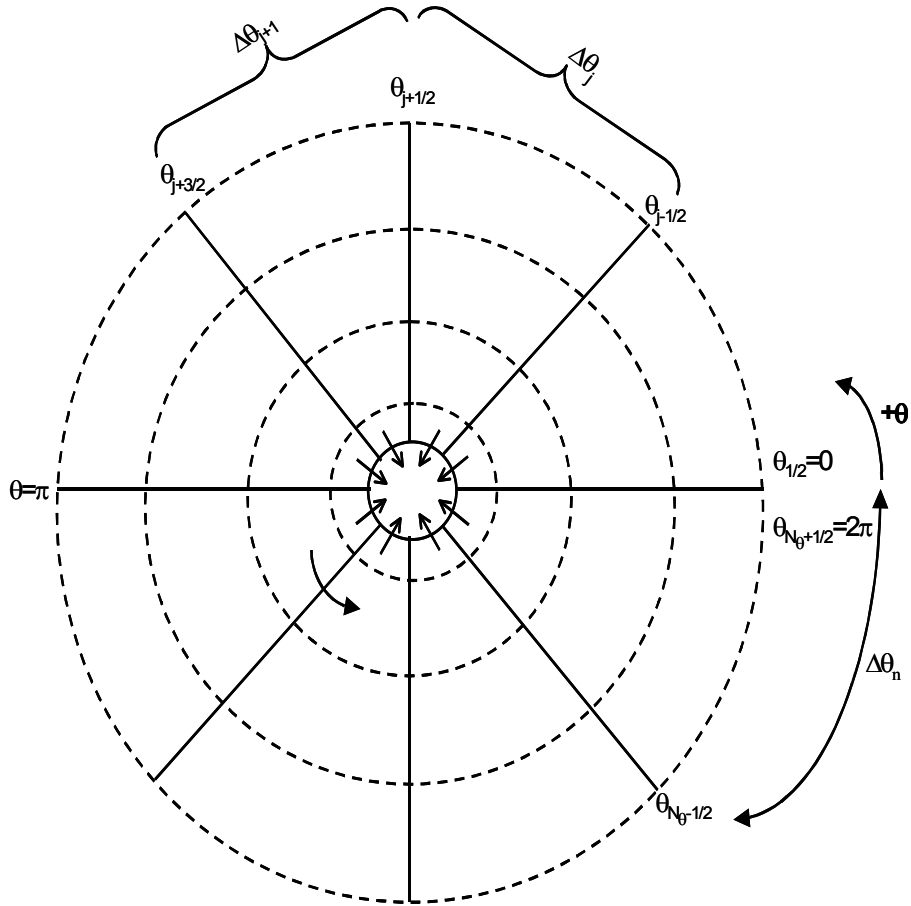


Figure 3.4 : Schematic presentation of grids in $r - \theta$ direction (taken from Gok, 2004).

As we present our gridding system briefly, we can now consider the structure of matrix for Newton and IMPES method for simple case.

Assume that we have cylindrical reservoir and well is located at the center. If we use $N_r = 4$, $N_\theta = 3$, and $N_z = 2$, we will have reservoir structure as given in **Figure 3.5**.

N_r : number of grids in r direction

N_θ : number of grids in θ direction

N_z : number of grids z direction

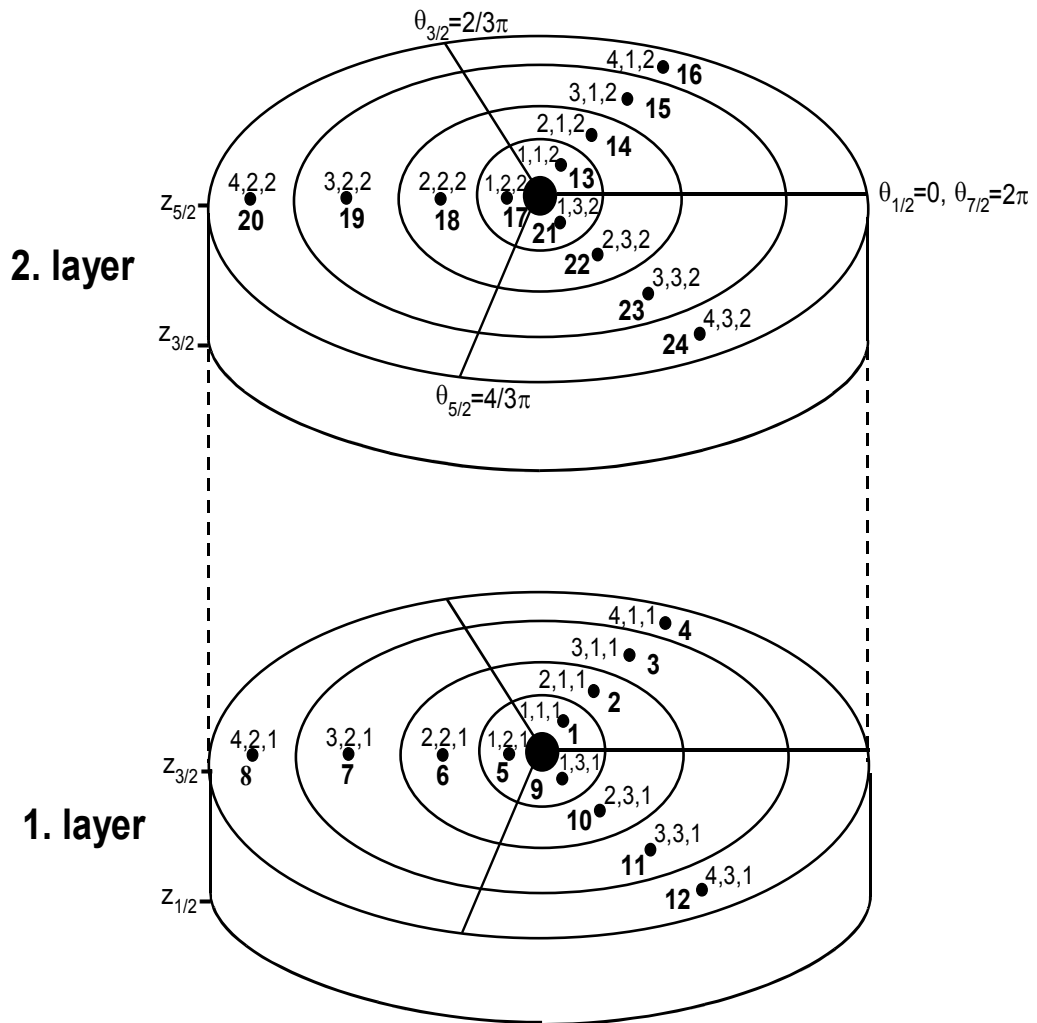
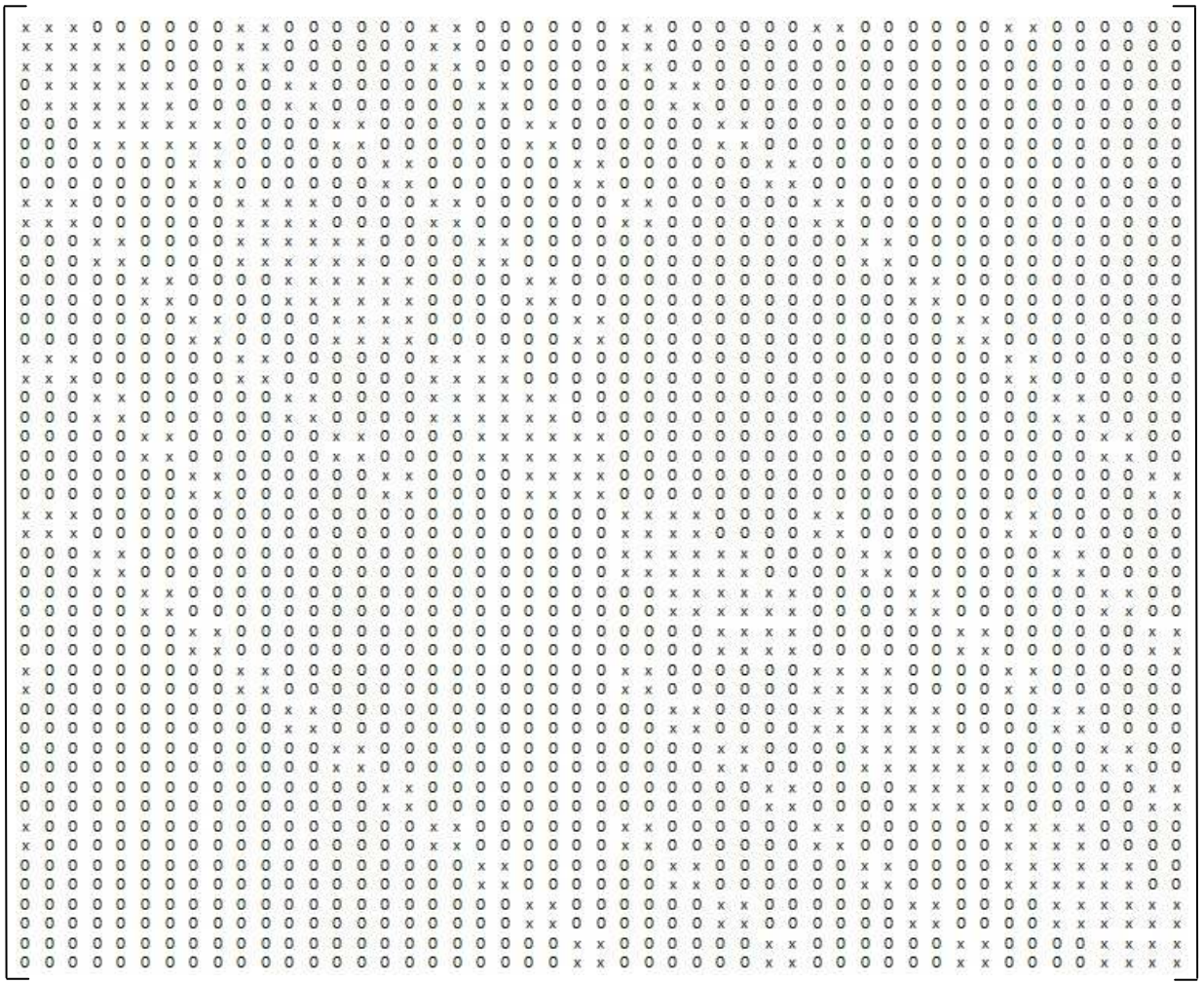


Figure 3.5 : Simple reservoir structure in $r-\theta-z$ direction.

Let us assume, we have a fully penetrating vertical well meaning all the grids around the well are open to flow. Under the assumptions, matrix structure for Newton and IMPES method are given in **Figure 3.6** and **Figure 3.7**, respectively.



49x49

Figure 3.6 : Jacobian matrix structure for the FIMPS (or Newton) method.

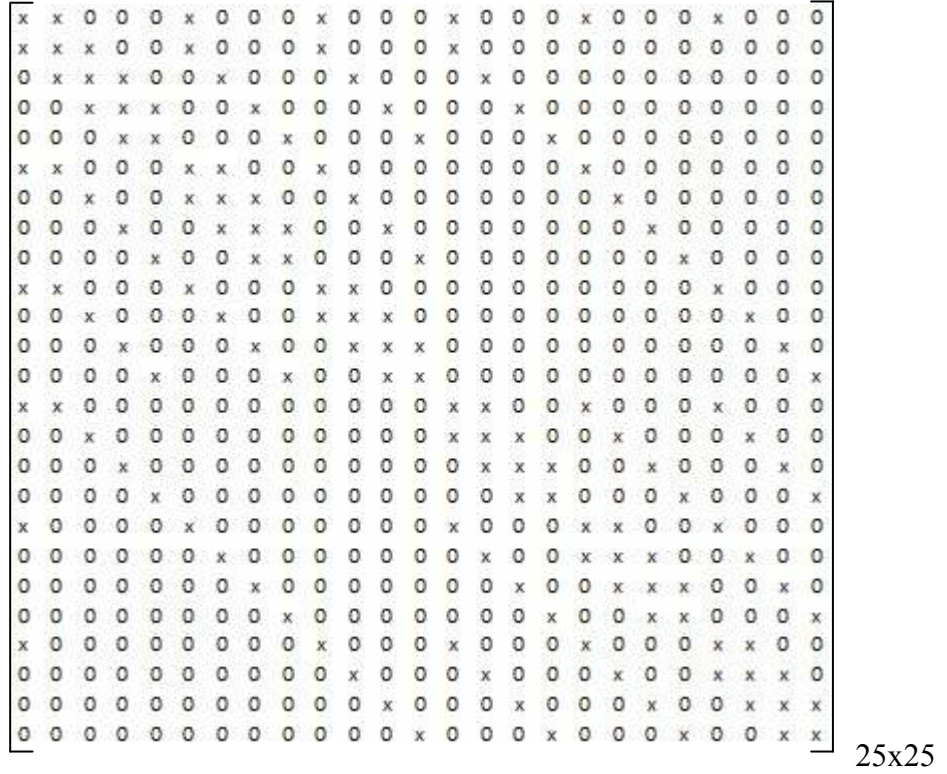


Figure 3.7 : Matrix structure for IMPES method.

It is worth noting that the matrices (Figs. 3.6 and 3.7) given for the Newton method and IMPES methods will be nonsymmetric matrices and require the use of nonsymmetric matrix solvers as discussed next.

3.3 Matrix Problem Solver

As it is clear from **Figure 3.6** and **Figure 3.7**, matrix size is bigger in the Fully Implicit Pressure and Saturation (FIMPS) method using the Newton's method since we solve pressures and saturations implicitly. However, as we solve only pressures in IMPES method, we have smaller size matrix. Specifically, in the FIMPS method, the total number of unknowns to be solved by the matrix problem is $2 \times N_{gb} + 1$, while in the IMPES method, the total number of unknowns to be solved by the matrix problem is $N_{gb} + 1$. Recall that N_{gb} is the total number of grid blocks, i.e., $N_{gb} = N_r \times N_\theta \times N_z$.

There exists different methods to solve matrix problem and most of the methods store all the elements of the matrix. This might be efficient when the matrix size is small. The amount of grid in typical reservoir simulation does not allow us to work with smaller size matrices. Therefore, we might have storage problem or long

solving time. To deal with these problems, we use special algorithms which only store non-zero elements of the matrix.

In this study, we used matrix solver package by Yale University (Eisenstat, 1979) to avoid storage and inefficient solving time problem. Moreover, this solver uses the compressed row storage scheme to store the matrix.

4. VERIFICATION OF THE RESULTS

After deriving the difference equation, we developed a simulator to solve the oil and water flow problem in 3D $r-\theta-z$ coordinate system using both FIMPS and IMPES method. Microsoft Visual C# is used for the development of simulator. It is important to note that we use FIMPS and Newton methods interchangeably. Results are compared with commercial IMEX (2010) software for the validation of the simulator developed in this study.

4.1 Case 1-Injection

In case 1, we will simply compare the results for Newton and IMPES method with IMEX. Therefore, we will only consider injection period of 16 hours with an injection rate of $q_w = -3000 \text{ STB} / D$ flow rate. For this case, we consider that flow occurs in only r direction and we have a fully penetrating vertical well. So, we simulate pressure and saturation behavior for 1-D radial flow case. This case has been previously considered by Chen (2007). Unless otherwise stated, we use $N_r = 200$ grid block in the r -direction, generated by using the McDonalds-Coats method. Moreover, in this study, we used 200 grids in r -direction for all the cases for CMG. Time steps are generated based on a scheme using logarithmically distributed time points. Relative permeability data for oil and water were generated by using a power-law model (see Appendix A, Eqs. A.18 – A.20). Other input data are given in Table 4.1.

A comparison of the bottom-hole pressure vs. time data obtained from IMEX-CMG, Newton and IMPES methods is presented in **Figure 4.1**. As can be seen from Fig. 4.1, the bottom-hole pressures from our simulator agrees very well with those from the IMEX for the entire duration of the injection. It is interesting to note that both the bottom-hole pressures obtained from the Newton and IMPES methods are also in good agreement.

Next, we investigate the accuracy of the saturation profiles. For instance, the water saturation vs. radial distance data computed from the IMPES, FIMPS, and IMEX methods at the end of injection period is shown in **Figure 4.2**. As can be seen, the agreement between the saturations computed from our simulator using the Newton method and IMEX is perfect. However, the saturations computed by our simulator using the IMPES method show some differences, particularly near the front. This indicates that IMPES method cannot produce saturation profiles as accurate as the FIMPS (or Newton) method. This is in fact not surprising because the saturation is solved explicitly and hence the accuracy of saturation in the IMPES method is more susceptible to the grid size and time steps than that in the FIMPS.

To further investigate the accuracy and stability issues with the IMPES method, we consider two different number of grid blocks; $N_r = 90$, $N_r = 200$, and $N_r = 400$. In other words, we investigate the effect of number of grid blocks (or equivalently the grid block size) on the pressure and saturation solutions to be obtained from the IMPES method. Comparisons of the bottom-hole pressures and saturations are shown in **Figure 4.3** and **Figure 4.4**, respectively. As it is seen from these figures, the pressure and saturations computed from the IMPES method is very susceptible to the grid block size. It should be noted that increasing the number of grid blocks (or decreasing the grid block sizes) decreases the accuracy of the pressure and saturations computed from the IMPES method and even can cause stability problems in the saturation values (e.g., see saturation profile for the case $N_r = 400$). The results shown in **Fig. 4.3 and 4.4** for the IMEX case is generated by $N_r = 200$.

As Coats and McDonalds method is used for grid construction in r direction, when we increase the grid number, grid size around the well decreases. In IMPES method, we obtain good match only when the grid size are sufficiently big to not cause stability issues.

Eventhough, we do not show it in this study, time step has the same effect on IMPES method. In order the work properly with IMPES method, we need to use small time steps.

Table 4.1 : Data for Case 1 and Case 2.

Property	Value
h	60 ft.
r_w	0.35 ft.
r_e	6800 ft.
k	300 md.
S_{iw}	0.1
S_{or}	0.25
P_i	2500 psi
ϕ	0.22
B_o	1.0 RB/STB
B_w	1.0 RB/STB
c_o	$8 \times 10^{-6} \text{ psi}^{-1}$
c_w	$3.02 \times 10^{-6} \text{ psi}^{-1}$
c_r	$5.0 \times 10^{-6} \text{ psi}^{-1}$
$k_{ro@S_{nw}}$	1
$k_{rw@(1-S_{or})}$	0.5
m	2
n	2
μ_o	3 cp.
μ_w	0.5 cp.

In reservoir simulation, we want to use small grids around the wellbore and small time steps at the beginning of the operation for better accuracy in the solutions. Usually, time steps increases with time to have a faster solution. Therefore, although IMPES method works well when the conditions are met, we decided to continue with Newton's method to not suffer because of stability problem. To further support this, we present the pressure and saturation solutions obtained from the our simulator based on the Newton method in **Figures 4.5 and 4.6** for three different values of $N_r = 90, 200, \text{ and } 400$. As can be seen, unlike the accuracy and stability of the solutions from the IMPES method, the accuracy and the stability of the solutions from the Newton method are not strongly dependent on the number of grid blocks in the r-direction for this example case.

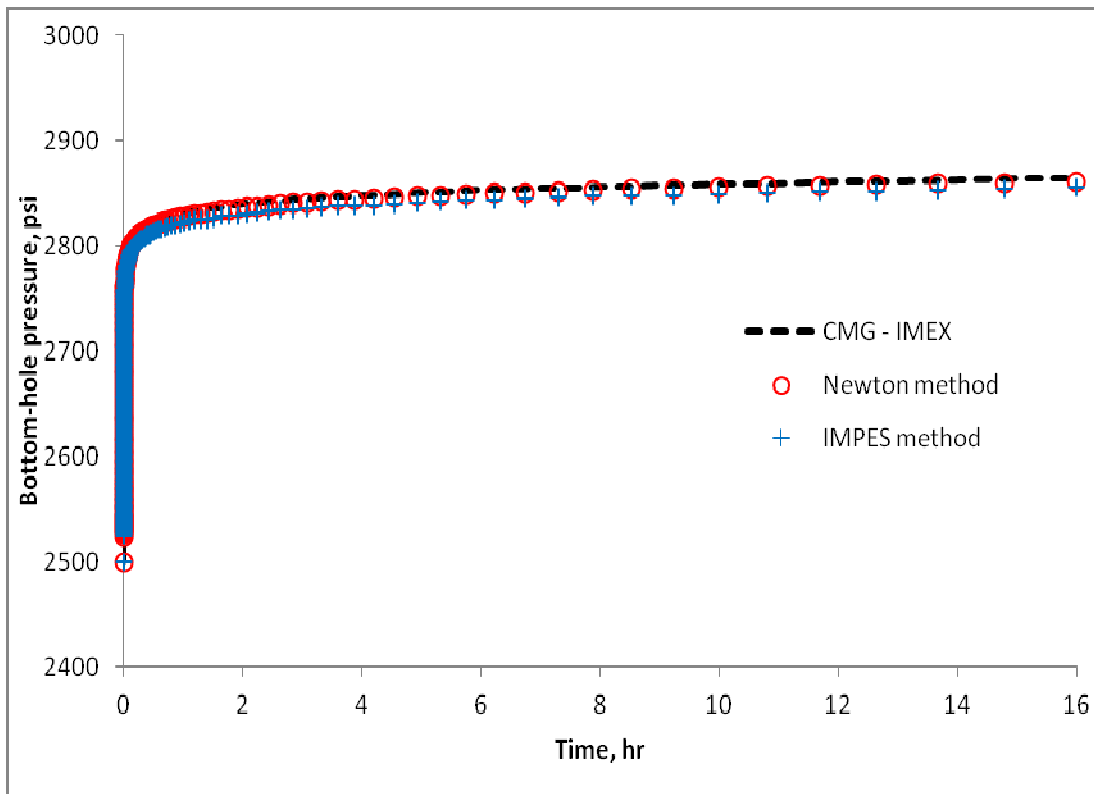


Figure 4.1 : Pressure vs. time for Case 1 ($N_r = 200$).

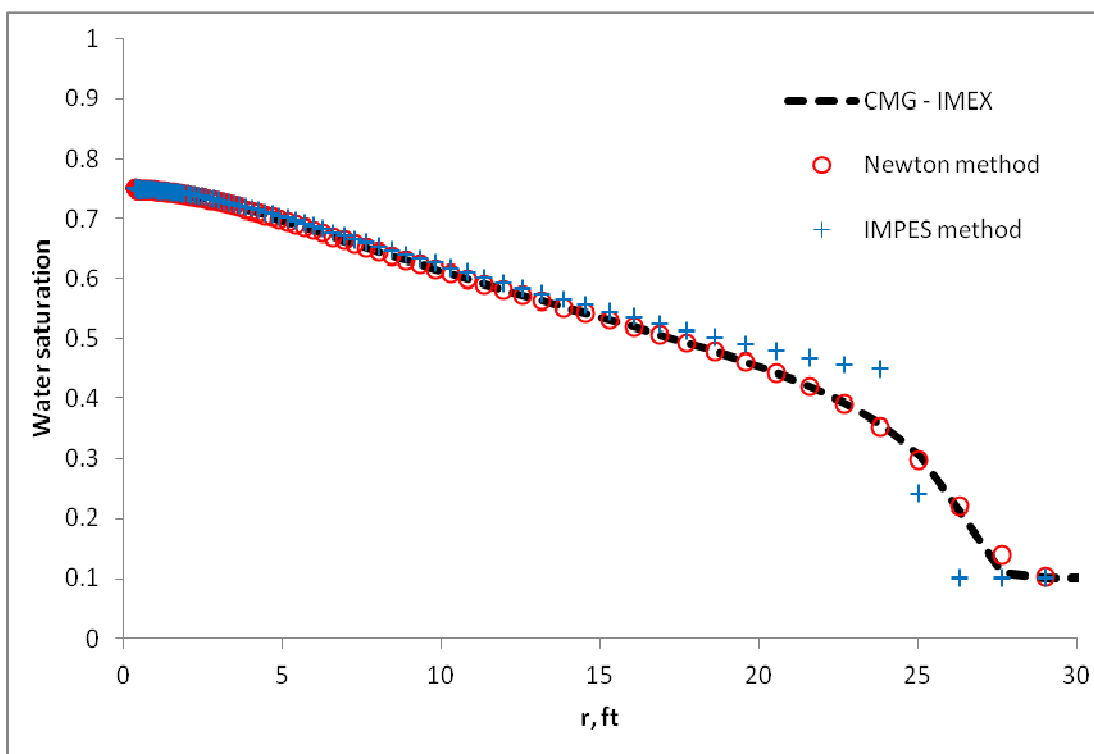


Figure 4.2 : Saturation profile in r direction for Case 1 (end of injection) ($N_r = 200$).

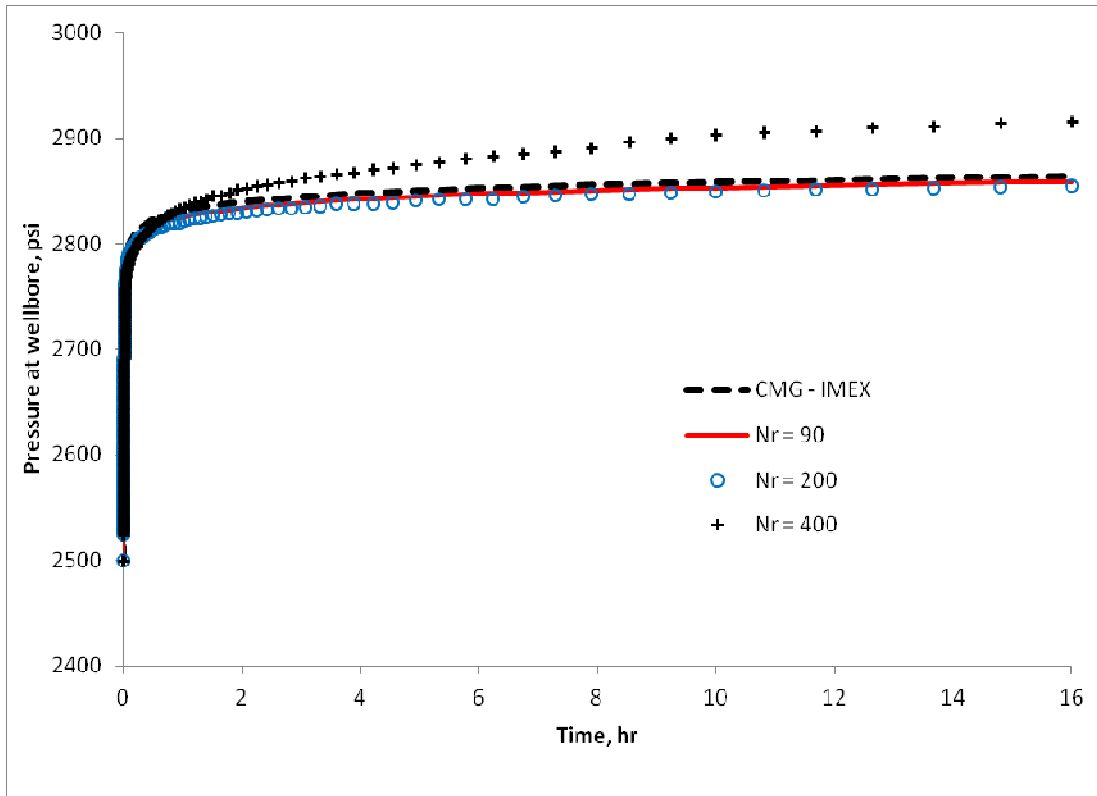


Figure 4.3 : Bottom-hole pressures from IMPES method for different values of N_r for Case 1.

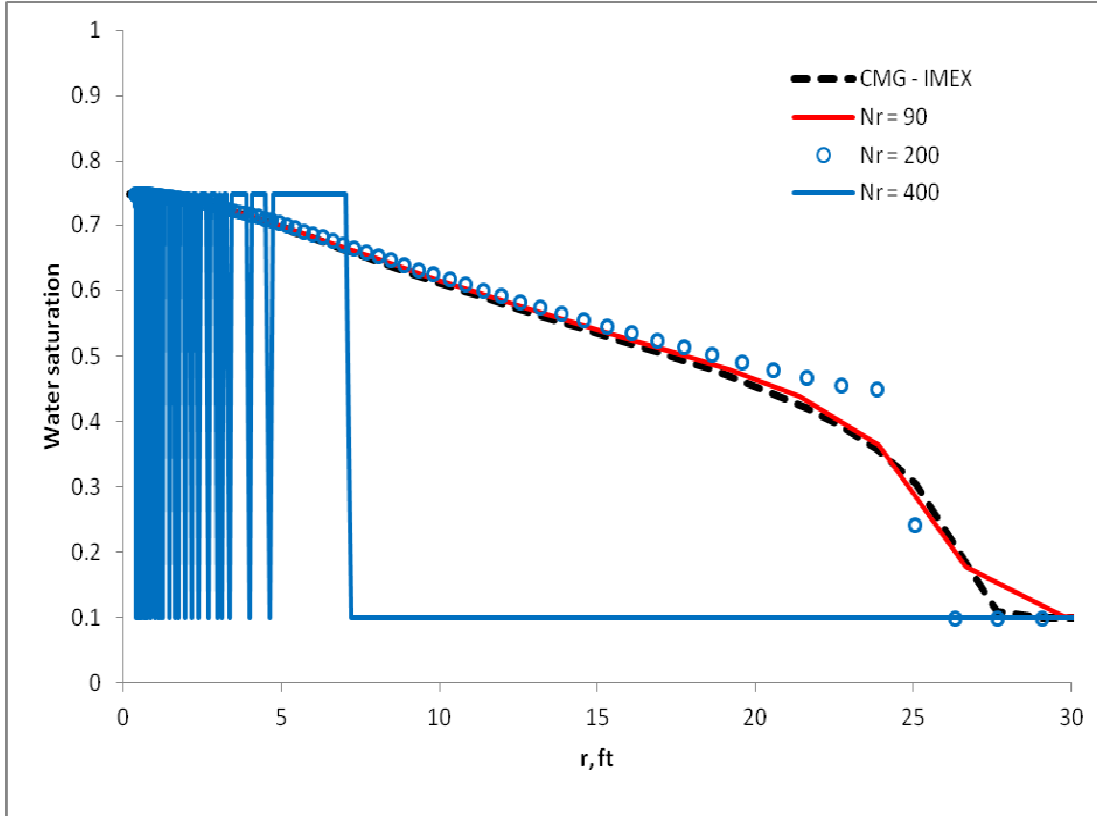


Figure 4.4 : Water saturation versus radial distance from IMPES method for different values of N_r for Case 1.

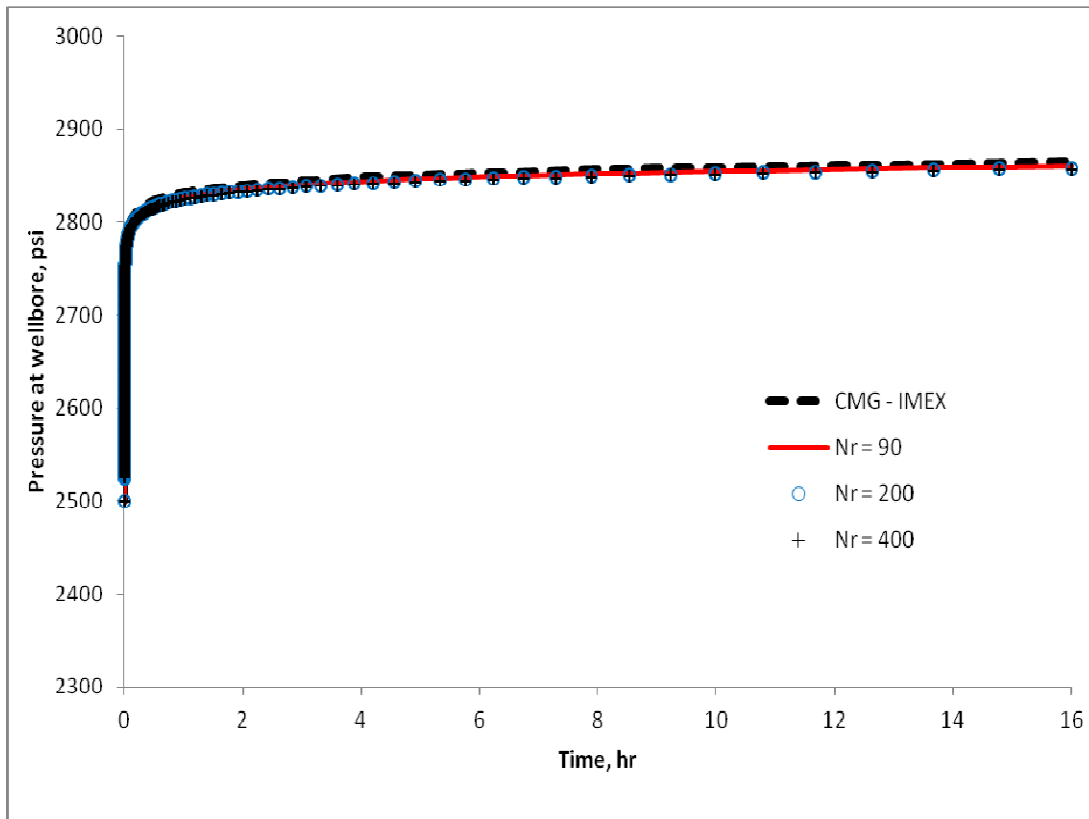


Figure 4.5 : Bottom-hole pressures from Newton method for different values of N_r for Case 1.

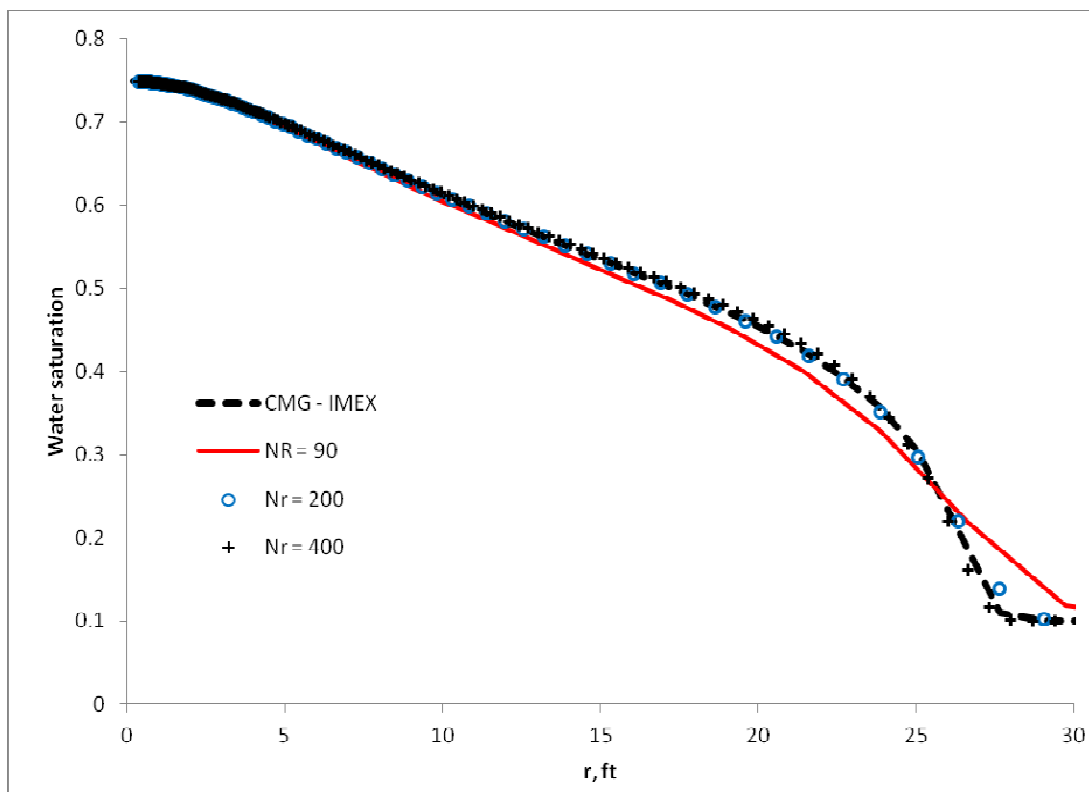


Figure 4.6 : Water saturation versus radial distance from Newton method for different values of N_r for Case 1.

4.2 Case 2 - Injection-Fall off-Production

As we decided to work with Newton's method, we consider a more complicated case to validate our results with the results from the IMEX software.

Here, we will use the same input data given in Table 4.1 for Case 1. However, we will change the flow rate history. Firstly, we will inject water with the flow rate of $q_w = -3000 \text{ STB}/D$ for 16 hours. Secondly, we will have fall off period for 16 hours (i.e., $q_w = 0 \text{ STB}/D$). Finally, we will have a total production of $q_{surface} = 3000 \text{ STB}/D$ for 24 hours. We use $N_r = 200$ grid block in the r -direction, generated by using the McDonalds-Coats method.

The results for the bottom-hole pressure vs. time are compared in **Figure 4.7**. As it is clear that the bottom-hole pressure data generated from the simulator developed in this study match quite well with the bottom-hole pressure data from the commercial software IMEX-CMG. In the first 16 hours, bottom-hole pressure increases as it is expected. During fall-off period between 16 hr. and 32 hr., we see a decrease in bottom-hole pressure since the pressure stabilizes. Finally, after 32 hr., we see a decrease in pressure because of production. Moreover, we see two sharp decrease in pressure during production period. The reason for this is that we first produce only the water in the near wellbore region formed during the injection period, and then we start producing both water and oil from the reservoir. Although it is difficult to see from **Figure 4.7**, after 45. hr., there is a small increase in pressure even though we still produce from the reservoir.

As it is expected, the saturation profiles are very similar at the end of injection and at end of falloff periods. Saturation profile given in **Figure 4.2** also represents the saturation profile at the end of injection for Case 2.

The saturation profiles obtained from our simulator and the IMEX for the end of fall-off and production periods are compared in **Figure 4.8** and **Figure 4.9**, respectively.

The results presented in **Figures 4.7-4.9** for Case 2 were generated by considering flow only in the r -direction, i.e., $N_r = 200$, $N_t = N_z = 1$. To validate that the simulator works satisfactorily when we allow flow in the theta and z directions, we run the simulator for Case 2 with $N_r = 200$, $N_\theta = 6$, and $N_z = 10$. The bottom-hole pressures computed with $N_r = 200$, $N_\theta = N_z = 1$ and with $N_r = 200$, $N_\theta = 6$, $N_z = 10$ together with

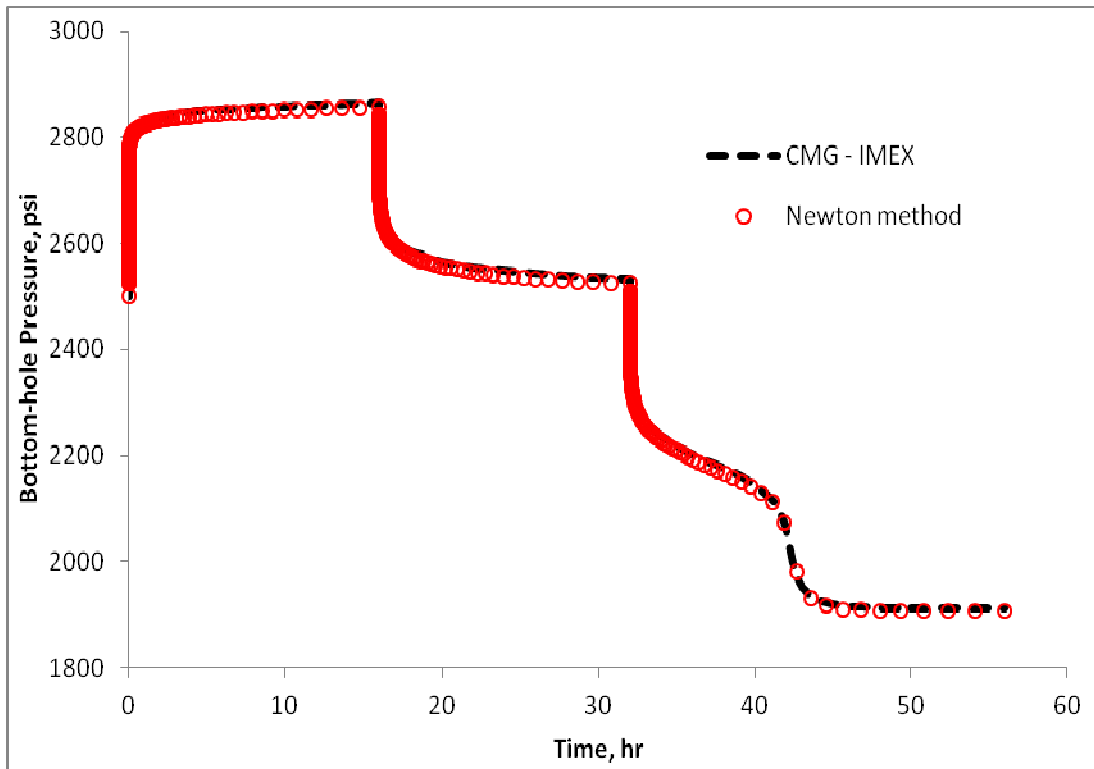


Figure 4.7 : Pressure vs. time plot for Case 2.

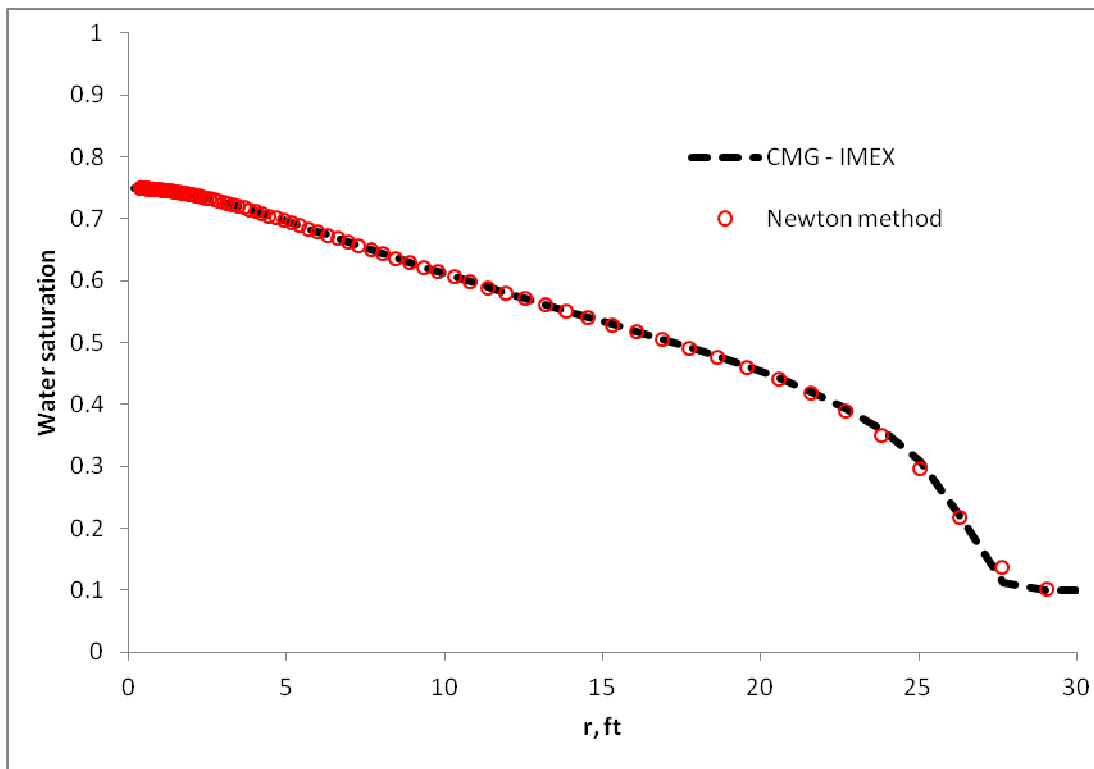


Figure 4.8 : Saturation profile in r direction (end of fall off) for Case 2.

those from IMEX are compared in **Figure 4.10**. As expected, the pressures are the same as the pressures when we consider only flow in the r direction for this fully penetrating vertical case because we do not consider gravity effect and the well is fully penetrated. Although not shown here, we also compared the saturation profiles generated with $N_r = 200, N_\theta = N_z = 1$ and with $N_r = 200, N_\theta = 6, N_z = 10$ and the agreement between them were excellent. So, these comparisons validate that the simulator is working properly for three-dimensional flow case since we have excellent matches for pressure and saturation generated for the 1-D and the equivalent 3-D flow cases.

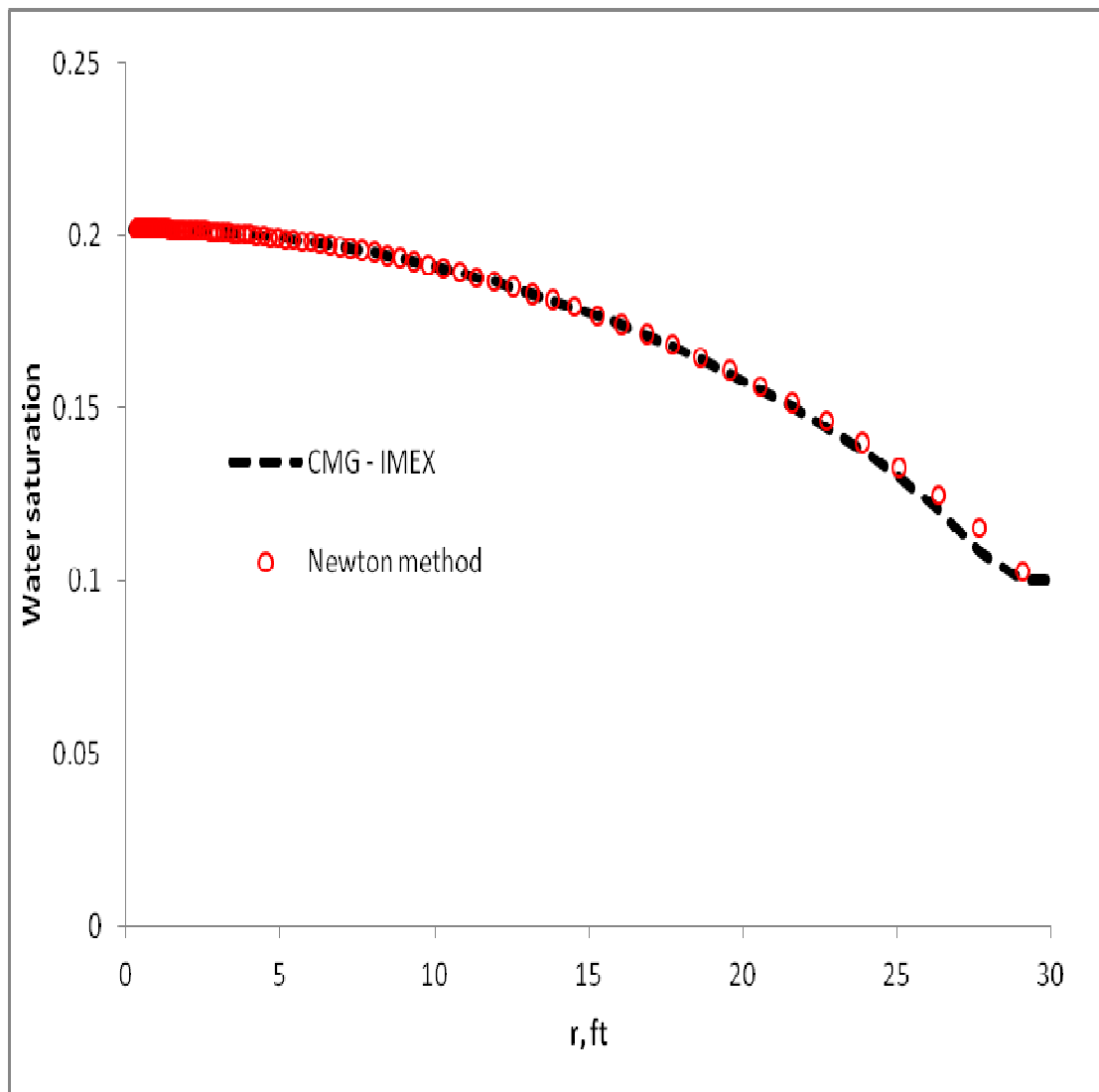


Figure 4.9 : Saturation profile in r direction for Case 2 (end of production).

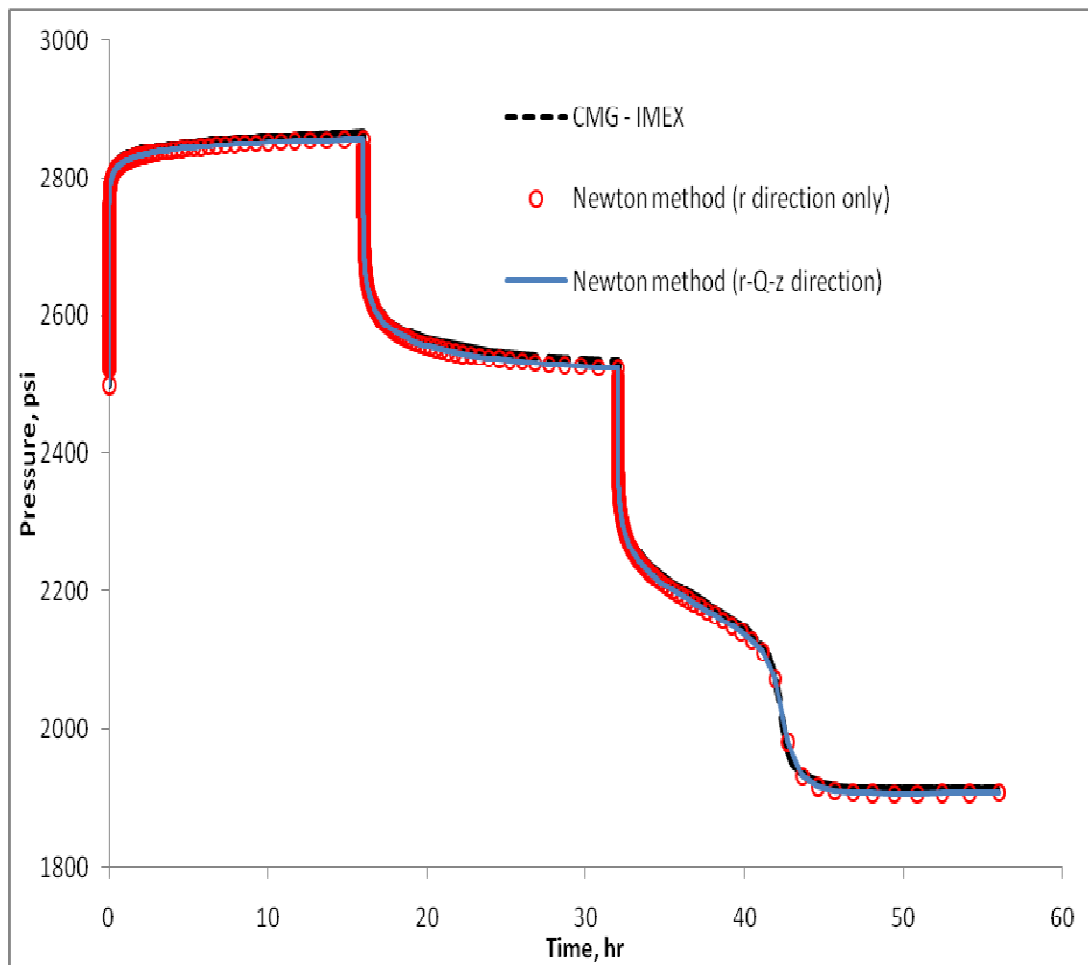


Figure 4.10 : Pressure vs. time plot for Case 2.

4.3 Case 3-Injection

In the first two cases, we compared our simulator results with IMEX-CMG software. Now, we compare our results with some results presented in the literature. Here, for comparison, we consider the results presented by Levitan (2003) for an injection case (see Fig. 5 of Levitan, 2003). Table 4.2 contains the input data for Levitan's case (or referred to as Case 3 here).

Since he did not present any value for formation volume factor of oil and water, we used 1 RB/STB for both oil and water. Moreover, we also need the external radius of the reservoir. Since his results do not show any boundary effect, we used sufficiently large external radius ($r_e = 6800$ ft.) to avoid boundary effects on the solutions. For the comparison, we inject water with the flow rate of $q_w = -500$ RB/STB for 10 hours.

We use $N_r = 400$ grid block in the r -direction, generated by using the McDonalds-Coats method.

Figure 4.11 presents a comparison of the Levitan's results for the rate normalized pressure changes and its Bourdet derivative for a finite wellbore vertical well with the corresponding results from our simulator. Here the Bourdet derivative refers to the derivative of rate-normalized pressure change with respect to the natural logarithm of time (Bourdet et al. 1989). As it is clear, an excellent agreement exists between the solutions, validating our simulator.

Finally, we compare the results of Levitan (see Fig. 4 of Levitan) for the case where the wellbore is treated as line-source (well radius is vanishingly small) with the corresponding results from our simulator for the same case. This comparison is presented in **Figure 4.12**. Note that we consider a sufficiently small wellbore radius (0.0357 ft.) so that we can obtain a match with Levitan's solutions. As it is seen from **Fig. 4.12**, again, we have an excellent match with Levitan's analytical solution assuming a line-source wellbore. It should be noted that although we simulate pressure and saturation using a well bore radius of 0.0357 ft, we print the pressures at the actual wellbore radius of 0.357 ft.

Table 4.2 : Data from Levitan's paper

Property	Value
h	100 ft.
r_w	0.357 ft.
k	1000 md.
$S_{w,ir}$	0.2
S_{or}	0.25
P_i	5000 psi
ϕ	0.2
c_o	9×10^{-6} psi ⁻¹
c_w	3×10^{-6} psi ⁻¹
c_r	5.0×10^{-6} psi ⁻¹
$k_{ro@S_{rw}}$	0.8
$k_{rw@(1-S_{or})}$	0.2
m	2
n	2
μ_o	0.3 cp.
μ_w	0.25 cp.

So, the pressure change and the pressure derivative shown in **Figure 4.12** represents the pressure and derivative data computed at $r_w = 0.357$ ft. In other words, while we inject water at 0.0357 ft, we actually observe the pressure inside reservoir at the radial distance equal to the actual wellbore radius of 0.357 ft. Hence, we observe a rapid change in pressure-derivative for the "infinitesimally small" wellbore radius case. This is in fact not surprising if we realize, the pressures are given at $r_w = 0.357$ ft, and until the water front reaches the radius of 0.357 ft, we first observe a radial flow reflecting the properties of the oil zone. Hence, when the front reaches the radius of 0.357 ft, we start to observe the radial flow reflecting the properties of the water zone. This is reflected as a rapid change in derivative as the response goes from the oil zone to water zone.

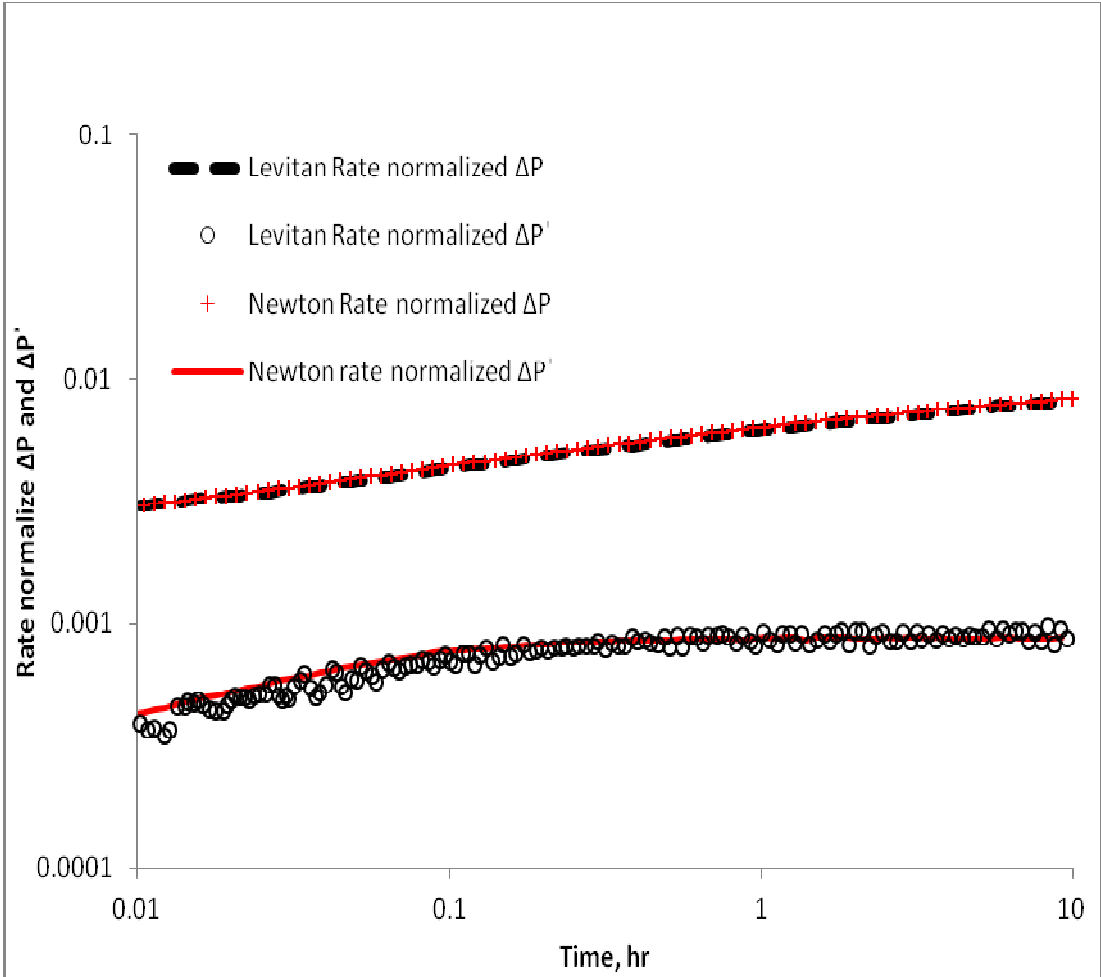


Figure 4.11 : Rate normalized ΔP and $\Delta P'$ vs time (finite wellbore) for Levitan's (2003) case (Case 3).

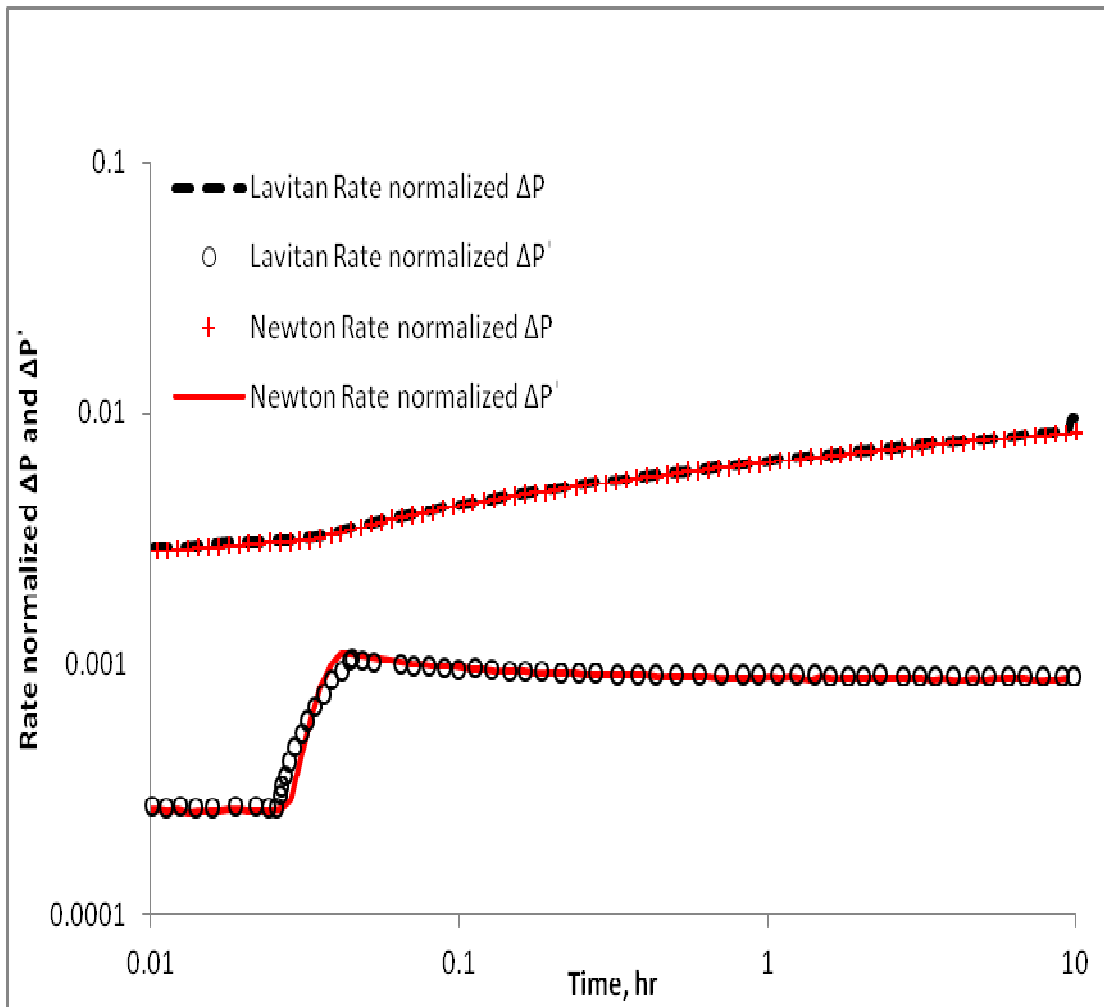


Figure 4.12 : Rate normalized ΔP and $\Delta P'$ vs time (linesource wellbore) for Levitan's (2003) case (Case 3).

5. APPLICATIONS

In previous chapter, accuracy of the simulator is validated. In this chapter, effects of some parameters such as end point mobility ratio and skin will be presented. Moreover, simple analysis will be performed on diagnostic plot.

5.1 Effect of Initial Time Step of Simulation

During our work, we observed that starting simulation time (denoted by t_s here) has important effect on the simulated pressure and saturation by the FIMPS method. Here, we investigate the effect of t_s on the solutions and for this investigation, we consider Case 3 (Levitan's finite wellbore injection example) given in Chapter 4.

Figure 5.1 illustrates the effect of starting time on pressure-derivative curve for Levitan's finite wellbore case. Recall that pressure difference and derivative of pressure difference are calculated by the commercial well-test software ECRIN (2009). Although we did not consider wellbore storage and skin effects, we observe a hump on Bourdet derivative if the starting time of simulation is not sufficiently small. We believe that this is because of non-linearity of the problem. Therefore, one should be careful when selecting the starting time t_s . Incorrect selection of t_s may give appearance of wellbore storage and skin effects on the pressure solutions.

5.2 Analysis of Derivatives for Injection-Falloff-Production Periods

One of the objectives of this study is to understand the pressure response of two-phase flow condition. In previous chapter, we validated our simulator for various cases. Here, we will interpret the injection-fall-off-production case given in Chapter 4 (see **Figure 4.7** for Case 2).

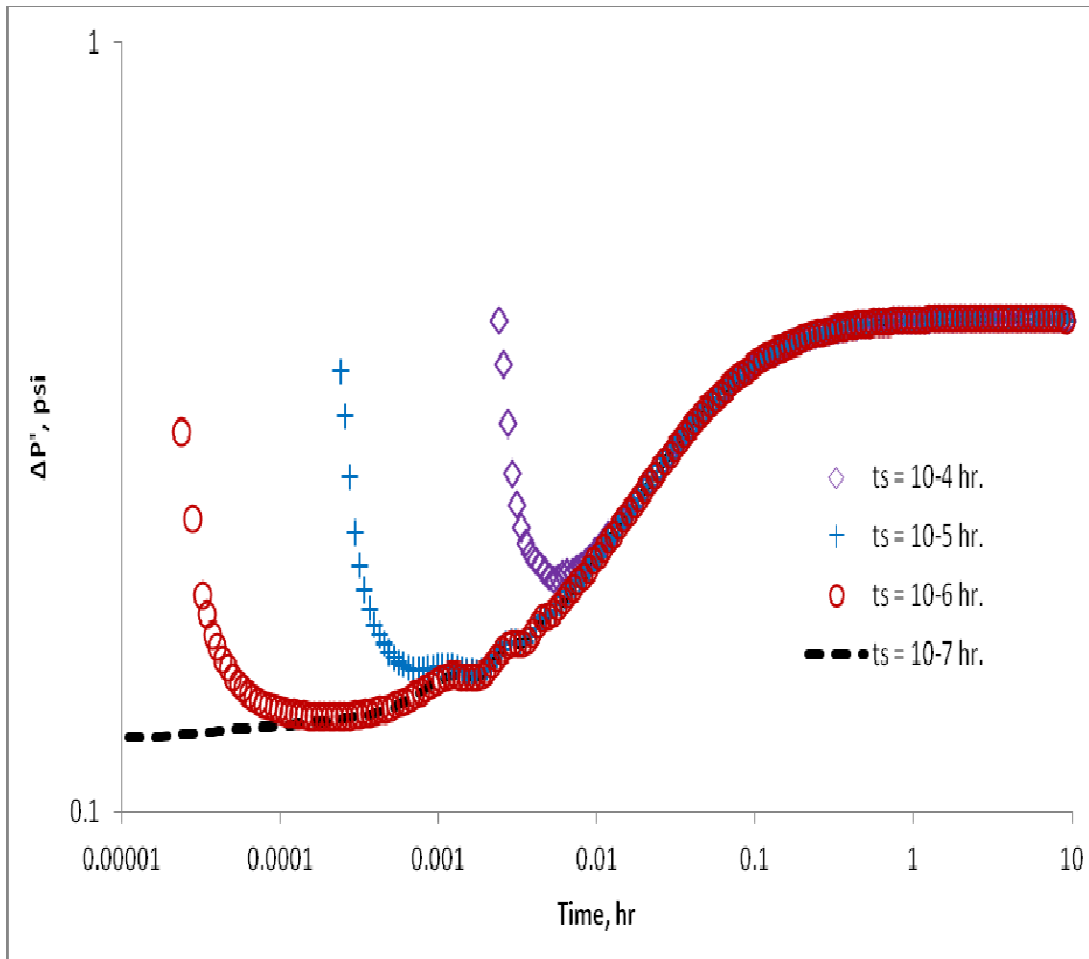


Figure 5.1 : Rate normalized ΔP and $\Delta P'$ vs time (infinite wellbore).

Figure 5.2 illustrates the pressure difference and its Bourdet derivative of injection period. Two radial flows are observed since there exists two zero-slope lines on the derivative data. The first radial flow occurs between 0.0003 hr. and 0.001 hr. When we inject water into reservoir, pressure propagation is ahead of the water front at early times. Therefore, pressure response comes from the oil zone. Based on the work of Amina (2007), we can also calculate the early-time Bourdet derivative from the formula given by

$$\Delta P' = \frac{70.6 \times q_{inj} \times B_w}{kh \left(\frac{k_{ro}^0}{\mu_o} \right)} = \frac{70.6 \times 3000 \times 1}{300 \times 60 \times \left(\frac{1}{3} \right)} = 35.3 \text{ psi} \quad (5.1)$$

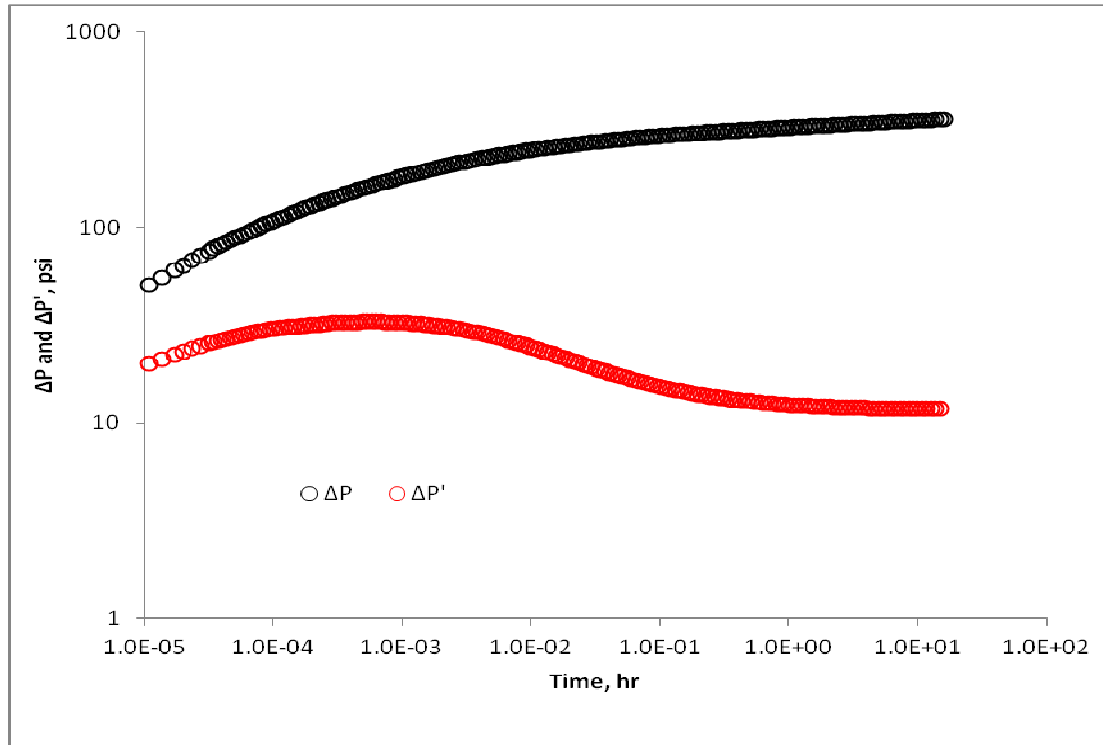


Figure 5.2 : ΔP and $\Delta P'$ vs time for injection period.

We observe a second radial flow starting about from 1 hr. to the end of injection period. As some amount of water is injected into the reservoir, pressure propagates in the water zone. Therefore, second radial flow contains information about the water zone. Based on the work of Amina (2007), the late time Bourdet-derivative reflecting radial flow for injection period can be calculated by

$$\Delta P' = \frac{70.6 \times q_{inj} \times B_w}{kh \left(\frac{k_{rw}^0}{\mu_w} \right)} = \frac{70.6 \times 3000 \times 1}{300 \times 60 \times \left(\frac{0.5}{0.5} \right)} = 11.77 \text{ psi} \quad (5.2)$$

k_{ro}^0 / μ_o and k_{rw}^0 / μ_w in Eq. 5.1 and Eq. 5.2 are called end point mobility for oil and water, respectively. In oil water two phase problem, end point mobility have significant effect on flow.

Figure 5.3 presents the pressure difference and its derivative of the falloff period. We also observe two radial flow periods as in the case for the injection period. As water is present around the wellbore, pressure propagates in the water zone first. Therefore, the early-time radial flow for the falloff contains information about water

zone, whereas the late-time (or second) radial flow reflects the properties of the oil zone. Eq. 5.1 and Eq. 5.2 are still valid for the Bourdet derivative for these radial flow periods.

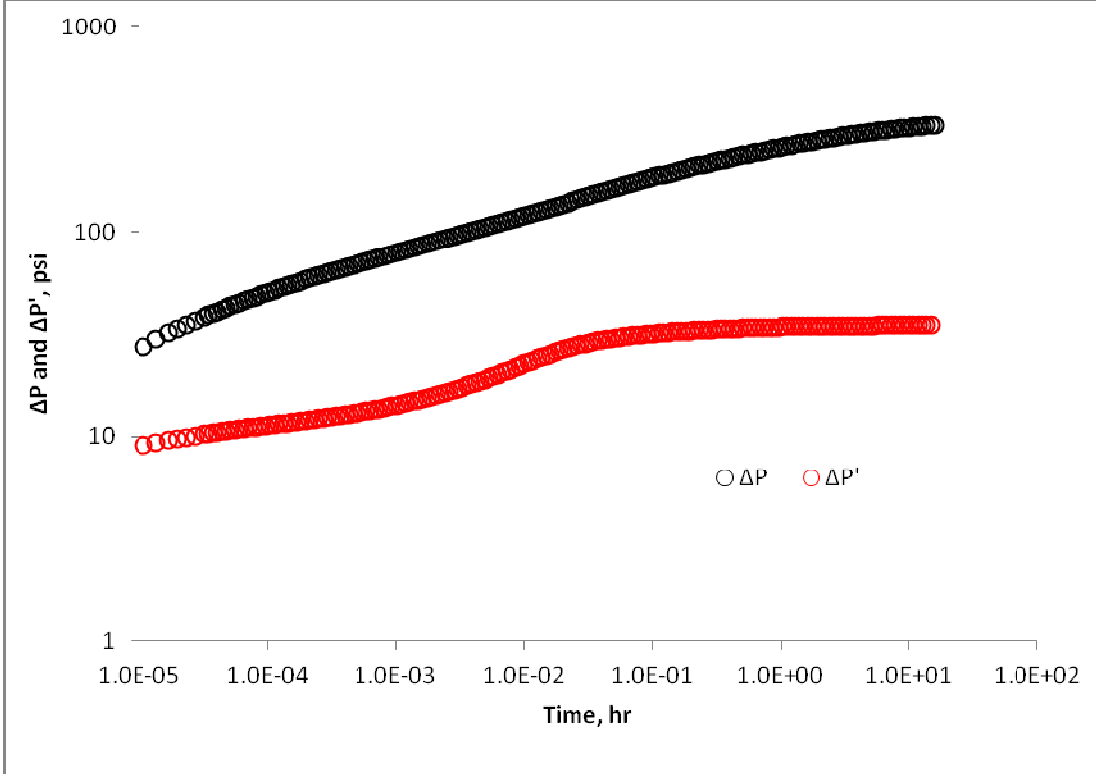


Figure 5.3 : ΔP and $\Delta P'$ vs time for falloff period.

Finally, we present the pressure difference and its Bourdet derivative for the production period in **Figure 5.4**. Note that a comparison of **Figures 5.3 and Figure 5.4** indicates that falloff and production periods give similar derivative responses . However, we observe rapid change in the pressure and derivative data, and the derivative data go to negative values at time of oil breakthrough during production period. The reason for the rapid change in pressure and derivative data is due to the rapid change in total mobility at the time of oil breakthrough. Recalling the definition of total mobility gives

$$\lambda_t = \frac{k_{rw}}{\mu_w} + \frac{k_{ro}}{\mu_o} \tag{5.3}$$

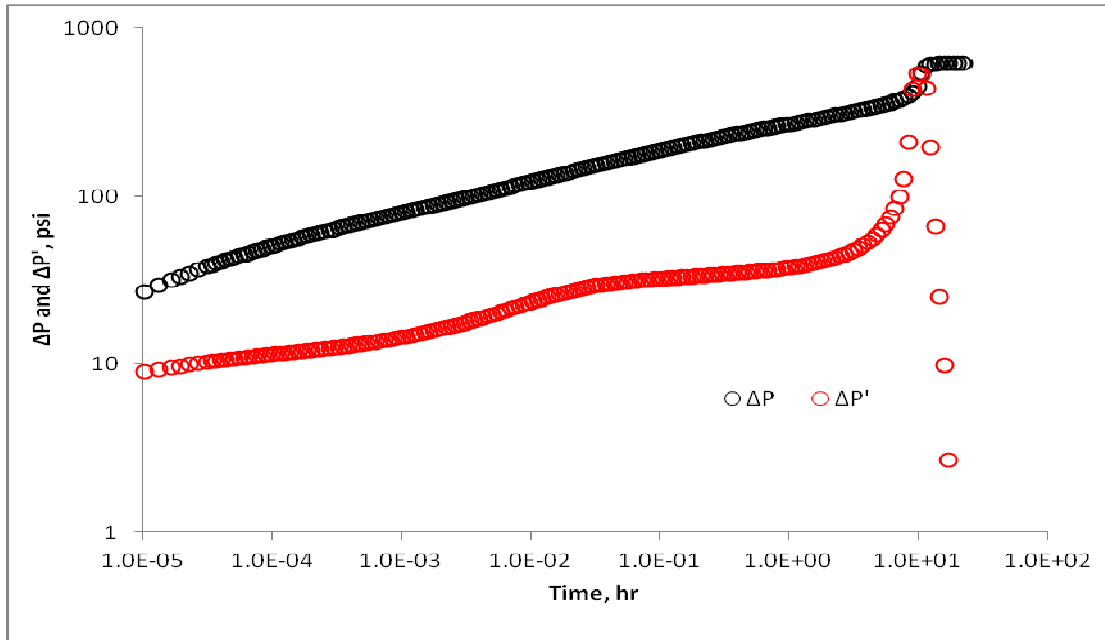


Figure 5.4 : ΔP and $\Delta P'$ vs time for production period.

Figure 5.5 represents the total mobility change with water saturation. Since water mobility is higher than oil mobility, with the increasing water saturation total mobility increases sharply. For the production period, we first produce the water and when the oil breakthrough occurs, total mobility decreases significantly.

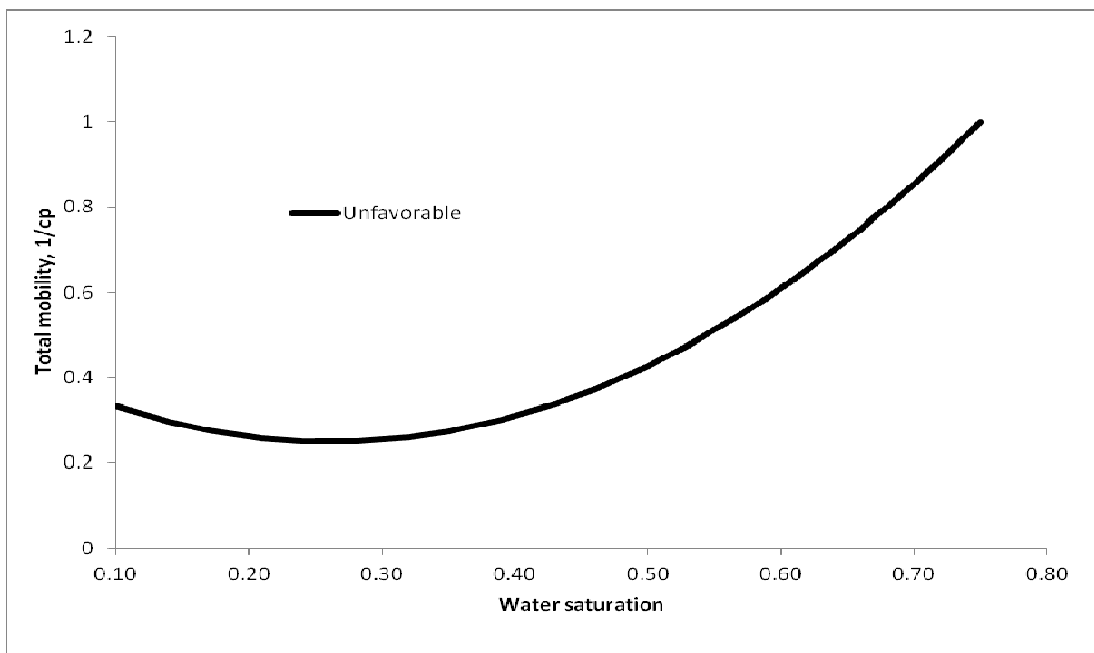


Figure 5.5 : Total mobility change ($\mu_o = 3$ cp, $\mu_w = 0.5$)

5.3 Effect of End Point Mobility Ratio

The mobility ratio is defined as the ratio of the mobility of the displacing phase divided by the mobility of the displaced phase (for example see Willhite 1986). There are various definitions of the mobility ratio. For the oil-water two-phase problem, mobility ratio can be defined by using the end point of values of the oil and water relative permeability. It is also referred to as the end-point mobility ratio, which is defined by

$$M^* = \frac{k_{rw}^0 \mu_o}{k_{ro}^0 \mu_w} \quad (5.4)$$

The water displacement is called as favorable if M^* is smaller than one and as unfavorable if M^* is greater than one.

Here, we will consider an example of favorable and unfavorable of oil-water flow for injection-falloff test. The input data used for simulation are given in Table 5.1, and the same data was considered by Amina (2007).

Here, we will compare the diagnostic pressure change and its Bourdet derivative data plots for the unfavorable case with $\mu_o = 5.1$ cp and for the favorable case with $\mu_o = 0.85$ cp. We assume that water viscosity is the same for both cases and is equal to $\mu_w = 0.516$ cp. Water is injected with a flow rate of $q_w = -18869$ STB/D for a 3-day period. Then, we will have a falloff period of 3 days.

Table 5.1 : Injection-falloff data.

Property	Value
h	78.74 ft.
r_w	0.35 ft.
r_e	10000 ft.
k	2700 md.
S_{iw}	0.25
S_{or}	0.28
P_i	3461.4 psi
ϕ	0.32
B_o	1.318 RB/STB

B_w	1.008 RB/STB
c_o	$8 \times 10^{-6} \text{ psi}^{-1}$
c_w	$2.84 \times 10^{-6} \text{ psi}^{-1}$
c_r	$5.63 \times 10^{-6} \text{ psi}^{-1}$
$k_{ro@S_{iw}}$	0.55
$k_{rw@(1-S_{or})}$	0.175
m	2
n	2

Figure 5.6 illustrates the diagnostic plots for the injection period. During early times of injection period, the pressure propagates first in the oil zone. Since we only change the oil viscosity, we observe two different radial flow periods at early times. However, at late time, both derivative curves are identical since we used same water viscosity for both cases.

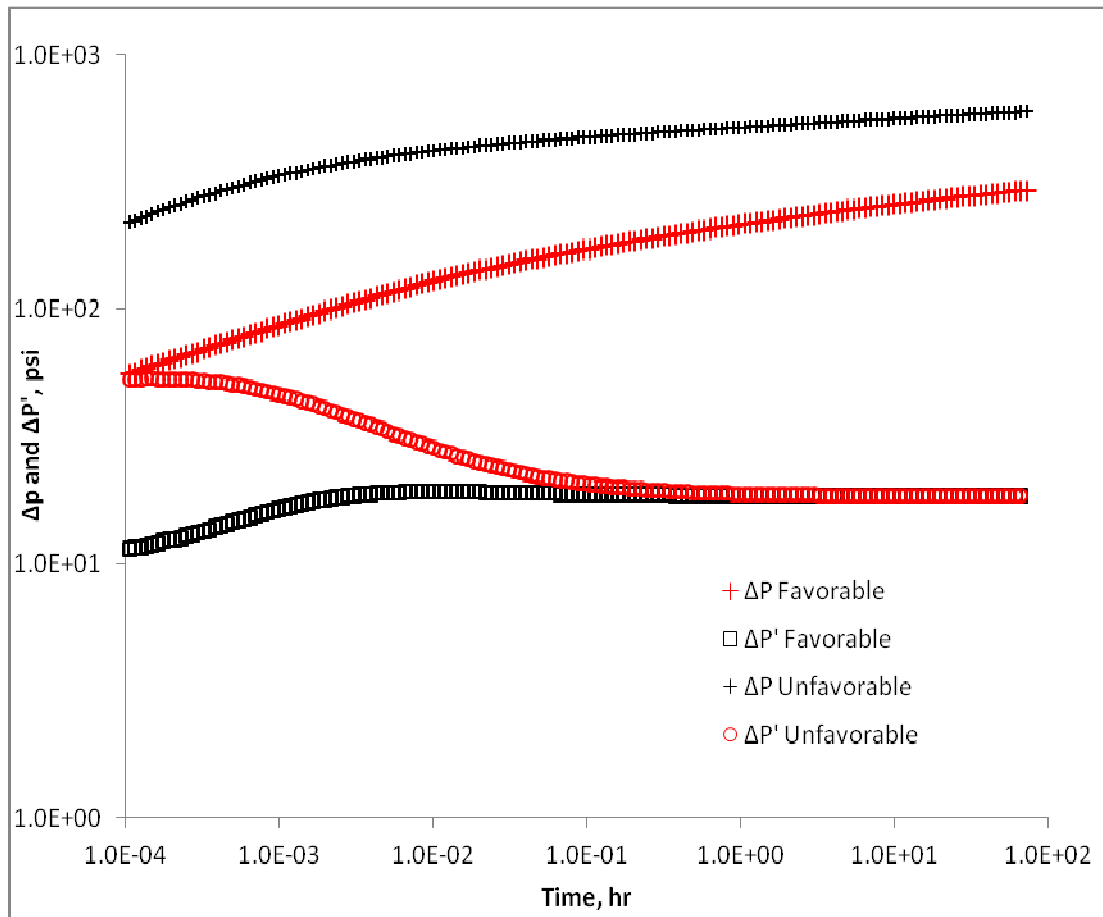


Figure 5.6 : Comparison of favorable and unfavorable case for injection period.

Figure 5.7 illustrates the diagnostic plot of the falloff period. As the pressure response comes from water zone at early times and the viscosities are equal for water for both cases, we observe identical zero slope line at early times. Similar to the injection period, since we used different oil viscosity, we observe two different zero slope lines at late times. As the beginning time of falloff is the same for both cases, pressure difference is identical at early time as the response comes from water zone. However, as soon as pressure starts propagating in the oil zone, we start to observe the difference on pressure difference. As in the injection test, pressure difference is higher for unfavorable case.

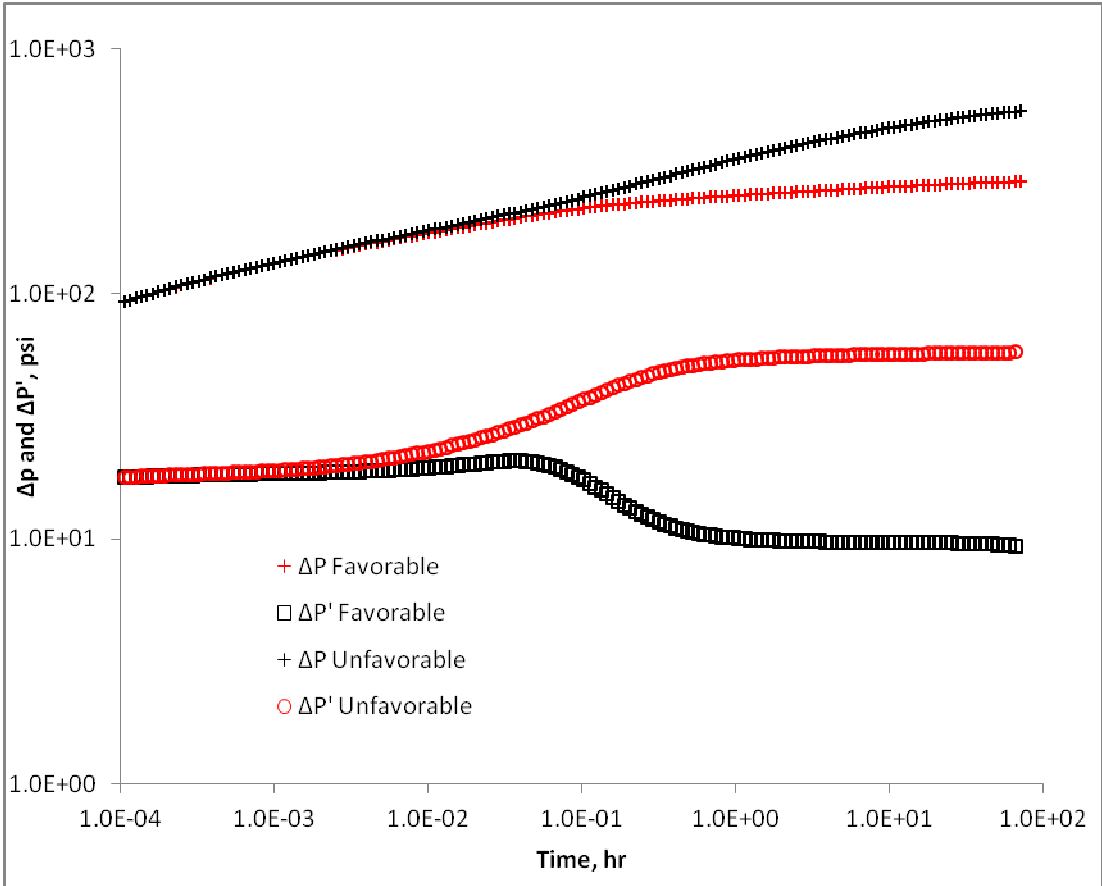


Figure 5.7 : Comparison of favorable and unfavorable case for fall-off period.

5.4 Effect of Skin on Injection-Falloff Tests

Here, we will consider the effect of skin on pressure difference and its Bourdet derivative. The formulation of skin used in the simulator is given in Appendix A.

Hawkins' formula (Hawkins 1956) indicates that, if we know the skin factor and the radius of the skin zone, we can calculate the skin zone permeability. For the following example we will compare three different value of skin, $S = 0$, $S = 4.75$, and $S = -1$. We assumed that the skin zone extends from r_w to $r_s = 1.15$ ft. Using Hawkins' formula, permeability of the skin zone is calculated approximately 540 md. for positive skin case ($S = 4.75$) and 16942 md. for the negative skin case ($S = -1$). Other input data are given in Table 5.1, and hence we consider the same injection and falloff test sequence considered in the previous example for both favorable and unfavorable cases.

Figure 5.8 shows the effect of skin on diagnostic plots for injection period for a favorable case. Firstly, Let us start to analyze the case where skin factor equals to zero. At early time of injection, pressure propagates on oil zone. We calculate the derivative of early time as follows.

$$\Delta P' = \frac{70.6 \times q_{inj} \times B_w}{kh \left(\frac{k_{ro}^0}{\mu_o} \right)} = \frac{70.6 \times 18869 \times 1.008}{2700 \times 78.74 \times \left(\frac{0.55}{0.85} \right)} = 9.76 \text{ psi} \quad (5.5)$$

As times goes on, water saturation increases in the reservoir. Therefore, pressure propagates on water zone and we observe a second radial flow period from the response of water zone. The numeric value of derivative can be calculated as follows.

$$\Delta P' = \frac{70.6 \times q_{inj} \times B_w}{kh \left(\frac{k_{rw}^0}{\mu_w} \right)} = \frac{70.6 \times 18869 \times 1.008}{2700 \times 78.74 \times \left(\frac{0.175}{0.516} \right)} = 18.62 \text{ psi} \quad (5.6)$$

Secondly, if we analyze the case with positive skin, we observe a sharp increase in both pressure difference and its Bourdet derivative at early time. If the skin zone radius is large enough, we expect that a radial flow occurs at early time, reflecting oil zone properties, and the Bourdet derivative for this radial flow period is given by the following formula (Amina 2007):

$$\Delta P' = \frac{70.6 \times q_{inj} \times B_w}{k_s h \left(\frac{k_{ro}^0}{\mu_o} \right)} = \frac{70.6 \times 18869 \times 1.008}{540 \times 78.74 \times \left(\frac{0.55}{0.85} \right)} = 48.80 \text{ psi} \quad (5.7)$$

According to the Amina (2007), once the flood front moves outside the skin zone, regardless of flow condition, pressure derivative can be negative only if the following condition is satisfies.

$$\left(\frac{k}{k_s} - 1 \right) \left(\frac{\lambda_w}{\lambda_t(r_s, t)} - 1 \right) > 1 \quad (5.8)$$

λ_w : water mobility

As there is a rapid increase in total mobility, pressure decreases during injection period. Therefore, discontinuity at the derivative occurs when the water front reaches the skin zone diameter and has a negative value.

As sufficient amount of water is injected into a reservoir, pressure propagates on water and we observe a zero-slope line which indicates radial flow. The numerical value of derivative at late time is calculated from.

$$\Delta P' = \frac{70.6 \times q_{inj} \times B_w}{kh \left(\frac{k_{rw}^0}{\mu_w} \right)} = \frac{70.6 \times 18869 \times 1.008}{2700 \times 78.74 \times \left(\frac{0.175}{0.516} \right)} = 18.62 \text{ psi} \quad (5.9)$$

Finally, we discuss the results for the negative skin case. We expect that first radial flow will occur in the skin zone. However, as the skin zone permeability is sufficiently high we do not observe the first radial flow which should be the response from oil present in the skin zone. Actually, if we could have data at earlier time, derivative would be constant. The derivative is calculated from

$$\Delta P' = \frac{70.6 \times q_{inj} \times B_w}{kh \left(\frac{k_{ro}^0}{\mu_o} \right)} = \frac{70.6 \times 18869 \times 1.008}{16942 \times 78.74 \times \left(\frac{0.55}{0.85} \right)} = 1.55 \text{ psi} \quad (5.10)$$

However, since the permeability is too high because of negative skin, pressure propagation is fast. Second derivative that we observe on derivative is caused by oil zone response, since after passing the skin zone pressure propagates on oil zone. The value of derivative can be calculated from

$$\Delta P' = \frac{70.6 \times q_{inj} \times B_w}{kh \left(\frac{k_{ro}^0}{\mu_o} \right)} = \frac{70.6 \times 18869 \times 1.008}{2700 \times 78.74 \times \left(\frac{0.55}{0.85} \right)} = 9.76 \text{ psi} \quad (5.11)$$

As the time goes on, water saturation increases and pressure propagates on water zone. Therefore, we observe a second radial flow containing information about water zone. The late-time derivative is calculated from

$$\Delta P' = \frac{70.6 \times q_{inj} \times B_w}{kh \left(\frac{k_{rw}^0}{\mu_w} \right)} = \frac{70.6 \times 18869 \times 1.008}{2700 \times 78.74 \times \left(\frac{0.175}{0.516} \right)} = 18.62 \text{ psi} \quad (5.12)$$

When we consider three cases, we observe that the case with no-skin effect reach the late radial before the others. So, displacement efficiency is better. Moreover, we observe that we need much more pressure drop in the case of positive skin case.

Figure 5.9 illustrates the effect of skin on unfavorable flow. Similarly, we can find the value of derivative for early time radial flow for no-skin case as follows.

$$\Delta P' = \frac{70.6 \times q_{inj} \times B_w}{kh \left(\frac{k_{ro}^0}{\mu_o} \right)} = \frac{70.6 \times 18869 \times 1.008}{2700 \times 78.74 \times \left(\frac{0.55}{5.1} \right)} = 58.59 \text{ psi} \quad (5.13)$$

and late time derivative,

$$\Delta P' = \frac{70.6 \times q_{inj} \times B_w}{kh \left(\frac{k_{rw}^0}{\mu_w} \right)} = \frac{70.6 \times 18869 \times 1.008}{2700 \times 78.74 \times \left(\frac{0.175}{0.516} \right)} = 18.62 \text{ psi} \quad (5.14)$$

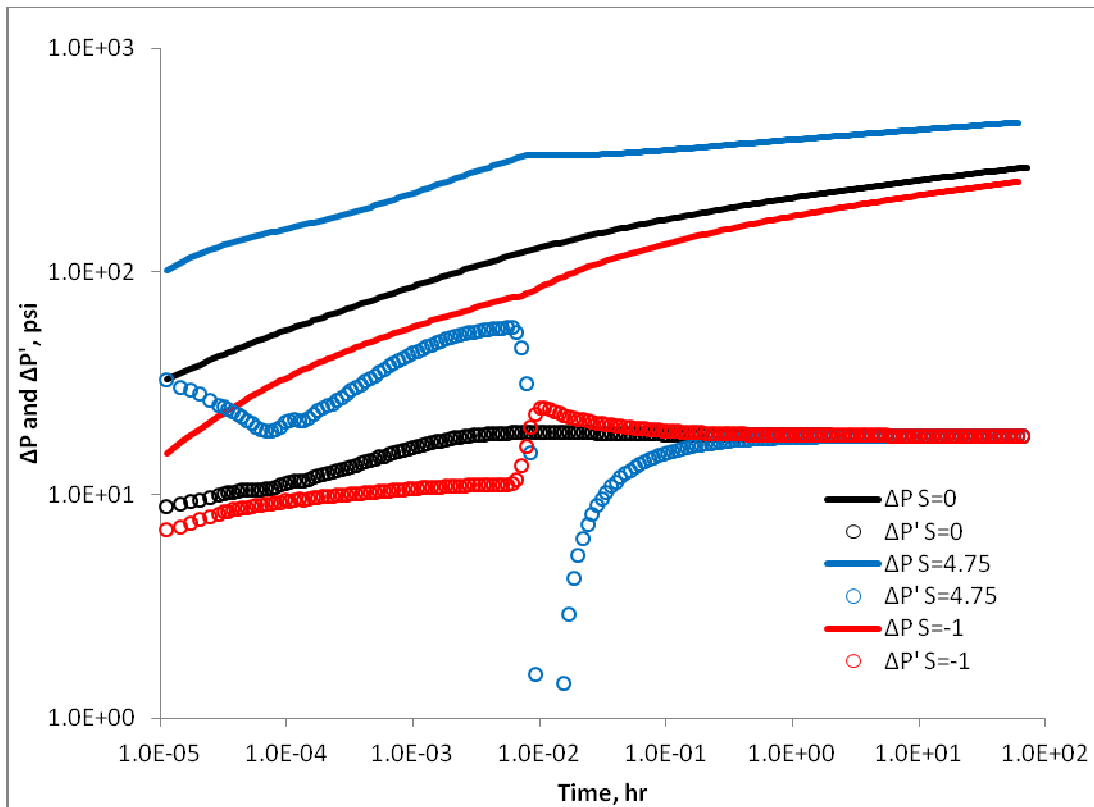


Figure 5.8 : Effect of skin on injection period (favorable).

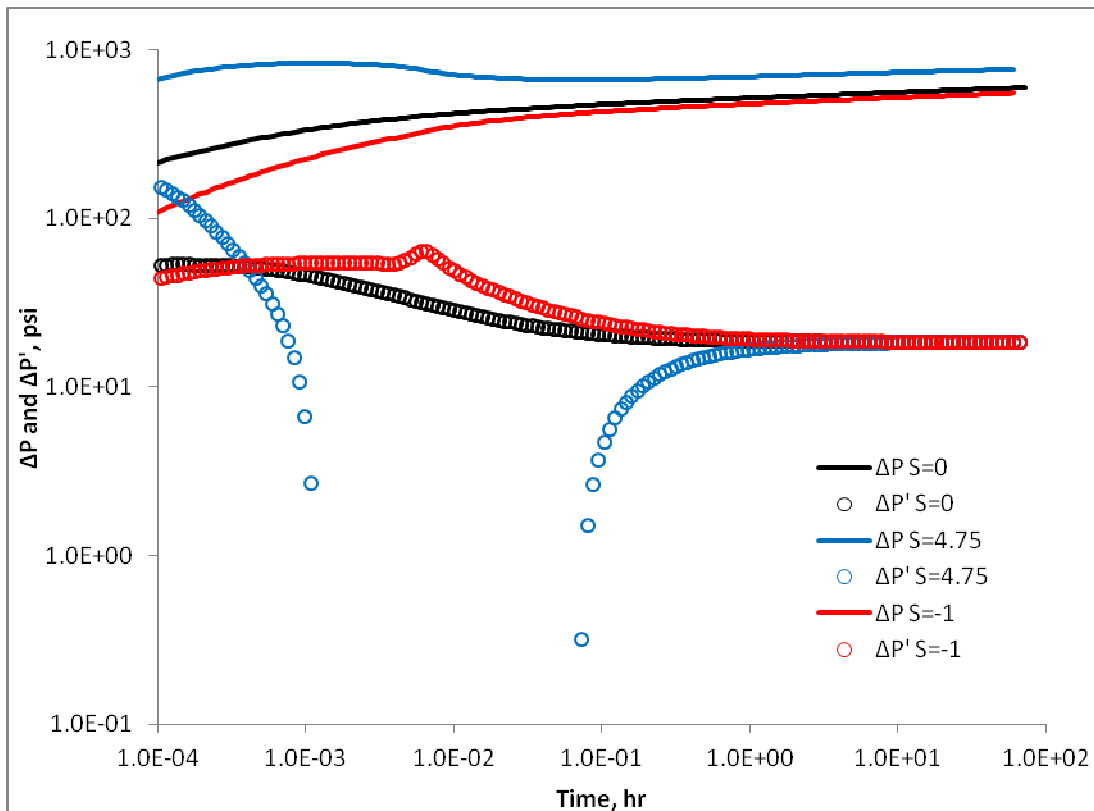


Figure 5.9 : Effect of skin on injection period (unfavorable).

For the positive skin case, we observe a discontinuity in derivative as in favorable case. According to Amina (2007), discontinuity occurs for unfavorable flow and derivative can be negative at early times if the following condition is present.

$$M^* \left(1 - \frac{k_s}{k} \right) > 1 \quad (5.15)$$

He also mention that it is possible only when the well is damaged and the mobility ratio is unfavorable. When the water zone goes out of skin zone and the water saturation increases, we observe a zero slope which indicates the radial flow with same value as calculated in Eq. 5.14.

Recall that we should also see a radial flow because of the skin zone if we could start the simulation at earlier times. The value of derivative would be,

$$\Delta P' = \frac{70.6 \times q_{inj} \times B_w}{kh \left(\frac{k_{ro}^0}{\mu_o} \right)} = \frac{70.6 \times 18869 \times 1.008}{540 \times 78.74 \times \left(\frac{0.55}{5.1} \right)} = 292.8 \text{ psi} \quad (5.16)$$

Finally, for negative skin case, we expect that early time response comes from the oil which is in skin zone. However, as in the favorable case, pressure propagates fast and that is why we do not see it on the plot. derivative of first radial flow which should be the response of oil in skin zone can be calculated as follow.

$$\Delta P' = \frac{70.6 \times q_{inj} \times B_w}{kh \left(\frac{k_{ro}^0}{\mu_o} \right)} = \frac{70.6 \times 18869 \times 1.008}{16942 \times 78.74 \times \left(\frac{0.55}{5.1} \right)} = 0.108 \text{ psi} \quad (5.17)$$

Socondly, we should observe a response of oil zone. Numeric value of derivative is calculated as follows.

$$\Delta P' = \frac{70.6 \times q_{inj} \times B_w}{kh \left(\frac{k_{ro}^0}{\mu_o} \right)} = \frac{70.6 \times 18869 \times 1.008}{2700 \times 78.74 \times \left(\frac{0.55}{5.1} \right)} = 58.59 \text{ psi} \quad (5.18)$$

We observe a small pick on derivative around 0.007 hr. We believe that water front reaches the skin zone radius. As the permeability decreases after this radius for negative skin case, we start observing decrease on derivative. Finally, when

sufficient amount of water is injected to the reservoir, pressure propagates on water zone and we observe a zero slope. The value of derivative is calculated from

$$\Delta P' = \frac{70.6 \times q_{inj} \times B_w}{kh \left(\frac{k_{rw}^0}{\mu_w} \right)} = \frac{70.6 \times 18869 \times 1.008}{2700 \times 78.74 \times \left(\frac{0.175}{0.516} \right)} = 18.62 \text{ psi} \tag{5.19}$$

Figure 5.10 and **Figure 5.11** illustrates the effect of skin on falloff period. We can use the same analysis technique to determine the value of derivative. However, since the water is present in the reservoir, we would observe a early radial flow from the response of water zone and late radial flow from the response of oil zone.

One can see easily that, during fall off period, it is impossible to observe difference on derivative. The only difference occurs at really early times. However, as in the injection case, pressure change in the reservoir is different and higher for positive skin case.

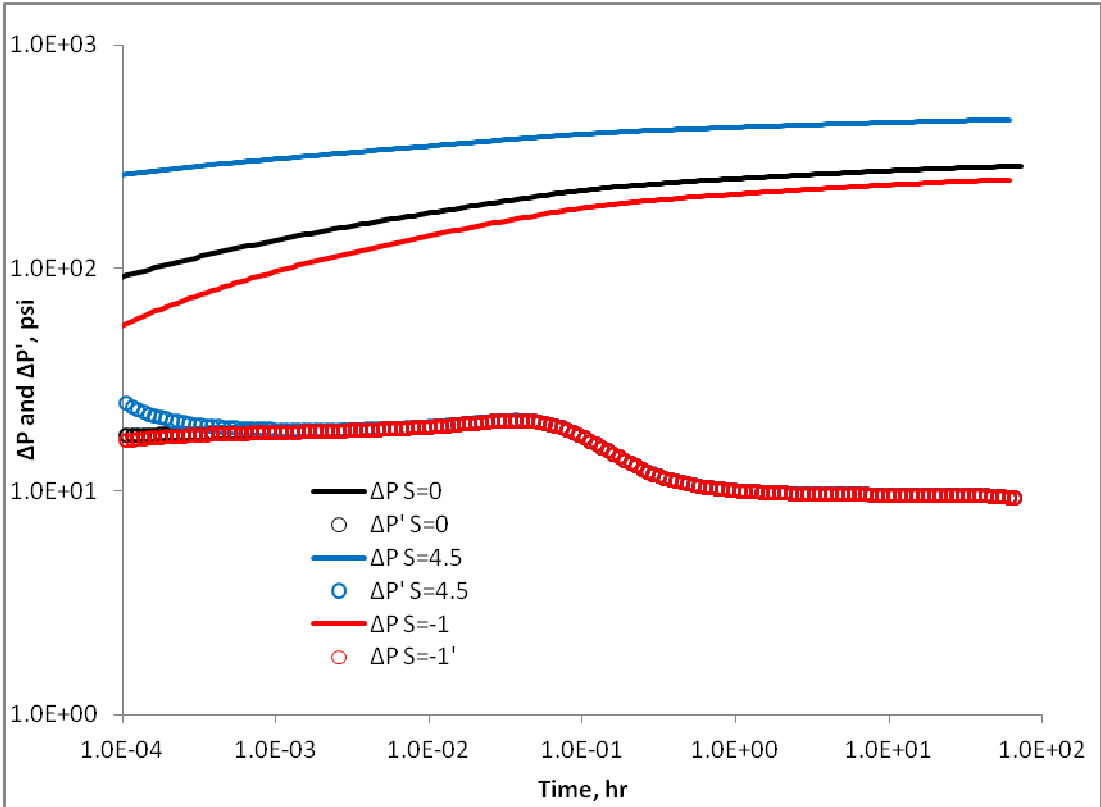


Figure 5.10 : Effect of skin on fall-off period (favorable)

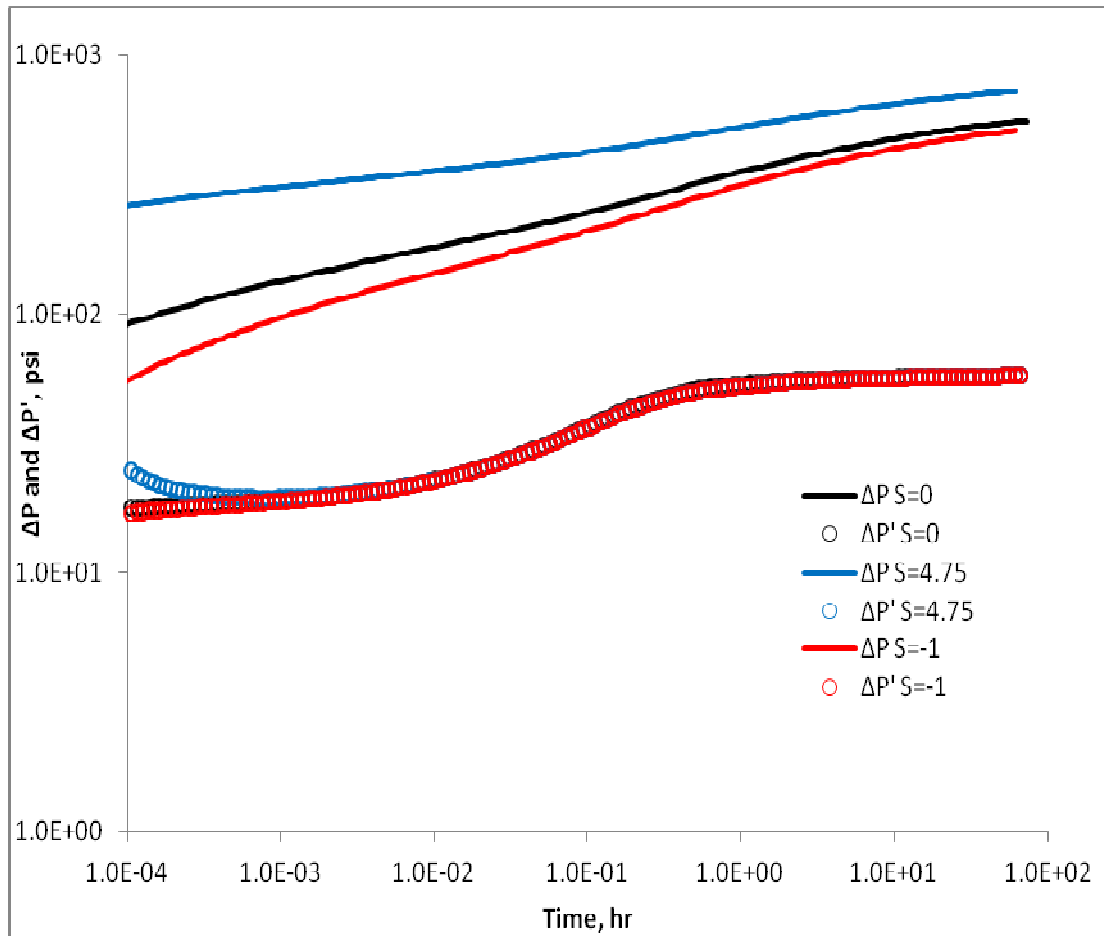


Figure 5.11 : Effect of skin on fall-off period (unfavorable).

Here, we applied the Hawkins formula to implement the skin in our solution. In the formula, we use skin radius and actually for each well it may differ. Therefore, we present the effect of skin zone radius on diagnostic plot in **Figure 5.12**. We used same data that used previously and constant skin of 4.5 for unfavorable flow case.

As it is clear from **Figure 5.12**, skin radius does not significantly affect the pressure difference. However, it shifts the derivative curve. As much as skin radius bigger, pressure propagation is longer in skin zone. Therefore, derivative curve shifts righthand side. Moreover, if the skin radius is small, late time radial flow occurs at earlier time.

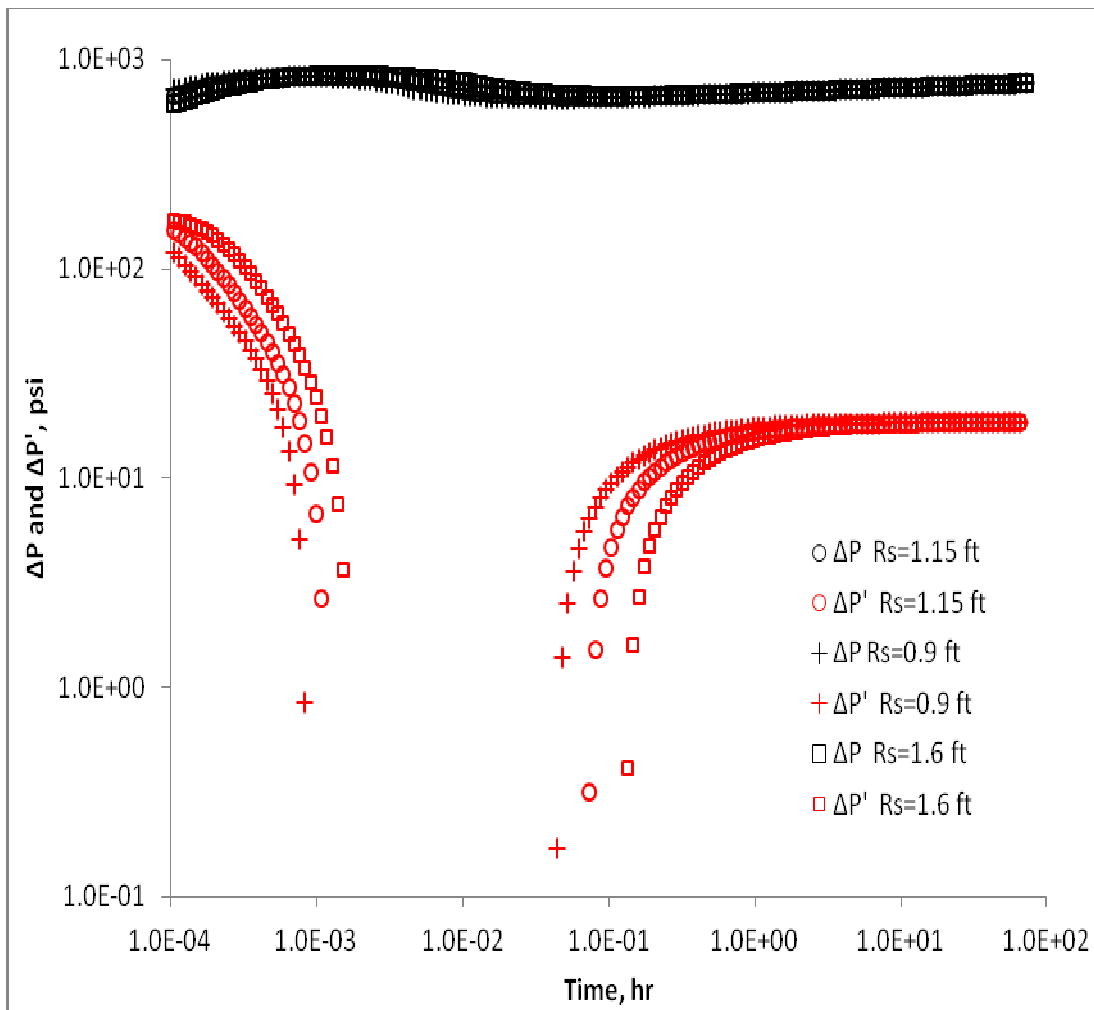


Figure 5.12 : Effect of skin radius (unfavorable, $s = 4.75$).

6. CONCLUSIONS AND RECOMMENDATIONS

On the basis of this study, following conclusions are warranted:

- Although it is widely used, IMPES method may suffer because of stability problems since saturation equation is solved explicitly if the number of grid blocks is not appropriately chosen. The results indicate that the IMPES requires sufficiently large sized grid blocks should be used in simulation to improve the accuracy and avoid the stability problems of the solutions.
- It is found that the FIMPS method is not susceptible as the IMPES method to the number of grid blocks, and provides very accurate solutions without any stability problem. However, the cost of the computations is larger for the FIMPS as the matrix size to be solved in the FIMPS is about twice the size of the matrix problem to be solved in the IMPES method.
- It is found that initial time step of simulation has a great affect on the Bourdet-derivative of pressure difference.
- Unlike single phase flow, two radial flow is observed in two phase flow of oil and water. In the injection period, first radial flow occur because of the response of oil zone and second radial flow because of water zone that is injected. However, during fall of period, first radial flow is the response of water zone where second radial is the response of oil zone.
- It is observed that the end point mobilities of oil and water have a great affect on injection pressure response.
- In injection tests, the derivative of pressure difference can be negative not only because of positive damage around the wellbore but also rapid change in total mobility.

- It is observed that better analysis can be applied on injection test when skin is present because effect of skin on falloff tests occurs at sufficiently early times.

The following recommendations are given:

- One should be careful to stability problem of IMPES method especially when using MacDonaldis and Coats method for gridding.
- Because of the non-linearity of the problem, starting time of simulation must be sufficiently small in order to avoid misinterpretation of diagnostic plot.
- In this work, only forward problem solution is considered. It is recommended that inverse problem should be studied to infer absolute and relative permeability data as well as skin factor from observed pressure and saturation data in a future work.

REFERENCES

- Abbaszadeh, M., Kamal, M.** (1989). Pressure - Transient Testing of Water - Injection Wells, *SPE Reservoir Engineering*, February 1989.
- Amina, B.** (2007). *Injection/Falloff Testing of Vertical and Horizontal Wells* (Doctoral dissertation).
Retrieved from <http://edt.missouri.edu/>
- Aziz, K., Settari, A.** (1979). Petroleum Reservoir Simulation, Applied Science Publishers, England.
- Bourdet, D., Ayoub, J.A., and Pirard, Y.M.** 1989. Use of Pressure Derivative in Well Test Interpretation. *SPE Form Eval* 4 (2): 293–302; *Trans.*, AIME, 287.
- Bratvold, R. B., Horne, Ronald N.** (1990). Analysis of Pressure - Falloff Tests Following Cold - Water Injection, *SPE Formation Evaluation*, September 1990.
- Chen, S.,** (2007). *A Well Test for In-situ Determination of Relative Permeability Curves* (Doctoral dissertation)
Retrieved from <http://edt.missouri.edu/>
- Chu, W. C.,** (1981). *Well Test Analysis for Two-Phase Flow* (Doctoral dissertation)
Retrieved from <http://edt.missouri.edu/>
- Craig, F.F.,** (1971). The Reservoir Engineering Aspects of Waterflooding, SPE Monograph Vol. 3, Society of Petroleum Engineers (2nd edition), Richardson, TX.
- Eisenstat, S.C., Gursky, M.C., Schultz, M.H., and Sherman, A.H.** (1979). Yale Sparse Matrix Package, II. The Nonsymmetric Codes, Yale University, Department of Computer Science, Technical Report #114.
- Ecrin v4.12.02.,** Integrated Software Platform for Dynamic Flow Analysis. 2009.
Sophia Antipolis, France: Kappa Engineering.
- Ertekin, T., Abou-Kassem, J.H., King, G.R.,** (2001). Basic Applied Reservoir Simulation, Richardson, TX.
- Gök, Ihsan M.,** (2004). *Düşey Girişimli Basınç Testlerinin Modellenmesi ve Parametre Tahmini* (Doktora tezi).
Retrieved from <http://edt.missouri.edu/>
- Hawkins, M. F. Jr.** (1956). A note on the Skin Effect, *SPE Technical Note* , December 1956.
- IMEX Version 2010** User's Guide, Computer Modeling Group, Ltd, Calgary.
- Killough, J. E.** (1976). Reservoir Simulation With History Dependent Saturation Functions, *SPE-AIME 49th Annual Fall Meeting*, Houston, 6 - 9 October 1974.

- Kreyszig, E.**, (1979). *Advanced Engineering Mathematics*, John Willey and Sons Inc., (4th Edition), New York, USA.
- Levitan, Michael. M.** (2003). Application of Water Injection/Falloff Tests for Reservoir Appraisal: New Analytical Solution Method for Two-Phase Variable Rate Problems, *SPE Journal*, 2002 SPE Annual Technical Conference and Exhibition, , San Antonio, 29 September - 2 October.
- MacDonald, R. C., Coats, K. H.** (1970). Methods for Numerical Simulation of Water and Gas Coning, *SPE, Second Symposium on Numerical Simulation of Reservoir Performance*, Dallas, 5 - 6 February.
- Peres, A.M.M., Amina A., B., Reynolds, A. C.** (2006). Rate Superposition for Generating Pressure Falloff Solutions, *SPE Journal*, 2004 SPE Annual Technical Conference and Exhibition, Houston, 26 - 29 September.
- Thompson, L. G., Reynolds, A. C.** (1997). Well Testing for Radially Heterogeneous Reservoirs Under Single and Multiphase Flow Conditions, *SPE Formation Evaluation*, 1995 SPE Annual Technical Conference and Exhibition, , Dallas, 22 - 25 October.
- Willhite, P.G.**, (1986). Waterflooding. SPE Textbook Series, Vol. 3, SPE Richardson, TX.

APPENDICES

APPENDIX A.1 : Calculation of Parameters

APPENDIX A.1

Calculation of parameters at grid boundaries

Let us recall the general finite difference equation given in Eq. 3.41 for oil and water flow.

$$\begin{aligned}
& T_{m,r,i+\frac{1}{2},j,k}^{n+1} \left(P_{i+1,j,k}^{n+1} - P_{i,j,k}^{n+1} \right) - T_{m,r,i-\frac{1}{2},j,k}^{n+1} \left(P_{i,j,k}^{n+1} - P_{i-1,j,k}^{n+1} \right) \\
& + T_{m,\theta,i,j+\frac{1}{2},k}^{n+1} \left(P_{i,j+1,k}^{n+1} - P_{i,j,k}^{n+1} \right) - T_{m,\theta,i,j-\frac{1}{2},k}^{n+1} \left(P_{i,j,k}^{n+1} - P_{i,j-1,k}^{n+1} \right) \\
& + T_{m,z,i,j,k+\frac{1}{2}}^{n+1} \left(P_{i,j,k+1}^{n+1} - P_{i,j,k}^{n+1} \right) - T_{m,z,i,j,k-\frac{1}{2}}^{n+1} \left(P_{i,j,k}^{n+1} - P_{i,j,k-1}^{n+1} \right) \\
& = \frac{V_{b,i,j,k}}{c_1 \Delta t} \left[(b_m \phi S_m)_{i,j,k}^{n+1} - (b_m \phi S_m)_{i,j,k}^n \right]
\end{aligned} \tag{A.1}$$

As stated in Chapter 3, we solve Eq. A.1 with FIMPS (or Newton) and IMPES methods. To do that, we need to discretize the partial differential equations as given in Eq. A.1 for a grid system. From Eq. A.1, it is clear that we first need calculate transmissibility in Eq. A.1 to solve the general finite difference equations. Definitions of transmissibility are as follows.

$$T_{m,r,i+\frac{1}{2},j,k}^{n+1} = c_1 r_{i+\frac{1}{2}} \frac{\Delta \theta_j \Delta z_k}{(r_{i+1} - r_i)} \left(\frac{b_m k_r k_{rm}}{\mu_m} \right)_{i+\frac{1}{2},j,k}^{n+1} \tag{A.2}$$

$$T_{m,r,i-\frac{1}{2},j,k}^{n+1} = c_1 r_{i-\frac{1}{2}} \frac{\Delta \theta_j \Delta z_k}{(r_i - r_{i-1})} \left(\frac{b_m k_r k_{rm}}{\mu_m} \right)_{i-\frac{1}{2},j,k}^{n+1} \tag{A.3}$$

$$T_{m,\theta,i,j+\frac{1}{2},k}^{n+1} = c_1 \ln \left(\frac{r_{i+\frac{1}{2}}}{r_{i-\frac{1}{2}}} \right) \frac{\Delta z_k}{(\theta_{j+1} - \theta_j)} \left(\frac{b_m k_\theta k_{rm}}{\mu_m} \right)_{i,j+\frac{1}{2},k}^{n+1} \tag{A.4}$$

$$T_{m,\theta,i,j-\frac{1}{2},k}^{n+1} = c_1 \ln \left(\frac{r_{i+\frac{1}{2}}}{r_{i-\frac{1}{2}}} \right) \frac{\Delta z_k}{(\theta_j - \theta_{j-1})} \left(\frac{b_m k_\theta k_{rm}}{\mu_m} \right)_{i,j-\frac{1}{2},k}^{n+1} \quad (\text{A.5})$$

$$T_{m,z,i,j,k+\frac{1}{2}}^{n+1} = \frac{c_1}{2} \left(r_{i+\frac{1}{2}}^2 - r_{i-\frac{1}{2}}^2 \right) \frac{\Delta \theta_j}{(z_{k+1} - z_k)} \left(\frac{b_m k_z k_{rm}}{\mu_m} \right)_{i,j,k+\frac{1}{2}}^{n+1} \quad (\text{A.6})$$

$$T_{m,z,i,j,k-\frac{1}{2}}^{n+1} = \frac{c_1}{2} \left(r_{i+\frac{1}{2}}^2 - r_{i-\frac{1}{2}}^2 \right) \frac{\Delta \theta_j}{(z_k - z_{k-1})} \left(\frac{b_m k_r k_{rm}}{\mu_m} \right)_{i,j,k-\frac{1}{2}}^{n+1} \quad (\text{A.7})$$

Let us consider first the oil and water viscosity. In this study, we assumed that constant viscosity. However, it may differ from grid to grid. We calculate the viscosity at boundaries using simple arithmetic averaging formula given as follows.

$$\mu_{i+\frac{1}{2},j,k} = \frac{\mu_{i,j,k} + \mu_{i+1,j,k}}{2} \quad (\text{A.8})$$

$$\mu_{i,j+\frac{1}{2},k} = \frac{\mu_{i,j,k} + \mu_{i,j+1,k}}{2} \quad (\text{A.9})$$

$$\mu_{i,j,k+\frac{1}{2}} = \frac{\mu_{i,j,k} + \mu_{i,j,k+1}}{2} \quad (\text{A.10})$$

We use the same averaging technique for the calculation of formation volume factors. However, as we assume that formation volume factor changes with pressure we use simple formulation to calculate the inverse of volume factor as follows to calculate them in grid centers.

$$b_{m,i,j,k} = b_m^0 \left(1 + c_m (P_{i,j,k} - P_b) \right) \quad (\text{A.11})$$

$b_{m,i,j,k}$: inverse of formation volume factor for phase m

b_m^0 : inverse of formation volume factor at base pressure for phase m

c_m : isothermal compressibility of fluid phase m

$P_{i,j,k}$: pressure of the grid block with indices i,j,k

P_b : base pressure (14.7 psi)

Once we calculate the inverse of formation volume factor, we use arithmetic averaging to calculate the inverse formation volume factors at grid boundaries.

$$b_{i+\frac{1}{2},j,k} = \frac{b_{i,j,k} + b_{i+1,j,k}}{2} \quad (\text{A.12})$$

$$b_{i,j+\frac{1}{2},k} = \frac{b_{i,j,k} + b_{i,j+1,k}}{2} \quad (\text{A.13})$$

$$b_{i,j,k+\frac{1}{2}} = \frac{\mu_{i,j,k} + \mu_{i,j,k+1}}{2} \quad (\text{A.14})$$

Harmonic averaging technique applied to calculate the absolute permeability at grid block boundaries. The definitions for harmonic average for absolute permeability are as follows.

$$k_{r,i+\frac{1}{2},j,k} = \frac{k_{r,i,j,k} k_{r,i+1,j,k} \ln\left(\frac{r_{i+1}}{r_i}\right)}{k_{r,i,j,k} \ln\left(\frac{r_{i+1}}{r_{i+\frac{1}{2}}}\right) + k_{r,i+1,j,k} \ln\left(\frac{r_{i+\frac{1}{2}}}{r_i}\right)} \quad (\text{A.15})$$

$$k_{\theta,i,j+\frac{1}{2},k} = \frac{k_{\theta,i,j,k} k_{\theta,i,j+1,k} (\theta_{j+1} - \theta_j)}{k_{\theta,i,j+1,k} \left(\theta_{j+\frac{1}{2}} - \theta_j\right) + k_{\theta,i,j,k} \left(\theta_{j+1} - \theta_{j+\frac{1}{2}}\right)} \quad (\text{A.16})$$

$$k_{z,i,j+\frac{1}{2},k} = \frac{k_{z,i,j,k} k_{z,i,j,k+1} (z_{k+1} - z_k)}{k_{z,i,j,k} \left(z_{k+1} - z_{k+\frac{1}{2}}\right) + k_{z,i,j,k+1} \left(z_{k+\frac{1}{2}} - z_k\right)} \quad (\text{A.17})$$

Finally, the last parameter that we need to calculate in transmissibility terms is relative permeability. There are different approaches to construct relative permeability curves such as straight-line method and power law method. In this

study, we use the power-law model to construct relative permeability curves. Model parameters calculated as follows.

$$k_{ro} = k_{ro}^0 (1 - S_{wD})^m \quad k_{ro}^0 \leq 1 \quad \text{and} \quad m = 2, 3, 4 \quad (\text{A.18})$$

$$k_{rw} = k_{rw}^0 (S_{wD})^n \quad k_{rw}^0 \leq 1 \quad \text{and} \quad n = 2, 3, 4 \quad (\text{A.19})$$

Where,

$$S_{wD} = \frac{S_{w,i,j,k} - S_{w,ir}}{1 - S_{w,ir} - S_{or}} \quad (\text{A.20})$$

k_{ro}^0 : oil relative permeability at irreducible water saturation

k_{rw}^0 : water relative permeability at residual oil saturation

$S_{w,i,j,k}$: water saturation of specified grid

$S_{w,ir}$: irreducible water saturation

S_{or} : residual oil saturation

S_{wD} : dimensionless water saturation

An example relative permeability curves are given in **Figure A-1**. For the construction of the curves we used $k_{ro}^0 = 0.55$, $k_{rw}^0 = 0.175$, $S_{w,ir} = 0.25$, $S_{or} = 0.28$, $n = m = 2$.

Once we calculate the relative permeability values, we used up winding technique to calculate the values at grid boundaries. Basically, up winding technique is a method to find the value at the grid boundary using flow direction. In this study, we used the pressure to find the flow direction. We check the pressure between two grids and, assumed flow will occur from higher pressured grid to lower one.

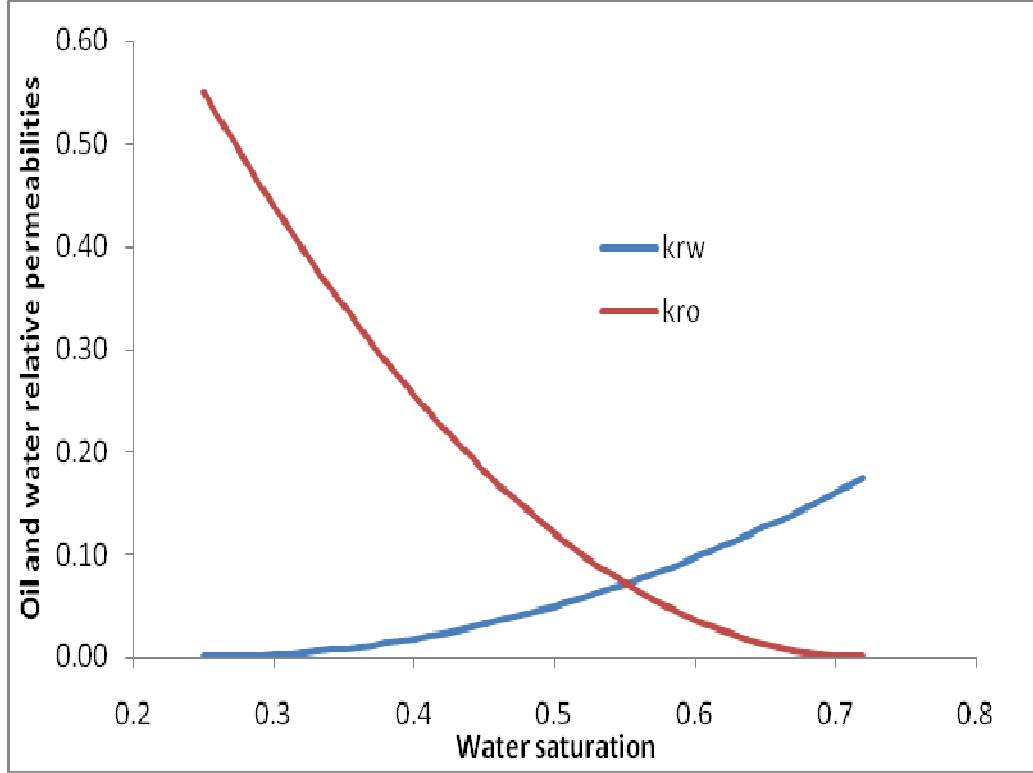


Figure A.1 : Example relative permeability curves

Calculation of parameters at inner boundary

We call the first grid boundary located at well radius at r direction as inner boundary. If we rewrite the transmissibility,

$$T_{m,r,\frac{1}{2},j,k}^{n+1} = c_1 r_1 \frac{\Delta\theta_j \Delta z_k}{2(r_1 - r_w)} \left(\frac{b_m k_r k_{rm}}{\mu_m} \right)_{\frac{1}{2},j,k}^{n+1} \quad (\text{A.21})$$

We use the grid viscosity value for inner boundary since it is constant.

$$\mu_{\frac{1}{2},j,k} = \mu_{1,j,k} \quad (\text{A.22})$$

We do the same approach for absolute permeability.

$$k_{s,\frac{1}{2},j,k} = k_{s,1,j,k} \text{ for } s = r, \theta, \text{ or } z \quad (\text{A.23})$$

However, inverse of formation volume factor is calculated using first grid and well pressure using Eq. A.11. Then, we use arithmetic averaging to find the inverse of formation volume factor at inner boundary as follows.

$$b_{m,\frac{1}{2},j,k} = \frac{b_{m,@P_{0,j,k}} + b_{m,@P_{1,j,k}}}{2} \quad (\text{A.24})$$

Calculation of relative permeability differ according to the operation. In injection period, we assume that relative permeability of water equals to the value at residual oil saturation. Similarly, we do the same approach for oil relative permeability. Mathematically, for injection,

$$k_{rw,\frac{1}{2},j,k} = k_{rw@(1-S_{or})} \quad (\text{A.25})$$

$$k_{ro,\frac{1}{2},j,k} = k_{ro@(1-S_{or})} = 0 \quad (\text{A.26})$$

During falloff and production period, we use the value of the grid same as we did for viscosity and absolute permeability.

Calculation of parameters at outer boundaries

Since we assumed that, no-flow boundaries are present at the edge of the reservoir, outer boundaries conditions at $r - z$ directions are as follows.

$$T_{m,r,N_{r+\frac{1}{2}},j,k}^{n+1} = 0 \quad (\text{A.27})$$

$$T_{m,r,i,j,\frac{1}{2}}^{n+1} = 0 \quad (\text{A.28})$$

$$T_{m,r,i,j,N_{z+\frac{1}{2}}}^{n+1} = 0 \quad (\text{A.29})$$

For θ direction, we need to consider two options. If $\theta \neq 360^\circ$,

$$\mu_{m,i,\frac{1}{2},k} = \mu_{m,i,1,k} \quad (\text{A.30})$$

$$\mu_{m,i,N_\theta+\frac{1}{2},k} = \mu_{m,i,N_\theta,k} \quad (\text{A.31})$$

$$k_{i,\frac{1}{2},k} = k_{i,1,k} \quad (\text{A.32})$$

$$k_{i,N_\theta+\frac{1}{2},k} = k_{i,N_\theta,k} \quad (\text{A.33})$$

$$b_{m,i,\frac{1}{2},k} = b_{m,i,1,k} \quad (\text{A.34})$$

$$b_{m,i,N_\theta+\frac{1}{2},k} = b_{m,i,N_\theta,k} \quad (\text{A.35})$$

$$k_{rm,i,\frac{1}{2},k} = k_{rm,i,1,k} \quad (\text{A.36})$$

$$k_{rm,i,N_\theta+\frac{1}{2},k} = k_{rm,i,N_\theta,k} \quad (\text{A.37})$$

If $\theta = 360^\circ$,

$$\mu_{m,i,\frac{1}{2},k} = \mu_{m,i,N_\theta+\frac{1}{2},k} = \frac{\mu_{m,i,1,k} + \mu_{m,i,N_\theta,k}}{2} \quad (\text{A.38})$$

$$k_{\theta,i,\frac{1}{2},k} = k_{\theta,i,N_\theta+\frac{1}{2},k} = \frac{k_{\theta,i,1,k} k_{\theta,i,N_\theta,k} (\theta_{N_\theta} - \theta_1)}{k_{\theta,i,N_\theta,k} \left(\theta_1 - \theta_{\frac{1}{2}} \right) + k_{\theta,i,1,k} \left(\theta_{N_\theta+\frac{1}{2}} - \theta_{N_\theta} \right)} \quad (\text{A.39})$$

$$b_{m,i,\frac{1}{2},k} = b_{m,i,N_\theta+\frac{1}{2},k} = \frac{b_{m,@P_{1,j,k}} + b_{m,@P_{N_\theta,j,k}}}{2} \quad (\text{A.40})$$

Finally, up-winding (or upstream) method applied between first and last grid at θ direction to find the relative permeability at the boundary located at $\theta = 0^\circ = 360^\circ$.

Calculation of Skin Factor

Skin can be applied either rearranging transmissibility term or by well known Hawkins formula given as follows. In this study, we applied the skin using Hawkins formula.

$$s = \left(\frac{k}{k_s} - 1 \right) \ln \left(\frac{r_s}{r_w} \right) \quad (\text{A.41})$$

s : skin

k_s : permeability of invaded zone

k : permeability of uninvaded zone

r_s : radius of invaded zone

r_w : wellbore radius

Calculation of derivatives in Jacobian Matrix

In this study, derivatives in Jacobian matrix is calculated numerically. Our experiments show that the best results are obtained when using a central difference method. Derivative of oil and water residual is calculated as follows.

$$\frac{\partial f_o}{\partial P}(P) = \frac{f_o(P + \omega) - f_o(P - \omega)}{2 \times \omega} \quad (\text{A.42})$$

$$\frac{\partial f_o}{\partial S_m}(S_m) = \frac{f_o(S_m + \omega) - f_o(S_m - \omega)}{2 \times \omega} \quad (\text{A.43})$$

$$\frac{\partial f_w}{\partial P}(P) = \frac{f_w(P + \omega) - f_w(P - \omega)}{2 \times \omega} \quad (\text{A.44})$$

$$\frac{\partial f_w}{\partial S_m}(S_m) = \frac{f_w(S_m + \omega) - f_w(S_m - \omega)}{2 \times \omega} \quad (\text{A.45})$$

Moreover, we also applied the central difference method for well equation as follows.

$$\frac{\partial f_{well}(P)}{\partial P} = \frac{f_{well}(P + \varepsilon) - f_{well}(P - \varepsilon)}{2 \times \varepsilon} \quad (\text{A.46})$$

Log Time Step Selection

Beginning time for simulation : t_b

End time for simulation : t_e

$npts = 10$

Step 1 – Compute the ratio

$$R = \frac{t_e}{t_b} \quad (\text{A.47})$$

Step 2 – Compute the number of log cycles

$$ncyc = \text{int}[\log_{10}(R)] + 1 \quad (\text{A.48})$$

Step 3 – Compute the total number of time points to be generated.

$$ncyc = ncyc \times npts \quad (\text{A.49})$$

Step 4 – Compute the factor to be used for geometric progression.

$$FACT = R^{\frac{1}{NTP}} \quad (\text{A.50})$$

Then set $NTP = NTP + 1$

Step 5 – Generate the time points from t_b to t_e .

```
set  $t(1) = t_b$   
do  $i = 2$  NTP  
 $t(i) = FACT \times t(i-1)$  (A.51)  
 $\Delta t(i) = t(i) - t(i-1)$   
End do
```

CURRICULUM VITAE



ame Surname: Atakan Sever

Place and Date of Birth: Aydin / 01.04.1982

Address: Halaskargazi M. Kuyumcu Irfan S. No : 40 / 3 Sisli / Istanbul

E-Mail: atakansever@gmail.com

B.Sc.: Istanbul Technical University

Professional Experience and Rewards:

He was born in 01 April 1982 in Aydin. He completed Aydin High School between 1996 and 1999. After high school education, he studied Refinery and Petro-chemistry in Kocaeli University as a pre-licence. He joined the Istanbul Technical University Petroleum and Natural Gas Engineering Department in 2005. After his bachelor, he started his master at Istanbul Technical University Petroleum and Natural Gas Engineering Department in 2010. During his studies, he started working as a research assistant Petroleum and Natural Gas Engineering Department. He has a award from SPE Paper Contest Turkey Section Undergraduate Division 2009 with the title of "Numerical Simulation of 1-D Linear Waterflooding Problem".